Stony Brook University

The Chemical Composition and Evolution of the Martian Upper Crust and Near Surface Environment

A Dissertation Presented

by

Brian Charles Hahn

to

The Graduate School

in Partial Fulfillment of the

Requirements

for the Degree of

Doctor of Philosophy

in

Geosciences

Stony Brook University

December 2009

Stony Brook University

The Graduate School

Brian Charles Hahn

We, the dissertation committee for the above candidate for the
Doctor of Philosophy degree, hereby recommend
acceptance of this dissertation.

Scott M. McLennan, Dissertation Advisor
Professor, Department of Geosciences

Daniel M. Davis, Chairperson of Defense
Professor, Department of Geosciences

Lianxing Wen
Professor, Department of Geosciences

Timothy Glotch
Professor, Department of Geosciences

Bradley L. Jolliff
Professor, Department of Earth and Planetary Sciences
Washington University in St. Louis

This dissertation is accepted by the Graduate School

Lawrence Martin
Dean of the Graduate School

Abstract of the Dissertation

The Chemical Composition and Evolution of the Martian Upper Crust and Near Surface Environment

by

Brian Charles Hahn

Doctor of Philosophy

in

Geosciences

Stony Brook University

2009

The Martian crust is an important geochemical reservoir that has received a great deal of study through the success of several recent spacecraft missions utilizing both orbital remote sensing and in situ lander analyses. Of principle use to this work is the surface chemical analyses returned by the Alpha-Proton X-Ray Spectrometers on the Mars Exploration Rovers (Spirit and Opportunity), which have operated for several years and continue to operate at this writing, and the global abundance maps of a suite of geochemically important elements produced by the Gamma-Ray Spectrometer instrument onboard the 2001 Mars Odyssey orbiter, which collected chemistry data through April

2009. Together, these data provide answers to a broad range of outstanding geochemical questions about the Martian crust.

For the first part of this work, using the most recent data returned from Mars orbital and landed missions, reported chemistries of the Martian meteorites, and cosmochemical relationships, an estimate is made for the bulk chemical composition of the upper Martian crust – the most complete such estimate to date. The results show a basaltic planet with a global sedimentary system dominated by physical processes rather than chemical weathering. Chemically, the Martian crust is far more homogeneous than the terrestrial upper crust. Also, quantifying secular variations in the chemical composition of the Martian crust provides unique insights into the processes that have guided the evolution of the Martian crust-mantle system. Calculating the average chemical abundances for geologic regions of the three Martian age epochs (Amazonian, Hesperian, and Noachian) show subtle, but statistically significant, variations in elemental composition over Martian geologic time.

Martian thermal state and evolution depend principally on the radiogenic heat-producing element distributions in the planet's crust and mantle. This suite of elements can be measured and mapped by the GRS instrument suite and are used in the second part of this work to generate the first global surface heat production and crustal heat flow models based on direct chemical measurements. Additional analyses of specific geologic provinces, regions of anomalous heat flow, and associated geology are discussed.

Table of Contents

List of Figures

Chapter 1

Chapter 2

Chapter 3

Chapter 4

Chapter 5

List of Tables

Acknowledgements

First and foremost, I would like to thank my advisor during this dissertation work, Scott McLennan…and there is much for which I owe thanks. Scott has been a superlative advisor in all matters scientific and I always value his insights. He has helped teach me to think like a scientist. He has also provided me the opportunity to work on both the Mars Exploration Rovers and the Mars Odyssey GRS science teams – a great honor, and the fulfillment of the dream of working on a space mission. I am deeply indebted to Scott and know I will work with him for many years to come. He has also been a great friend, and I wish him and his family the best.

I thank my dissertation committee for their time and effort in reviewing the work presented here. If anyone is actually reading these acknowledgements, it means I passed…so I've got that going for me…which is nice. Thank you: Dan Davis, Lianxing Wen, Tim Glotch, and Brad Jolliff. A special thanks to Brad for travelling a distance from St. Louis for my defense.

Studying under Scott has been rewarding in itself, but I've also been very fortunate to work with the wonderful people that have made up our research group over the past several years. Special thanks must go to Nick Tosca and Joel Hurowitz, who have been great friends for the last several years. They have made the stresses of graduate school much less of a burden. I expect (and hope) we shall be working together on various projects in the future. I'd also like to thank the other members of our lab group

through the years: Shannon Arlaukas; Scott Perl; Lauren Beavon; Yuyan Zhao; and Suniti Karunatillake. And, while not an official member of our group, I extend a special thanks to Alex Smirnov, too. Best wishes to all.

Additionally, I must thank Steve Squyres and William Boynton, the leaders of the MER Athena Science Team and Odyssey GRS Science Team, respectively. Participation in these missions has been a wonderful and gratifying experience.

I thank all the faculty, staff, and my fellow students of the Department of Geosciences at Stony Brook University for support and resources. Special thanks to: Owen Evans, for keeping the ship running smoothly and silently; Loretta Budd, who I hope enjoys her well-deserved retirement; and Diane Isgro and Yvonne Barbour, for much appreciated help.

I thank Zantac®, Tagamet® and Prilosec® for support through stressful times.

I also must extend thanks to several people and collaborators. Jeff Taylor has been one of the more interesting people I've come to know and work with; he's a great scientist, but I suspect he'd make an even better late night talk show host. Ross Taylor has been a source of wisdom, insight, and good humor. Also, special thanks to Hap McSween and Jeff Moersch for providing a place of employment after graduation.

Last, but certainly not least, my family has been a great source of encouragement and support over the past several years while I have worked to complete this dissertation. Thank you, Charles and Bridget Hahn and Jeanette Hahn for your love and support.

Chapter 1: Introduction

The Martian crust is an important geochemical reservoir. It is the only portion of the planet surveyed by broad-scale remote sensing observations or in situ lander and rover experiments. Mars experienced a unique mechanism for crustal emplacement, resurfacing, and recycling [*Nimmo and Tanaka, 2005*] – different from the broadly continuous plate tectonic regime of Earth or the highly episodic, widespread basalt flooding of Venus. The various Martian crustal age provinces are the only geologic records available that preserve evidence of the secular chemical variations produced by the planet's development and evolution [*Hahn et al., 2007*]. If Mars was ever a haven for life, it would have survived on or in the upper crust, and any evidence of its existence would be preserved in the geologic record [*Knoll et al., 2005*]. Accordingly, determining the bulk chemical composition of the Martian crust, constraining the crustal thermal regime, and understanding their relationships to the evolution of Mars are valuable and necessary scientific endeavors.

Further, it is well established that crusts of the inner terrestrial planets as well as many dwarf planets and large rocky satellites become substantially enriched in a suite of geochemically important elements during early differentiation and further evolution [*Taylor and McLennan, 20009; Taylor, 2001*]. Therefore, all planetary crusts have an enhanced chemical significance disproportional to their small relative volume with

respect to the parent planet. The Martian crust is especially significant in this respect since, compared to most other inner planets, the Martian crust is volumetrically larger compared to Mars as a whole (>4%) and is the primary repository for many incompatible trace elements, including the geochemically important heat producing elements (K, Th, and U). The Martian crust therefore serves as an important constraint on the chemical composition of the entire planet and on models of planetary differentiation and crust-mantle evolution.

Of the data used for the studies collected in this dissertation, of particular importance are the in situ lander measurements of soil and rock chemistry (especially the Spirit and Opportunity rovers) and orbital gamma-ray spectrometer measurements of regional and global elemental abundances. Several successful missions, both orbital remote-sensing spacecraft and surface landers, have returned a great deal of information about Martian crustal chemistry. Several landed missions have returned geographically disparate measurements of surface chemistry. However, the two Viking missions consisted of stationary landers and the Sojourner rover used by the Pathfinder mission had limited mobility and operating lifetime [*Soffen, 1977; Golombek et al., 1999*]. The successful – and surprisingly long-lived – Mars Exploration Rovers (MER), Spirit and Opportunity, provided many more detailed chemical and mineralogical analyses of soils and rocks from geographically diverse locales on opposite sides of the planet [*Squyres et al., 2004a,b*] and significantly expanded the catalog of chemical analyses. Apart from several notable exceptions, in situ lander measurements of Martian sediments show very little chemical variability across landing sites. Aside from discrete, local components that influence proximate sediment chemistries, most soils and dust analyses are chemically

indistinguishable. For example, **Figure 1** plots average elemental abundances for the soils of Meridiani Planum measured by the Opportunity rover, versus average soil abundances for Gusev Crater as measured by the Spirit rover on a log-log plot. The diagonal line indicates a 1:1 equivalence between landing sites, and most elements plot very close to or on this line – indicating near-identical chemistries. In orbit, the Gamma-Ray Spectrometer (GRS) instrument suite on board the Mars Odyssey spacecraft has mapped the surface distribution of several elemental abundances – the first robust determination of global surface chemistry [*Boynton et al., 2007*]. Chemical abundances for the suite of GRS detectable elements for the specific pixels that incorporate the Spirit and Opportunity landing sites are also plotted on **Figure 1** and agree well with lander values.

The Alpha-Particle X-ray Spectrometers (APXS) aboard the MER vehicles are the primary instruments for determining elemental compositions [*Gellert et al., 2006; Rieder et al., 2004*]. In conjunction with the Rock Abrasion Tool (RAT) (which can brush away dust coatings or grind away alteration rinds), chemical analyses have been performed on undisturbed rock surfaces, brushed rock surfaces, rock interiors, trenched subsurfaces, as well as disturbed and undisturbed soils. For a given target, the APXS provides reliable analysis for all the major elements and several trace elements (notably: Zn, Cr, Br, and Ni). However, even with MER's enhanced mobility, landed missions have only explored a miniscule fraction of the planet's surface in any detail.

Although limited to a narrower suite of elements than surface in situ observations (H, Fe, Si, Cl, K, Th, Al, and Ca), the GRS can reliably analyze most of the planet from

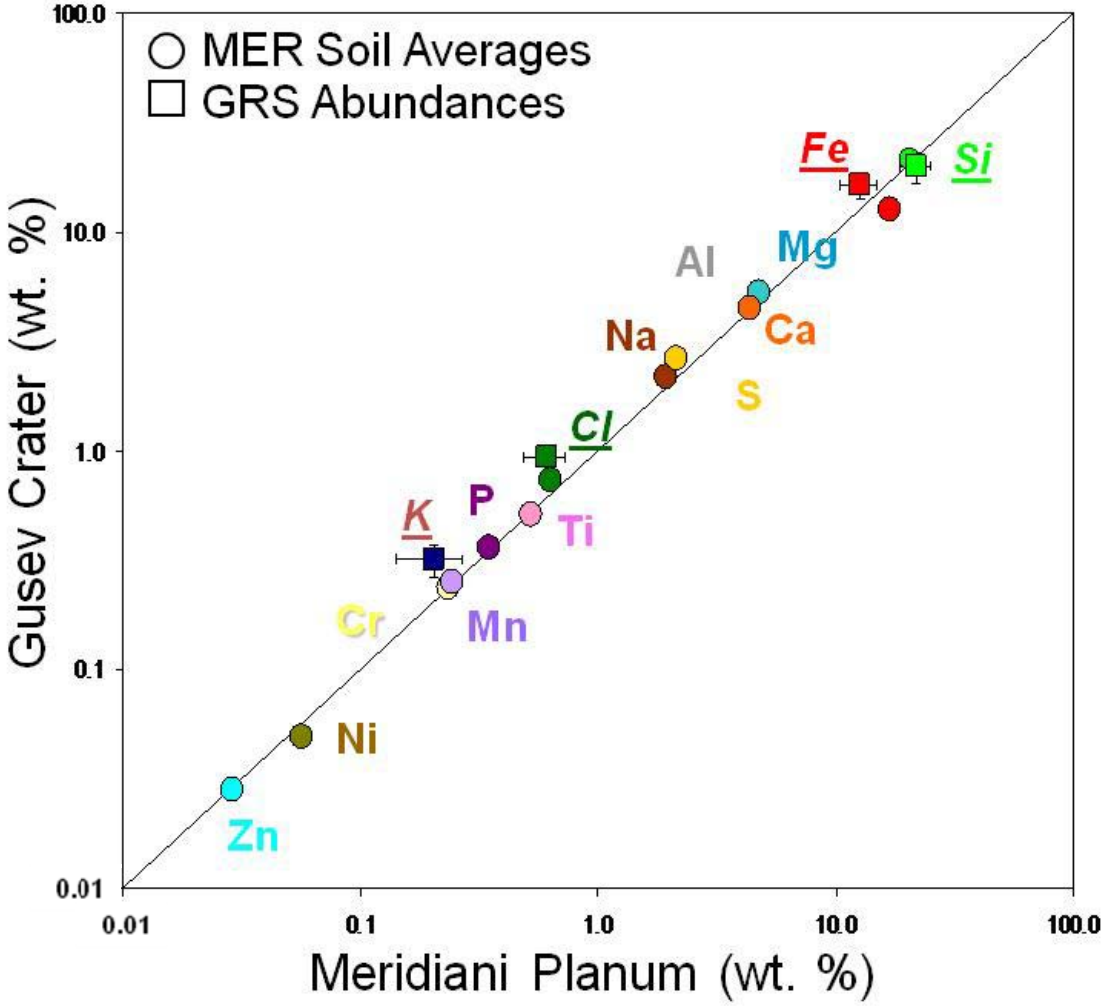

Figure 1. Log-Log plot of average soil compositions measured by the Opportunity rover at Meridiani Planum versus the average soil composition measured by the Spirit rover at Gusev Crater [*Gellert et al., 2006; Rieder et al., 2004*]. The diagonal line represents a 1:1 correlation of equivalent abundances. Generally, Martian soils are chemically indistinguishable across multiple landing sites. Also plotted, the GRS abundances for a suite of measured elements for the GRS pixels that cover the 2 landing sites. GRS abundances agree well with measured landing site averages.

orbit (high abundances of surface or sub-surface polar ice limit resolution at higher latitudes) [*Boynton et al., 2007*]. Penetration depths are mostly dependant on the density of the underlying matrix and the elements measured, but are on the order of tens of centimeters. This deeper penetration depth compared to most remote sensing techniques allows the GRS to be less sensitive to thin coatings of air-fall dust that obscure most other remote sensing data (e.g., TES, THEMIS, and OMEGA) [*Christensen et al., 2001, 2003; Bibring et al., 2005*]. However, the Odyssey GRS has an inherently low spatial resolving capacity with a large footprint and thus cannot be used effectively for fine-scale regional to local analysis. Additionally, element abundance maps are subject to considerable smoothing and auto-correlation effects due to element correction factors, the large footprint and necessary data processing. This too, limits GRS analysis to areally-large regional or global studies.

Using these data sources, the research described in this dissertation was undertaken in order to further understanding of the elemental composition of the upper Martian crust, its evolution through time, and the thermal behavior of the crust as an important reservoir of the incompatible heat producing elements. The results of this research are described in Chapters 2-5 of the dissertation. A brief summary of the major goals and findings for each chapter is provided below.

Overview of Chapter 2: The purpose of this study is to use the MER APXS soil composition data and orbital GRS Odyssey global abundance maps to constrain the bulk chemical composition of the upper Martian crust. For Earth, many past studies have used sediment compositions to help constrain estimates of the composition the terrestrial upper continental crust. Weathering, sedimentary transport, and deposition naturally sample a wide array of source rocks with the resultant chemistry being an efficient mixture of source terrains [*Taylor and McLennan, 1985, 1995, 2009; Condie, 1993; Plank and Langmuir, 1998; McLennan, 2001; Rudnick and Gao, 2003; McLennan et al., 2006*]. Therefore, knowledge of the total sedimentary rock budget (i.e., shales, carbonates, sandstones, and evaporites) provides an excellent proxy for the average bulk chemistry of the upper continental crust from which it is derived. On average, the bulk sedimentary mass appears to be slightly more mafic than the terrestrial upper crust as a whole, but this is probably due to recycling of ancient more mafic crust into the sedimentary record [*McLennan et al., 2006; Ronov, 1983; Veizer, 1979; Veizer and Mackenzie, 2003*].

However, on the Earth, there is significant partitioning of the major elements among distinct sedimentary lithologies through various aqueous processes. Accordingly, sediment chemistry alone is not the most reliable means of determining bulk major element chemistry of the upper continental crust and major element abundances are thus determined by using weighted averages of major rock provinces. Averages of sedimentary rock chemistry do provide a good proxy for the relatively insoluble trace element abundances found in the continental crust (e.g., REE, Th, Sc). By volume, marine shales dominate the sedimentary rock budget for Earth, and shales also tend to have high abundances of most trace elements. As such, chemical averages of sedimentary

products are dominated by an average shale chemistry that is broadly similar across the planet. Thus, the insoluble trace element abundances derived from an average of shale chemistry (with slight corrections for 'dilution' effects) best represents that of the upper terrestrial continental crust.

It is not yet clear whether or not Mars has a significant sedimentary component in the form of shale. Although phylosilicates have been observed by orbital remote sensing in Noachian layered sequences, the basic lithology of such deposits is not known [*Bibring and Langevin, 2008; Bishop et al., 2008*]. Sandstones have been observed and studied, such as those found at Meridiani Planum in the Burns Formation and in layered sequences in the Columbia Hills [*Grotzinger et al., 2005; McLennan et al., 2005; Arvidson et al., 2008; Lewis et al., 2008*]. Additionally, assortments of evaporites, clays and, most recently, carbonates have been detected in varying amounts at various locations around the planet through remote sensing and in situ rover observations. However, the dominant sedimentary products that have been recognized and characterized to date are the Martian dust and basaltic loose regolith or soils. Although different chemically and mineralogically, and resultant from different weathering processes, like terrestrial shales, Martian soils are derived from a large array of source materials from geographically large regions and thus chemical averages of these soils should represent a good proxy for the upper crust provinces from which they are produced. The major conclusions drawn from this study are:

- Most Martian soils are chemically similar representing an average "global" soil composition. Soils that show specific, chemically distinct signatures are explained

through physical mixing between the average global sediment and local, chemically distinct lithological sources (**Figure 2**), such as the Fe-enriched hematite concretions at Meridiani Planum or the P-enriched Wishstone class outcrops in the Columbia Hills at Gusev Crater.

- Like certain terrestrial sediments, Martian soils are derived from large source terrains and are the best chemical proxy for the composition of the upper Martian crust. Unlike terrestrial sediments, which can only provide insoluble trace element compositions of the upper continental crust, Martian soils are produced primarily through physical weathering processes and, more similar to terrestrial glacial sediments, also preserve the major elemental chemical abundances of the source terrains from which they were derived.
- This study uses carefully screened sediment chemical averages from all available lander mission data as well as orbital chemical abundances determined by the GRS instrument to derive the most comprehensive estimate for the bulk chemistry of the Martian crust to date. Average Martian crust is basaltic in composition and modestly enriched in the incompatible heat producing and most likely the light rare earth elements.
- The diversity of terrestrial sediments results from an environment dominated by aqueous alteration in a water-rich environment and most notably the presence of an ocean which fractionates sediments into diverse chemical compositions. In contrast, the primary sedimentary products of the Martian weathering environment over at least the past 3 billion years are the Martian soils and dust that are relatively

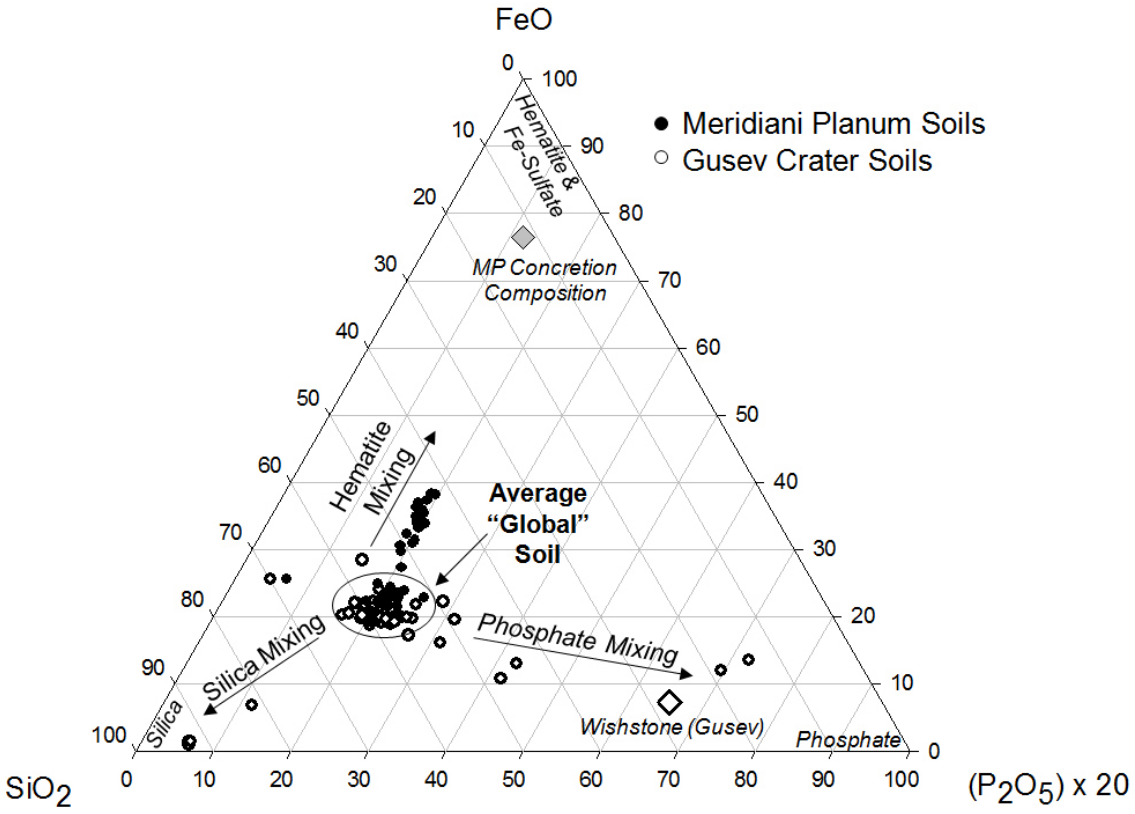

Figure 2. Ternary diagram illustrating average "global" soil composition versus mixtures with select local components. Most soils are chemically similar and represent an average "global" soil composition (circled). Specific, chemically distinct local sources create mixing trends whereas soils proximate to the local source will reflect mixing between the local source and the average composition. The apices are chosen to simply to illustrate chemically distinct locales and do not represent any particular geological process. For example, average soil mixed with end-member Meridiani Planum hematite concretions forms a trend toward the FeO apex [*Jolliff et al., 2007*]. At Gusev Crater, soils proximate to the P-rich Wishstone outcrop show enrichments in phosphate, and soils located near silica deposits near the Eastern Valley location show Si-enrichment [*Hurowitz et al., 2006; Squyres et al., 2008*]. Although not well illustrated here, there are also soils in the Eastern Valley characterized by extremely high sulfur content, also likely related to hydrothermal processes that operated in the vicinity [*Wang et al., 2008*]

Figure 3. (a; top) Total alkalis versus silica petrologic diagram of Martian sediments and APXS landing site rock analyses. Calculated average upper crust plots in the basalt field just below the subalkalic fractionation line. Martian soils plot within the cluster of Martian rock measurements and SNC analyses indicating they represent a physical mixture of primary sources without extreme chemical fractionation. (b; bottom) Plot of terrestrial average continental compositions, relative volumes of major terrestrial sedimentary rocks [*Taylor and McLennan, 2009*], and compositions of those specific sedimentary products with respect to bulk crustal chemistry. Unlike the Martian soils, terrestrial sediments are chemically diverse and represent products of aqueous chemical alteration resulting in considerable chemical fractionation.

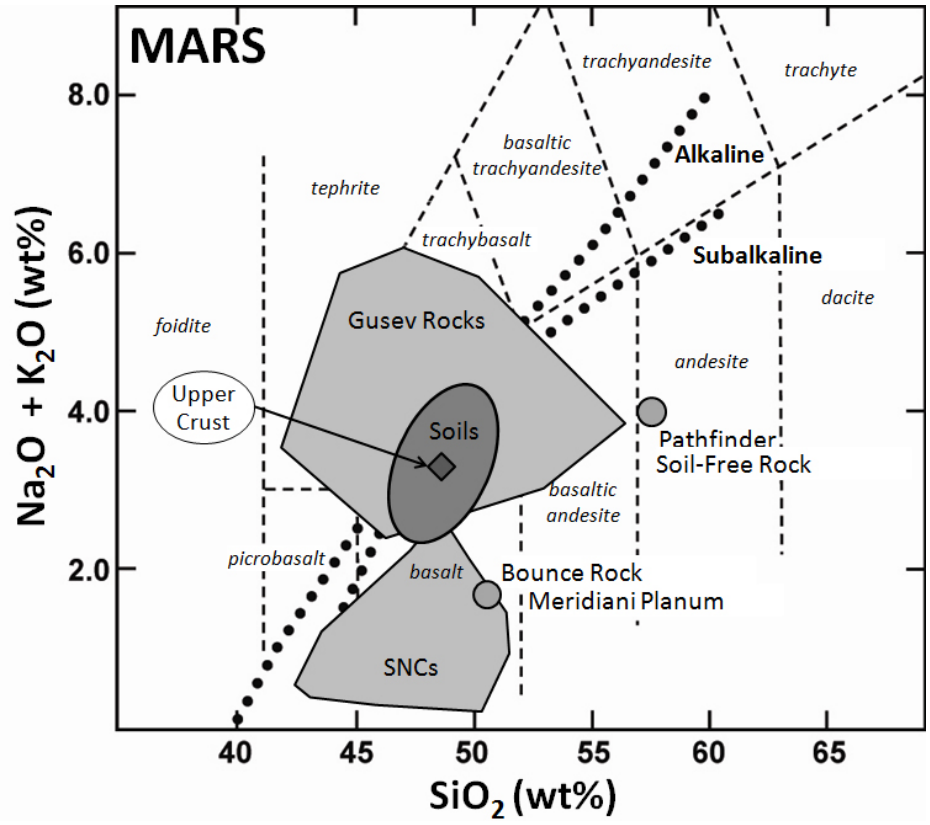
MARS
trachyandesite
trachyte
basaltic
trachyandesite
Alkaline
tephrite
trachybasalt
Subalkaline
dacite
foidite
Gusev Rocks
andesite
Upper
Crust
Soils
Pathfinder
Soil-Free Rock
basaltic
andesite
picrobasalt
basalt
Bounce Rock
Meridiani Planum
SNCs
8.0
6.0
4.0
2.0
40
45
50
55
60
65
Na2O + K2O (wt%)
SiO2 (wt%)

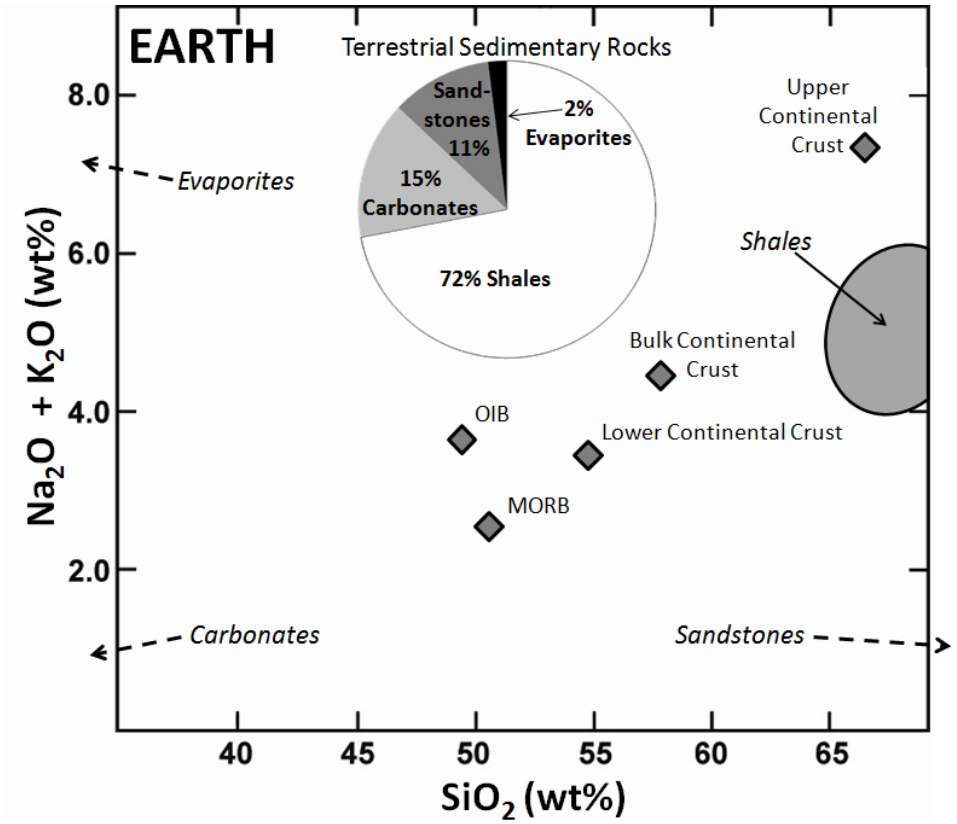
EARTH
Terrestrial Sedimentary Rocks
Sand-
stones
11%
2%
Evaporites
15%
Carbonates
72% Shales
Upper
Continental
Crust
Evaporites
Shales
Bulk Continental
Crust
OIB
Lower Continental Crust
MORB
Carbonates
Sandstones
8.0
6.0
4.0
2.0
40
45
50
55
60
65
Na2O + K2O (wt%)
SiO2 (wt%)

unaltered, homogeneous and chemically indistinct (**Figure 3**). This lack of compositional diversity strongly suggests an arid weathering environment with little long-term surface water and with sedimentary processes dominated by physical mixing. Global sedimentary chemistry, derived from either the in situ lander experiments or GRS global elemental mapping appear to provide no support for the presence of a Martian ocean during this time.

- Martian sediments only sample the upper crust and, as such, chemical composition estimates may not be applicable to the total Martian crust. However, unlike the terrestrial continental crust, the Martian crust is unlikely to be nearly as chemically heterogeneous vertically and there is no definitive evidence of the geologic processes that lead to widespread continental crustal differentiation on Earth. As such, the estimate for the chemical composition of the upper Martian crust likely also represents a reasonable first-order approximation to the chemical composition of the bulk total crust.

Overview of Chapter 3: This chapter reports the first results of correlations between element abundances determined by GRS and the apparent relative surface age of the Martian upper crust as determined by existing geologic mapping and explores some of the potential implications for better understanding Martian crustal evolution and global scale surficial processes.

Secular changes in element abundances, as recorded in age-specific provinces, reveal significant information about planetary crustal formation and evolution. Therefore, relating the age of a planetary crust to its chemical composition is of great geologic importance. On Earth, it is a relatively straightforward task to sample geographically wide-spread crustal materials, perform detailed chemical analyses of major and trace element abundances, and reliably date samples through a variety of field and laboratory methods. The relationship of age to chemistry has been used for decades to better understand the nature and evolution of the continental and oceanic crust [*Armstrong*, 1981; *Taylor and McLennan*, 1985], the reservoirs of heat producing elements throughout the crust-mantle system [*Taylor*, 2001], magmatic resurfacing histories [*Jerram and Widdowson*, 2005], sedimentary processes and recycling [*Veizer and Jansen*, 1985; *Taylor and McLennan*, 1985], plate tectonics [*Richter et al.*, 1992], and a wide array of other important geologic questions. Likewise, lunar samples returned by the Apollo missions, while more limited in sampling diversity, have been well characterized for chemistry and age and consequently, lunar science has made great progress (see reviews in *Taylor,* 1982, 2001). However, for planetary bodies outside the immediate terrestrial neighborhood, these data are difficult to obtain and highly limited.

Currently, the only means of constraining Martian surface age is through the analysis of crater count statistics, cross-cutting relationships, and stratigraphic position. Since the first orbital images of the Martian surface were returned, the USGS and other groups have been reliably mapping the geology of Mars. We have adapted a suite of these maps [*Scott and Tanaka*, 1986; *Greeley and Guest,* 1987; *Tanaka and Scott*, 1987] to create a global apparent relative surface age dataset of the Martian surface for

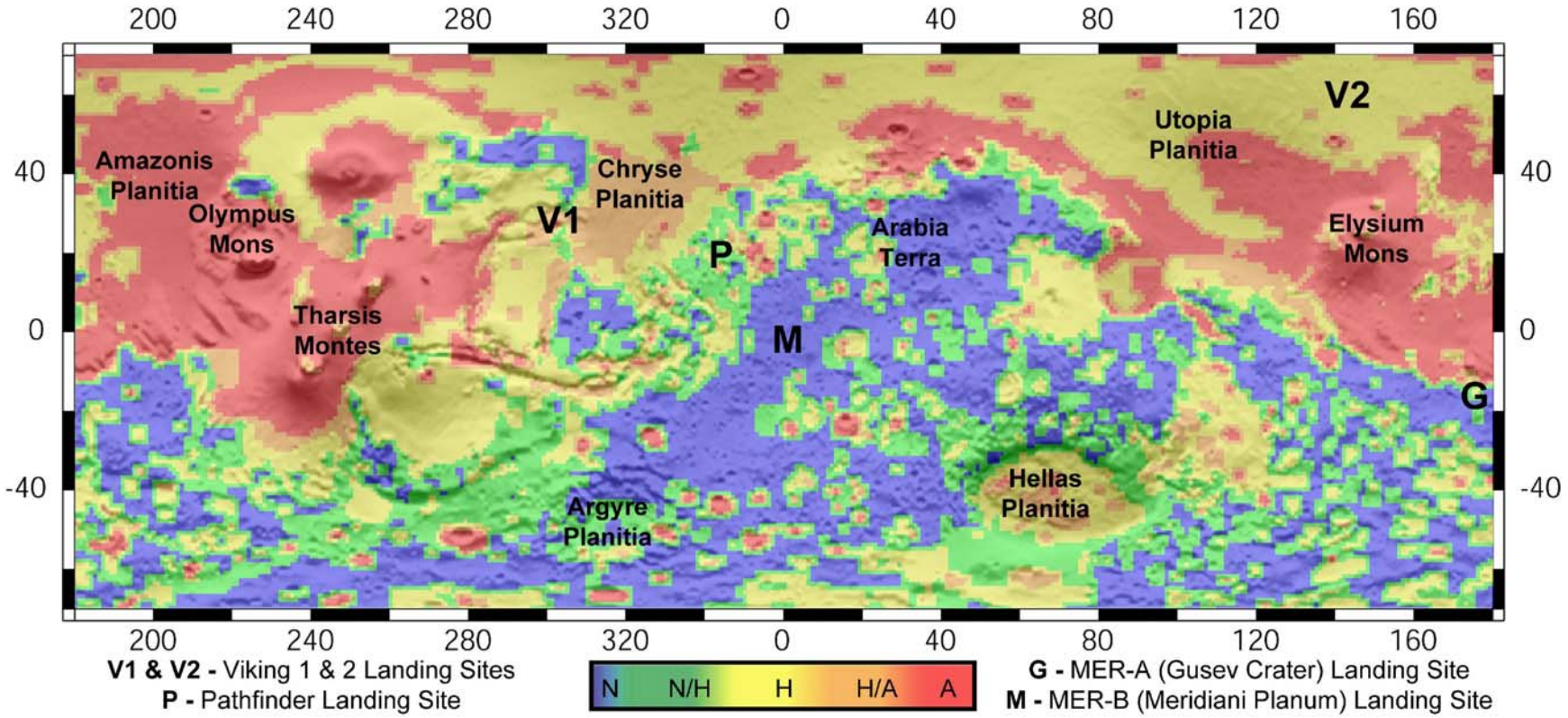

Figure 4. Global map of apparent surface age used in this study. Ages were adapted from the USGS Martian Geologic Investigations Series I-1802 (ABC) [*Scott and Tanaka*, 1986; *Greeley and Guest,* 1987; *Tanaka and Scott*, 1987], and binned into a 1ºx1º resolution grid. Three primary age categories have been assigned (N-Noachian, H-Hesperian, and A-Amazonian); as well as two, less areally extensive transitional age categories (N/H-Noachian-Hesperian and H/A-Hesperian-Amazonian). A gray-scale MOLA topography base-map and labels of prominent geologic features and landing sites have been provided for reference. For comparison to GRS element abundance datasets, we further re-binned age data to a 5ºx5º resolution.

comparison to GRS determined elemental abundances (**Figure 4**). Discussion continues about the uncertainties attached to relative ages derived by these methods; however, while absolute surface ages may not be well-constrained, relative ages between geologic provinces at regional scales are likely quite robust [*Dohm et al.*, 2001]. We examine chemical variations with respect to the three primary Martian age epochs from the formal stratigraphic systems devised by *Scott and Carr*, 1978: Noachian, Hesperian and Amazonian. The data reported and analyzed here support several important conclusions about the nature of the Martian crust:

- K and Th abundances both show significant decreases with younger apparent surface age. Although weathering and broad-scale transport in an acidic environment could cause some of the variation in these elemental abundances, the age relationship suggests an igneous origin. Younger resurfacing magmas were likely derived from a more evolved, depleted mantle source when compared to the older terrains derived from a more primitive mantle. All abundance averages for all age categories are higher than those determined for the SNC meteorites suggesting that, in this respect, the SNCs are not representative of the bulk Martian crust (**Figure 5**).
- Fe abundances show an increase with younger apparent surface age. However, the cause of this increase cannot be uniquely interpreted as igneous, alteration and weathering, or a combination of both. In a generally acidic Martian surface environment, Fe would be far more mobile than in typical terrestrial weathering scenarios. Alternately, a relatively modest change in primary igneous magma composition could lead to the abundance increase seen in the GRS data.

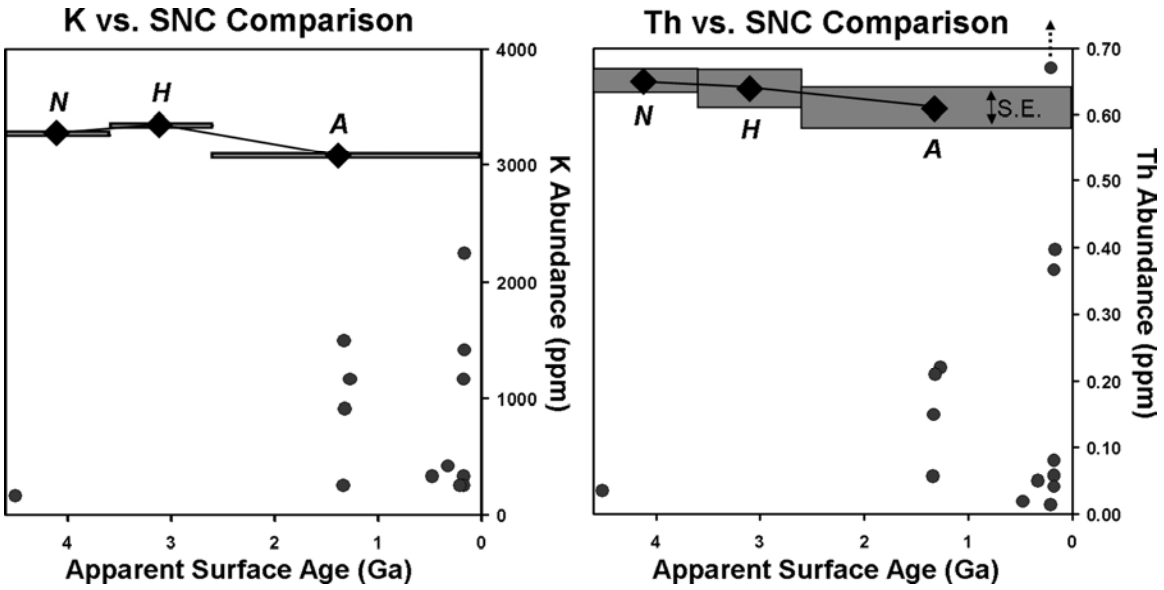

Figure 5. Plots of K and Th abundances with the calculated standard errors of the means represented by the thickness of the lines as well as elemental abundances of the Martian meteorites with reliable published dating and chemical analyses (see compilation in *Meyers*, 2003). Note that irrespective of the ages of the meteorites, all (save the Los Angeles meteorite with a non-characteristic high Th value) show significantly lower K and Th abundances than the broad-scale averages reported by the GRS instrument (age boundaries from *Hartmann*, 2005).

- Cl abundances increase with younger surface age, possibly the result of volcanic activity in younger provinces and the leaching of Cl from older, weathered terrains. The involvement of Cl in the Martian hydrologic cycle is supported by the close correlation between GRS determined Cl and H abundances. The global Cl averages determined for all age categories are lower than average soil compositions sampled at landing sites. However, given the site selection bias of landed missions and the disparate sampling depths of GRS versus in situ lander observations, higher Cl in individual measured soils is not unexpected.
- No statistically or geologically significant correlation was found between elemental abundance and apparent surface age for Si or H, nor was a correlation expected as Si varies little over the planet and H re-distribution occurs at faster timescales.

Overview of Chapter 4: This chapter presents the results of models calculating the crustal component of Martian crustal surface heat production and crustal heat flow as derived from GRS derived K and Th global distributions. Martian thermal state and evolution depend principally on the heat-producing element (HPE) distributions in the planet's crust and mantle, specifically the incompatible radiogenic isotopes of K, Th, and U. Normally these elements are preferentially sequestered into a planet's crust during differentiation [*Taylor and McLennan*, 2009], and this is especially true for Mars, which possesses a thick and mostly ancient crust that is proportionally large with respect to the planet's total volume. The GRS can detect all three of these elements and has been used to map the K and Th

abundances across nearly the entire Martian surface [*Boynton et al.*, 2007]. As the crust is a repository for approximately 50% of the radiogenic elements on Mars, these models provide important, directly measurable constraints on Martian thermal behavior. These results are valuable for better understanding Martian geodynamics, crust-mantle evolution, the cryosphere, formation and history of geologic provinces, and many other varied applications. Our calculations show considerable geographic and temporal variations in crustal heat flow, and demonstrate the existence of anomalous heat flow provinces.

Using smoothed GRS global K and Th maps where the data have been binned into 5°x5° pixels, we determined the radiogenic ^{40}K and ^{232}Th surface abundances for each GRS pixel based on well-determined isotopic fractions. Currently, ^{232}Th is 100% of total Th abundance with a heat release constant of 2.64×10^{-5} W·kg^{-1}; ^{235}U and ^{238}U are 0.7204% and 99.2742% of total U abundance with heat release constants of 5.69×10^{-4} W·kg^{-1} and 9.46×10^{-5} W·kg^{-1}, respectively; and ^{40}K is 0.012% of total K abundance with a heat release constant of 2.92×10^{-5} W·kg^{-1} [*Turcotte and Schubert*, 2001]. Uranium abundances (^{235}U and ^{238}U) were calculated using an assumed Th/U ratio of 3.8; a canonical cosmochemical value thought to be representative of most planetary bodies and that also agrees with analyses of most Martian meteorites unaffected by terrestrial weathering processes [*Meyers*, 2006]. The GRS instrument measures elemental abundances in the top-most tens of centimeters of the Martian surface, and accordingly is strongly influenced by near-surface soils, ice and dust deposits. These sediments broadly represent the bulk chemistry of the Martian upper crust when renormalized to a volatile-free basis [*Taylor and McLennan*, 2009] and as such, K and Th values must be

renormalized to a H_2O-, S-, and Cl-free basis to better reflect bulk crustal values. H_2O and Cl surface abundances are obtained by using smoothed 5°x5° GRS maps. Although the GRS instrument has not yet mapped surface S abundances at the required resolution, we use preliminary GRS estimates of a global S/Cl weight ratio of 5 to calculate the S content of each individual pixel. This ratio is also within the range of values measured in Martian soils at various landing site locations [*Bruckner et al.*, 2003; *Rieder et al.*, 2004; *Gellert et al.*, 2004]. These renormalizations are modest and equate to a 7-14% correction to the K, Th, and U abundances.

These calculations yield the following results for Martian crustal surface heat production and crustal Martian heat flow:

- We calculate a present day average surface heat production of 4.87×10^{-11} $W \cdot kg^{-1}$. Heat production varies significantly across the Martian surface (**Figure 6**), ranging from 2.52×10^{-11} $W \cdot kg^{-1}$ in the Hellas Basin and Solis Planum regions to 7.52×10^{-11} $W \cdot kg^{-1}$ in the Acidalia Planum region.
- Of all the GRS measured elemental abundances, K and Th most closely correlate with one another [*Taylor et al.*, 2006b]. In addition, Th is presently the largest heat source among the radiogenic isotopes. Consequently, present-day surface heat production closely correlates with Th surface abundances measured by the GRS (and especially as U is also a function of Th abundance).
- Using the crustal thickness model of *Neumann et al.*, 2004, smoothed to agree with the GRS 5°x5° pixel resolution, and an average uniform crustal density of 2,900 $kg \cdot m^{-3}$ [*Zuber*, 2001; *Spohn et al.*, 2001], we calculate the average crustal

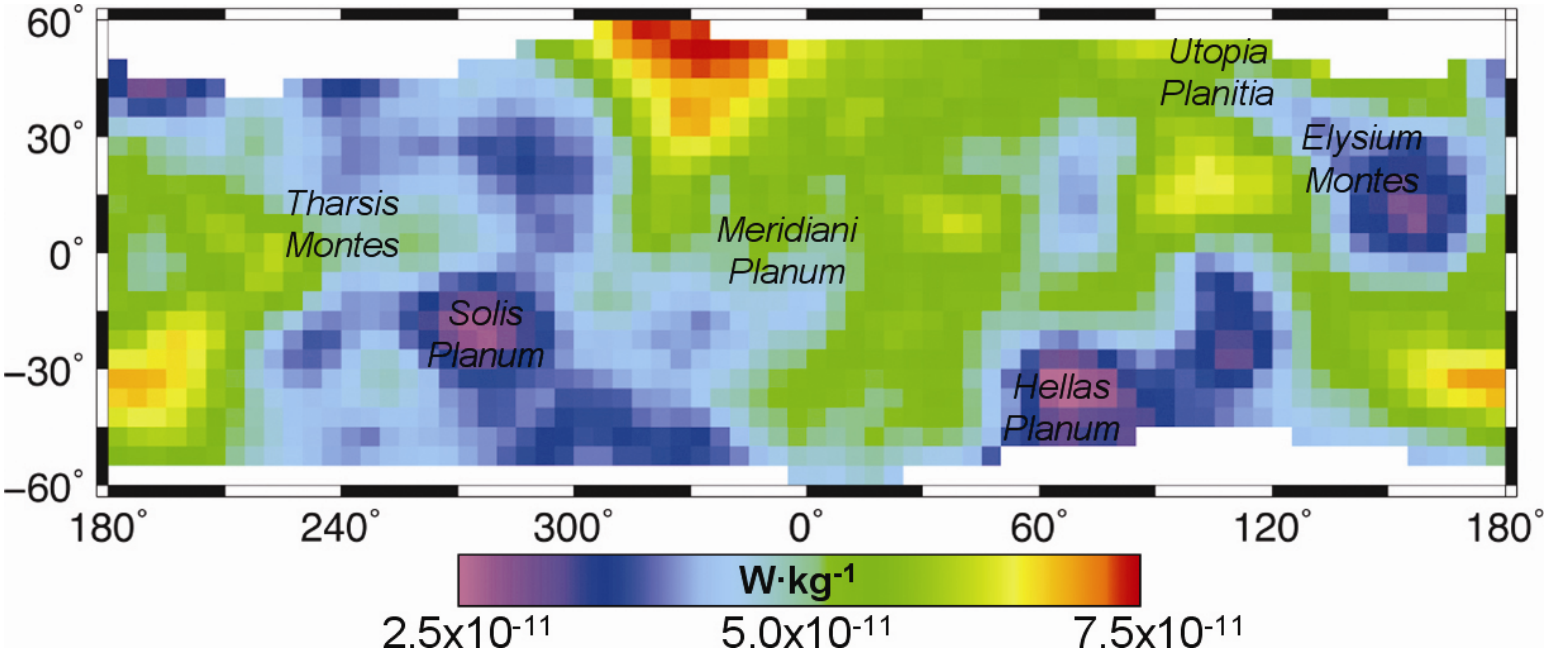

Figure 6: Surface heat production on Mars based on 5x5 smoothed re-binned global GRS K and Th abundance maps renormalized to an H_2O-, S-, and Cl-free basis and assuming Th/U=3.8.

component of heat flow of 6.43 $mW \cdot m^{-2}$ and ranging from <1 $mW \cdot m^{-2}$ in the Hellas Basin and Utopia Planitia regions to 12.6 $mW \cdot m^{-2}$ in the Sirenum Fossae region (**Figure 7**).

- Crustal thicknesses proportionately vary more across Mars than do heat producing elemental abundances. Therefore, although there are some significant deviations, the crustal component of heat flow generally correlates with crustal thickness – i.e., a thicker crust represents higher crustal heat flow.
- Because the respective half-lives of ^{40}K, ^{232}Th, ^{235}U, and ^{238}U are well-known, we can calculate the average crustal component of heat flow over geologic time. Furthermore, temporal regressions of the mapped data show crustal heat flow evolution. Crustal heat flow increases back through time and most dramatically before 2 Ga when the decay of ^{40}K becomes the dominant source of radiogenic heat. Average crustal heat flow at 4 Ga is almost five times that of present day (~28 $mW \cdot m^{-2}$), with some regions, specifically in some sections of the Southern Highlands, showing crustal heat flow of over 50 $mW \cdot m^{-2}$.

(4.) Overview of Chapter 5: Using elemental abundances measured by the Gamma-Ray Spectrometer (GRS) instrument suite onboard the 2001 Mars Odyssey spacecraft, *Hahn et al.* (Chapter 4) calculated and mapped the global distribution of the crustal component of Martian surface heat production and crustal heat flow. Evident from these maps are specific regions of anomalous heat flow, showing significant geographic

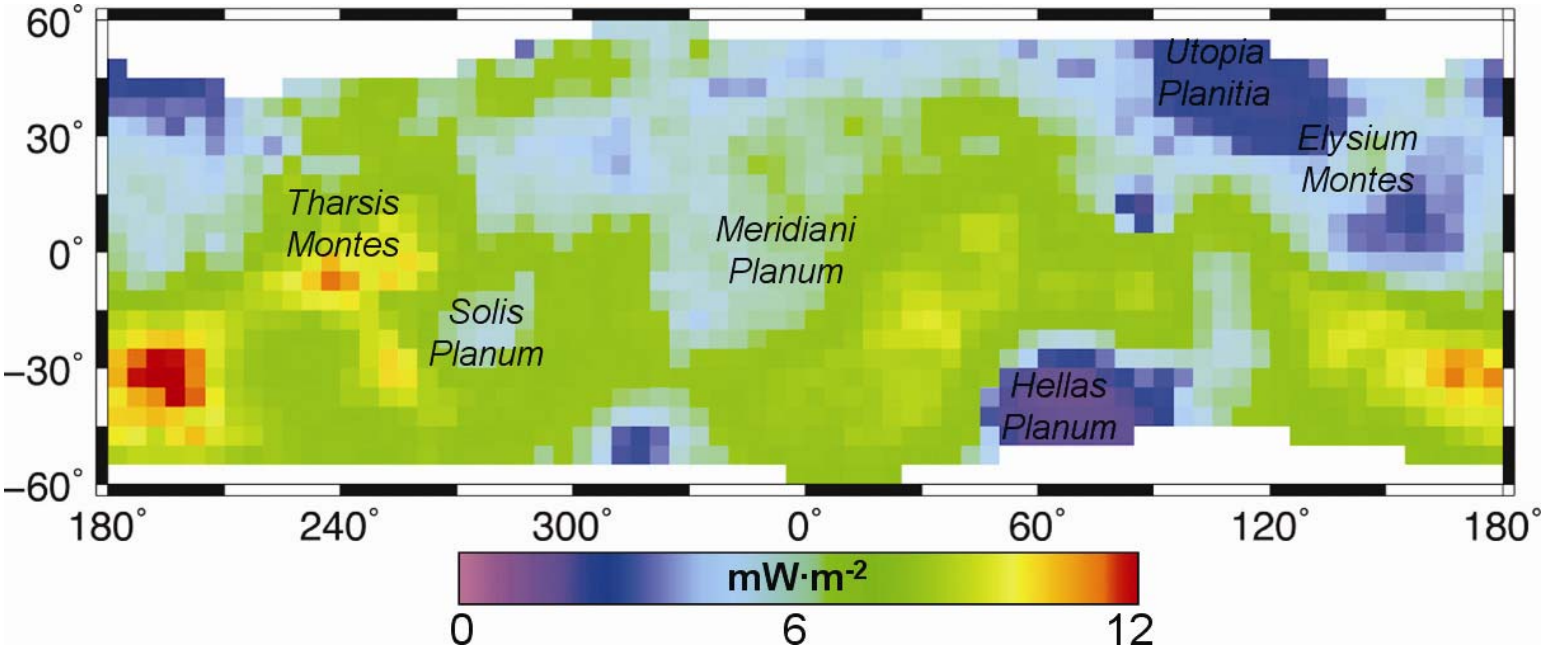

Figure 7: Crustal heat flow for low- and mid-latitudes based on 5x5 smoothed re-binned global GRS elemental abundances, an assumed average uniform crustal density of 2,900 kg·m^{-3} [*Spohn et al.,* 2001; *McLennan*, 2001], and the crustal thickness model of Neumann et al. (2004). Note that these heat flow calculations assume that the GRS-measured surface abundances of the radiogenic elements represent average crust.

variation in the crustal thermal reservoir. In this study, we explore in greater depth these specific regions of anomalous heat flow as well as the report the present crustal heat flow and heat flow at formation for certain geologically important terrains.

A number of previous studies have attempted to constrain Martian heat flow, primarily through indirect geophysical methods [*Zuber et al.*, 2000]. *McGovern et al.* (2002,2004) estimated heat flow for specific geologic regions and features using models determining the elastic or mechanical thickness of the Martian lithosphere. *Ruiz et al.*, 2006 used similar methods to argue for a differentiated Martian crust at Solis Planum. *Montesi and Zuber* (2003) used the distribution and horizontal length scale of wrinkle ridges in tectonic zones on the Martian surface to deduce flexural response to deformation and thus constrain heat flow. More recently, the results of the Shallow Radar (SHARAD) instrument onboard the Mars Reconnaissance Orbiter have been mapping layered deposits, specifically in the Polar Regions. The amounts of downward deflection these loads incur also provide constraints on the rheology and thermal properties of the underlying lithosphere [*Phillips et al.,* 2008; *Nunes and Phillips*, 2006].

Most of these previous studies were primarily interested in mantle heat flow as it relates to mantle convection or surface deformation. These studies estimate total heat flow; combining mantle and crustal heat flow due to the inability to distinguish between the two thermal reservoirs using existing methods. *Hahn et al.* (Chapter 4) and this follow-up study are the first to use elemental abundances, directly measured from recent orbital remote sensing, to constrain crustal heat flow [*Hahn and McLennan*, 2008]. The main findings and calculations of this chapter include:

- Using GRS derived K, Th and U elemental abundances and the method described in *Hahn et al.* (Chapter 4), crustal heat flow is calculated for a variety of Martian surface regions and geologic provinces. The geologic ages of such features can be constrained by crater count statistics and geological relationships and thus, an estimate can be made for the crustal component of heat flow at the time of formation of that feature (**Table 1**).
- We compare crustal heat flow calculations, both past and present, with previous estimates calculated primarily through geophysical observation methods. Some previous studies have calculated heat flow for small surface features and geologic sub-regions; however, do to the spatially large GRS footprint, and considerable smoothing of the GRS data, our study is restricted to relatively large regions.

Table 1: Geologic regions and approximate ages, GRS derived elemental abundances, and present and past heat flow

Geologic Feature/Region	**Feature Age**[†]	**Average Crustal Thickness (km)**[‡]	**GRS Average Abundances**		**Crustal Heat Flow ($mW \cdot m^{-2}$)**	
			K (ppm)	*Th (ppm)*	*Present*	*At Formation*
Olympus Mons	Amazonian	65	3340	0.67	8.9	~10-20
Elysium Mons	Late Hesperian, Early Amazonian	55	2900	0.53	5.9	~16
Tharsis Montes	Noachian and younger	60-65	3300-3700	0.55-0.73	8.4 (6.3-10.0)	~28-36
Solis Planum	Late Hesperian	65	2320	0.37	5.0	~12-14
Meridiani Planum *(Opportunity Landing Site)*	Late Noachian, Early Hesperian	40	3790	0.66	5.6	~20
High K-Th Northern Plains	Late Hesperian	25	6130	1.02	5.4	~16
Sirenum Fossae	Early-Mid Noachian	65	4340	0.98	11.9	~45-50
Hellas Basin	Early Noachian (Hesperian Sediments)	10	2830	0.34	0.9	~6
Utopia Planitia	Early Noachian (Hesperian Sediments)	15	4000	0.71	2.2	~12
Northern Lowlands[*]	N/A	30	4250	0.71	4.5	N/A
Southern Highlands[*]	N/A	60	3990	0.70	8.8	N/A
Global Average	**N/A**	**~50**	**3980**	**0.70**	**6.43**	**N/A**

[†][*Hahn et al.,* 2007; *Scott and Tanaka*, 1986; *Greeley and Guest*, 1987; *Tanaka and Scott*, 1987; *Carr and Head*, 2009; *Hynek et al.*, 2002]
[‡][*Neumann et al.*, 2004]
[*]**[***Taylor et al.,*** 2006b**]**

Chapter 2: Sediments and the Chemical Composition of the Martian Upper Crust

To Be Submitted to Earth and Planetary Science Letters

B. C. Hahn and S. M. McLennan

(1.) Introduction: The Martian crust is an important geochemical reservoir. It is the only portion of the planet surveyed by broad-scale remote sensing observations or in situ lander and rover experiments. Mars experienced a unique mechanism for crustal emplacement, resurfacing, and recycling [*Nimmo and Tanaka*, 2005] – different from the near continuous plate tectonic regime of Earth or the highly episodic, widespread basalt flooding of Venus. The various Martian crustal age provinces are the only geologic records available that preserve evidence of the secular chemical variations produced by the planet's development and evolution [*Hahn et al.*, 2007]. If Mars was ever a haven for life, it would have survived on or in the upper crust, and any evidence of its existence would be preserved in the geologic record [*Knoll et al.*, 2005]. Accordingly, determining the bulk chemical composition of the Martian crust and understanding its relationship to the evolution of Mars are valuable and necessary scientific endeavors.

Further, it is well established that crusts of the inner terrestrial planets as well as many dwarf planets and large rocky satellites become substantially enriched in a suite of geochemically important elements during early differentiation and further evolution

[*Taylor and McLennan*, 2009; *Taylor*, 2001]. Therefore, all planetary crusts have an enhanced chemical significance disproportional to their small relative volume with respect to the parent planet. The Martian crust is especially significant in this respect since, compared to other inner planets, the Martian crust is volumetrically larger compared to Mars as a whole (>4%) and is the primary repository for many incompatible trace elements, including the geochemically important heat producing elements (K, Th, and U). The Martian crust therefore serves as an important constraint on the chemical composition of the entire planet and on models of planetary differentiation and crust-mantle evolution.

(1.1.) The Chemical Compositions of the Terrestrial and Lunar Crusts: The terrestrial crust is easily and thoroughly sampled compared to other planetary bodies and as such, there are many estimates of its bulk chemistry. The oceanic crust is relatively chemically homogeneous and comparably quite young due to its continuous destruction through subduction processes. However, there is considerable geographic and temporal variation in continental crustal chemistries owing to such long-term and ongoing processes as weathering, sediment recycling, island-arc and hot-spot volcanism, plate tectonics, and biological activity. In addition, there are also systematic vertical variations in chemistry owing largely to intracrustal differentiation processes (i.e., crustal melting and fractional crystallization). The bulk of the continental crust (~60-85%) was likely in place by 2.5 Ga. Later growth has been relatively modest with much smaller episodic

crustal growth events [*Taylor and McLennan*, 2009; *Veizer and Jansen*, 1985].

Major element abundances from several studies – employing a variety of theoretical and analytical approaches – agree reasonably well, indicating a reasonably robust understanding of bulk chemistry. Trace element estimates, while more varied, nonetheless show that the chemistry of the terrestrial upper crust is well-understood. On the other hand, the trace element content for the bulk continental crust is more controversial, especially for the most incompatible elements. However, just as terrestrial crustal genesis and evolution have differed from Martian crustal evolution, the terrestrial weathering environment is fundamentally different from that of Mars. Mars has experienced a variable mechanical weathering environment [*Gooding et al.*, 1992; *Golombek et al.*, 2006], extensive impact gardening [*Hartmann et al.*, 2001], and a chemical weathering environment believed to be far more acidic and water limited on average than the terrestrial regime [*Tosca et al.*, 2005; *Hurowitz et al.*, 2006], and especially so since the end of the Hesperian, at about 3 Ga.

The Moon is the only large extraterrestrial body for which we have well-analyzed laboratory samples of known provenance; returned from the lunar surface by the Apollo and Luna mission landings. More recently, these have been supplemented by a suite of lunar meteorites, whose specific provenance is less well understood but on the other hand may provide a more random sampling of the lunar crust [*Korotev et al.*, 2003]. The crust is ancient (although not as ancient as the earliest Martian crust), having formed at about 4.4 Ga, shortly after the initial formation of the Moon likely the result of the solidification of a magma ocean [*Taylor*, 2001]. Although repeated impacts have caused

significant brecciation and physical mixing though impact gardening, the chemical makeup of the lunar crust is largely chemically unaltered since its initial formation. KREEP, a distinct but volumetrically lesser component of the lunar crust; is highly enriched in potassium, rare earth elements (REE), phosphorus, and other incompatible elements and was produced during the final crystallization stages of the ancient lunar magma ocean [*Haskin et al.,* 2000]. Despite encompassing a significant apparent areal fraction of the lunar surface (~17%), mare basalts are thin and make up a trivial volume of the lunar crust [*Taylor*, 2001]. Their iron-rich, basaltic compositions are derived from younger eruptions from a deeper mantle source and differ compositionally from both the lunar highlands and bulk crustal chemistry. The many analyses of the returned lunar surface samples and the Clementine and Lunar Prospector orbiters have provided robust determinations of bulk lunar crustal chemistry [*Taylor*, 1982; *Korotev*, 1998; *Gillis et al.*, 2004]. They reveal a dry crust depleted to various degrees in moderately to highly volatile elements and siderophile elements, but enriched in refractory lithophile elements.

(1.2.) The Martian Meteorites: To date, meteoriticists have identified more than 50 meteorite samples of Martian origin (often collectively referred to as the SNCs for the varieties Shergottites, Nakhlites and Chassignites) [*Meyer*, 2006]. The SNCs are generally accepted to be from Mars based primarily on analyses of gases trapped in glass inclusions that match atmospheric experiments performed by the Viking landers and the fact that their characteristic oxygen isotope ratios fall along a mass fractionation line that

does not conform to those of other planetary bodies or meteorite classes. They are the only in-hand sampling of Mars and, through detailed laboratory analysis, are the only means of determining most trace element abundances and absolute ages [*Wood and Ashwal*, 1981; *Banin et al.*, 1992; *Treiman et al.*, 2000]. Based on their cosmic-ray and terrestrial exposure ages, the SNCs were probably ejected from the Martian surface by 5-8 impact events [*Meyer*, 2003; *Eugster et al.*, 1997]. By Martian standards, the SNC meteorites are quite young. All, save one, have isotopically determined ages younger than or equal to about 1.3 Ga (the ancient ALH84001 is the sole reliable exception – dated between 4.5 and 4.0 Ga) [*Jagoutz*, 1991; *Nyquist et al.*, 2001].

The SNCs have been a vital resource for constraining the accretion history, evolution, and chemistry of the Martian system [*Dreibus and Wänke*, 1985; *Wänke and Dreibus*, 1988; *Halliday et al.*, 2001]. However, although ejected from the Martian surface, it is unclear to what degree they are representative of the Martian bulk crust [*McSween*, 2002]. Their generally young ages imply source regions that are not areally extensive and do not make up a majority of the crust. We cannot determine their geographic origin with any confidence, as they were removed by impact from unknown Martian provinces and attempts to constrain these locations using orbital data have not been successful [*Hamilton et al.*, 2003]. Consequently, additional chemical datasets must be analyzed for a robust determination of the Martian bulk crust.

(1.3.) The Martian Crust – Overview of Mission Data Sources: Several successful missions, both orbital remote-sensing spacecraft and surface landers, have returned a great deal of information about Martian crustal chemistry. Of particular interest for this study are in situ lander measurements of soil and rock chemistry and orbital gamma-ray spectrometer measurements of regional and global elemental abundances. Several landed missions have returned geographically disparate measurements of surface chemistry. However, the two Viking missions consisted of stationary landers and the Sojourner rover used by the Pathfinder mission had limited mobility and operating lifetime [*Soffen*, 1977; *Golombek et al.*, 1999]. The successful – and surprisingly long-lived – Mars Exploration Rovers (MER), *Spirit* and *Opportunity*, provided many more detailed chemical and mineralogical analyses of soils and rocks from geographically diverse locales on opposite sides of the planet [*Squyres et al.*, 2004a,b] and significantly expanded the catalog of chemical analyses. In orbit, the Gamma-Ray Spectrometer (GRS) instrument suite on board the Mars Odyssey spacecraft has mapped the surface distribution of several elemental abundances – the first robust determination of global surface chemistry [*Boynton et al.*, 2007]. The MER and GRS results are the primary data sources for this study.

The Alpha-Particle X-ray Spectrometers (APXS) aboard the MER vehicles are the primary instruments for determining elemental compositions [*Gellert et al.*, 2006; *Rieder et al.*, 2004]. In conjunction with the Rock Abrasion Tool (RAT) (which can brush away dust coatings or grind away alteration rinds), chemical analyses have been performed on undisturbed rock surfaces, brushed rock surfaces, rock interiors, trenched subsurfaces, as well as disturbed and undisturbed soils. For a given target, the APXS provides reliable

analysis for all the major elements and several trace elements (notably: Zn, Cr, Br, and Ni). However, even with MER's enhanced mobility, landed missions have only explored a miniscule fraction of the planet's surface in any detail.

Although limited to a narrower suite of elements than surface in situ observations (H, Fe, Si, Cl, K, Th, Al, and Ca), the GRS can reliably analyze most of the planet from orbit (high abundances of surface or sub-surface polar ice limit resolution at higher latitudes) [*Boynton et al.*, 2007]. Penetration depths are mostly dependant on the density of the underlying matrix and the elements measured, but are on the order of tens of centimeters. This deeper penetration depth compared to most remote sensing techniques allows the GRS to be less sensitive to thin coatings of air-fall dust that obscure most other remote sensing data (e.g., TES, THEMIS, and OMEGA) [*Christensen et al.*, 2001, 2003; *Bibring et al.*, 2005]. However, the Odyssey GRS has an inherently low spatial resolving capacity with a large footprint and thus cannot be used effectively for fine-scale regional to local analysis. Additionally, element abundance maps are subject to considerable smoothing and auto-correlation effects due to element correction factors, the large footprint and necessary data processing. This too, limits GRS analysis to areally-large regional or global studies.

(2.1.) Sediments as proxy for bulk upper crust: For Earth, many past studies have used sediment compositions to help constrain estimates of the composition of the

terrestrial upper continental crust. Weathering, sedimentary transport, and deposition naturally sample a wide array of source rocks with the resultant chemistry being an efficient mixture of source terrains [*Taylor and McLennan*, 1985, 1995, 2009; *Condie*, 1993; *Plank and Langmuir*, 1998; *McLennan*, 2001; *Rudnick and Gao*, 2003; *McLennan et al.*, 2006]. Therefore, knowledge of the total sedimentary rock budget (i.e., shales, carbonates, sandstones, and evaporites) provides an excellent proxy for the average bulk chemistry of the upper continental crust from which it is derived. On average, the bulk sedimentary mass appears to be slightly more mafic than the upper crust as a whole, but this is probably due to recycling of ancient more mafic crust into the sedimentary record [*McLennan et al.*, 2006; *Ronov*, 1983; *Veizer*, 1979; *Veizer and MacKenzie*, 2003].

However, on the Earth, there is significant partitioning of the major elements among distinct sedimentary lithologies through various aqueous processes. Accordingly, sediment chemistry alone is not the most reliable means of determining bulk major element chemistry of the upper continental crust and major element abundances are thus determined by using weighted averages of major rock provinces. Averages of sedimentary rock chemistry do provide a good proxy for the relatively insoluble trace element abundances found in the continental crust (e.g., REE, Th, Sc). By volume, marine shales dominate the sedimentary rock budget for Earth, and shales also tend to have high abundances of most trace elements. As such, chemical averages of sedimentary products are dominated by an average shale chemistry that is broadly similar across the planet. Thus, the insoluble trace element abundances derived from an average of shale chemistry (and corrected for the dilution effects of the other low trace element containing sedimentary lithologies) best represents that of the upper terrestrial continental crust.

It is not yet clear whether or not Mars has a significant sedimentary component in the form of shale. Although phylosilicates have been observed by orbital remote sensing in Noachian layered sequences, the basic lithology of such ancient deposits is not known [*Bibring and Langevin*, 2008; *Bishop et al.*, 2008]. Sandstones have been observed and studied, such as those found at Meridiani Planum in the Burns Formation and in layered sequences in the Columbia Hills [*Grotzinger et al.*, 2005; *McLennan et al.*, 2005; *Arvidson et al.*, 2008; *Lewis et al.*, 2008]. Additionally, assortments of evaporites, clays and, most recently, carbonates have been detected in varying amounts at various locations around the planet through remote sensing and in situ rover observations. However, the dominant sedimentary products that have been recognized and characterized to date are the Martian dust and basaltic loose regolith or soils. Although different chemically and mineralogically, and resulting from different weathering processes, like terrestrial shales, Martian soils are derived from a large array of source materials from geographically large regions and thus chemical averages of these soils should represent a good proxy for the upper crust provinces from which they are produced.

While specific, discrete, local sources do provide some significant variation in soil samples (**see 2.2 below**), most soils and soil averages at landing sites are chemically indistinguishable from one another – despite the fact that landing sites are geographically spread across the planet. Martian soils are quite homogeneous and represent a mixture of the igneous source materials with a moderate though ubiquitous enrichment of volatile rich salts. However, the landing sites do not entirely represent geographic diversity, both due to the limited number of successful landings (six, to date) and an understandable site selection bias that favors specific scientific goals (i.e., evidence of past or present water)

and a maximum probability of safe landing (e.g., low altitude and relatively smooth topography). Is the apparent chemical homogeneity of Martian soils at landing sites representative of global chemistry or merely an artifact of a landing site selection bias?

To answer this question, we note that the 2001 Mars Odyssey orbiter began its primary mapping mission in February 2002 and the Gamma Subsystem of the Gamma-Ray Spectrometer (GRS) instrument suite has since determined statistically reliable elemental abundance maps for H, Si, Fe, Cl, K, Th, and Ca (and with Al data currently being processed and S forthcoming in the near future). The GRS instrument is limited by a surface penetration depth of only a few tens of centimeters, but this is far deeper than other remote sensing instruments. It has an areally extensive resolution footprint of approximately 270 km radius, and while being an inherently low-resolution observational tool, GRS has provided the first detailed global maps of elemental abundances, and accordingly, has proven to be especially valuable for distinguishing the broad-scale variations in elemental compositions across the Martian surface.

GRS elemental abundance maps agree well with surface analyses and, with some notable exceptions, global GRS elemental abundance maps reveal less broad-scale chemical variation compared to the terrestrial or lunar surfaces. Additionally, global averages of GRS derived elemental abundances agree well with soil averages from landing site data, suggesting both that surface sediments dominate the fraction of upper crust measured by the instrument and also that landing site sediment chemistry is representative of global sediments and not an artifact of landing site selection.

Unlike terrestrial shales, which only provide a proxy for the insoluble trace

elements in the terrestrial continental crust, Martian soils can provide an estimate of full major element chemistry as well as a number of trace elements. The terrestrial environment is dominated by a chemical weathering regime with the presence of a large amount of liquid water - most notably the oceans - that causes significant major element fractionation between sedimentary lithological products (i.e., shales, sandstones, limestones, evaporites, siliceous sediments). However, Martian weathering that gives rise to surface soils is primarily physical in nature (see Discussion below). The Martian crust is broadly basaltic [*Taylor and McLennan*, 2009; *McSween et al.*, 2009], and there is little evidence of the geological processes that normally alter a primary igneous basaltic crust into more fractionated, highly evolved crustal products (both sedimentary and metamorphic). While several geophysical models suggest plate tectonics very early in Martian history, there is little definitive evidence for a younger active process. Likewise, some studies have speculated on the presence of a large, episodic ocean; however, the data remain inconclusive. While evidence of past glaciations and fluvial systems are evident in the geologic record, most sedimentary transport for the past ~3 Gyr years appears to be the result of eolian processes and impact gardening. As such, the Martian soils are a largely unaltered and unfractionated representative of the primary lithologies from which they have been derived and therefore generally preserve the bulk chemistry of those sources. While extensive chemical weathering has been observed at landing sites and by orbital remote sensing, such weathering is mostly local and often confined to the very near rock surfaces, as would be expected in a water-limited weathering environment [*Hurowitz et al.*, 2007; *Hurowitz and McLennan*, 2007. Therefore, such weathering products are not volumetrically significant with respect to bulk crustal chemistry.

Additionally, the Spirit and Opportunity rovers have measured the magnetic properties of dust samples and concluded that Martian dust samples are largely unaltered, again suggesting a surface environment mostly devoid of liquid water [*Goetz et al.*, 2008]. Martian dust is globally distributed by eolian processes and derived from physical weathering processes. As such, Martian dust may be more analogous to terrestrial loess, which are glacially derived and show less effects of chemical alteration compared to other terrestrial sedimentary products and therefore represent a good proxy for the chemistry of the upper terrestrial continental crust [*Taylor and McLennan*, 1985; *Rudnick and Gao*, 2003].

(2.2.) Selection and refinement of chemical averages and upper crustal chemistry estimates: In order to evaluate the relationship between the composition of Martian sediments and the bulk chemistry of the upper Martian crust, we must first compile an average soil composition from landing site measurements that most closely represents "global" Martian soil. It is important to note that this work does not claim that all of the Martian soils have been completely homogenized on a global scale and that soils everywhere across the surface are all the same. Rather, that the source terrains for most Martian soils are large enough that an average chemistry of sediments derived from these source terrains approximates upper crustal chemistry. While many measurements of landing site soils show broadly similar chemistries (which we will refer to as "average global soil"), some samples are clearly influenced by specific local processes and/or

exotic lithologies. To illustrate this, **Figure 1** plots measured soil elemental abundances for Fe, P, and Si for both MER rovers (the selection of plotted elements is for illustration purposes only, there is no special geological or petrogenetic significance to plotting these three elements on ternary format). A large majority (>70%) of soil samples at both rover sites plot in a tight cluster representing the average global soil composition. However, a few samples plot toward apices representing particular local variations. For example, a number of Meridiani Planum soils plot along a trend toward the Fe apex. This is due to the inclusion of hematite rich (i.e., Fe-rich) concretions or fragments of concretions as a surface lag deposit and specific to Meridiani Planum, mixed with a more typical soil [*McLennan et al.*, 2005; *Jolliff et al.*, 2007]. Also, a number of samples show evidence of P enrichment due to proximity to the distinctive Wishstone outcrop in the Columbia Hills at the Gusev Crater landing site [*Hurowitz et al.*, 2006] and similarly, several soils show considerable Si enrichment in the Eastern Valley region, also at Gusev, a reflection of local hydrothermal processes that have influenced the local soils [*Squyres et al.*, 2008]. In each case, these soil measurements indicate a varying amount of local source, enriched in a particular element, or suite of elements, mixed with an average global soil component.

Ideally, to best constrain the average global soil component chemically, soil averages should exclude those samples that exhibit evidence for mixing with local components that are not areally extensive or volumetrically significant with respect to the bulk chemistry of the upper crust. For example, including soil samples from Meridiani Planum that show Fe enrichment from concretions would artificially weight an average global soil toward a more Fe-rich composition. As such, we have screened the soil measurements for Opportunity, Spirit, Pathfinder and Viking and excluded soil samples

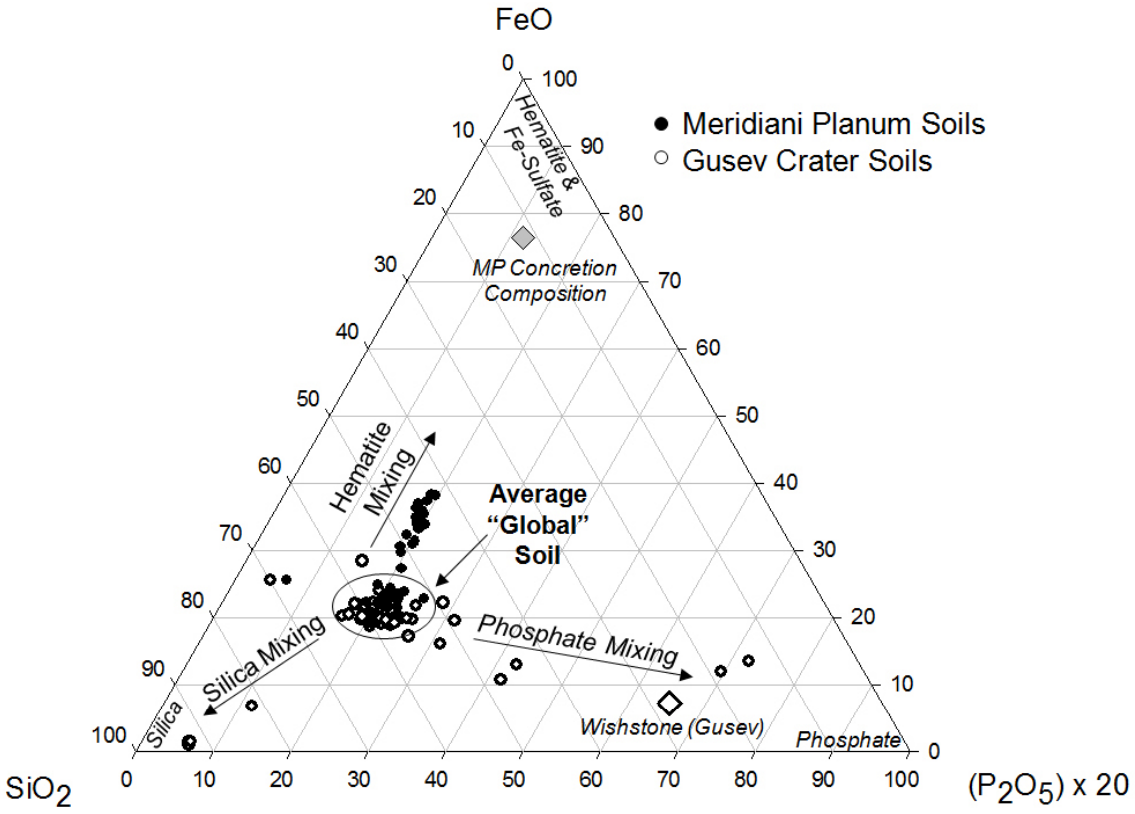

Figure 1. Ternary diagram illustrating average "global" soil composition versus mixtures with select local components. Most soils are chemically similar and represent an average "global" soil composition (circled). Specific, chemically distinct local sources create mixing trends such that soils that are proximate to the local source will reflect mixing between the local source and the average composition. The apices are chosen to illustrate some main chemically distinct locales and do not represent any particular geological or petrogenetic process. For example, average soil mixed with end-member Meridiani Planum hematite concretions forms a trend toward the FeO apex [*Jolliff et al.,* 2007]. At Gusev Crater, soils proximate to the P-rich Wishstone outcrop show enrichments in phosphate, and soils located near silica deposits near the Eastern Valley location show Si-enrichment [*Hurowitz et al.,* 2006*; Squyres et al.,* 2008]. Although not well illustrated here, there are also soils in the Eastern Valley characterized by extremely high sulfur content, also likely related to hydrothermal processes that operated in the vicinity [*Wang et al.,* 2008].

that show significant and obvious enrichments derived from local sources. Each soil sample was considered on a case by case basis. Soil samples evidencing unusual enrichment or depletion in plots of the major elements that can be related to proximate sources were removed from the population used for calculating the soil average. Note that the calculated chemical soil average derived from screened soil samples does not differ significantly from a chemical average calculated from averaging all unscreened soil samples; however, the standard deviation of the screened average is much smaller. The unscreened and screened soil averages and their respective standard deviations are listed in **Table 1**. Soil samples considered for this study include those from the first 1,500 Sols of the Spirit and Opportunity Mars Exploration Rovers, and the Pathfinder lander. Overall, of the 104 soil samples considered, 72 were used for determining a value for average global soil composition – these are listed in **Supplementary Table 1**.

All soils at every landing site location show various levels of enrichment in volatile elements such as S and Cl through the addition of certain evaporite salts. This sulfate-chloride component likely has a variable origin ranging from being fully detrital to being formed in place by various aqueous processes. Regardless of timing and precise origin, these volatile element enrichments are caused by surficial processes and are not representative of the total crustal chemistry. Therefore, all major element and trace element abundances derived from lander measurements have been renormalized to a S- and Cl-free basis to better reflect a bulk crustal chemistry (**Table 1**). This correction and renormalization leads to an increase in major element absolute abundances of between 5-10%.

Table 1. Unscreened/screened average soil compositions and renormalization corrections

	Unscreened		**Screened**		**CI Meteoritic**	**Screened and**
	value	*SD*	value	*SD*	**Component**[*†]	**Renormalized**
SiO_2	45.7	*9.7*	45.7	*1.9*	22.7	**49.0**
TiO_2	0.89	*0.2*	0.89	*0.2*	0.07	**0.95**
Al_2O_3	8.87	*2.1*	9.58	*1.0*	1.64	**10.3**
FeO	18.6	*6.3*	17.5	*2.9*	25.0	**18.8**
Cr_2O_3	0.35	*0.1*	0.37	*0.1*	0.39	**0.40**
MnO	0.31	*0.1*	0.34	*<0.1*	0.26	**0.34**
MgO	7.88	*1.9*	8.52	*1.6*	16.4	**9.13**
CaO	6.02	*1.4*	6.36	*0.6*	1.30	**6.82**
Na_2O	2.44	*0.7*	2.67	*0.5*	0.67	**2.86**
K_2O	0.41	*0.1*	0.45	*0.1*	0.07	**0.48**
P_2O_5	0.93	*0.7*	0.84	*0.1*	0.27	**0.90**
Ni (ppm)	540	*220*	500	*130*	11000	**305 (ppm)**
Zn (ppm)	310	*160*	310	*160*	312	**310 (ppm)**
SO_3[**]	6.94	*5.7*	5.92	*1.8*	15.6	
Cl[**]	0.67	*0.2*	0.70	*0.2*	0.07	
Σ	***100.0***		***100.0***			***100.0***

[*] *2% of CI Meteoritic component is subtracted from the Screened soil average and renormalized to 100%*
[**] *Screened SO_3 and Cl averages are subtracted from the Screened soil average and renormalized to 100%*
† [Anders and Grevesse, 1989]

In addition to S and Cl enrichments, heavy cratering of the Martian surface and the discovery of several meteorites on the Martian surface by the MER rovers imply some amount of a meteoritic component mixed with the soils [*Schröder et al.*, 2008]. Past estimates have been poorly constrained, ranging from 1% to up to 40% of the Martian soil composition (see review in *Yen et al.*, 2006). However, analyses of nickel concentrations and correlations with other elements in soil and sedimentary rocks samples analyzed by the MER rovers suggest a minor addition of meteoritic material amounting to 1-3% by weight [*Yen et al.*, 2006]. As this is a surface enrichment, and not representative of the bulk upper crust, soil compositions have had a 2% CI chondrite composition by weight subtracted from the soil averages (details of the calculation are provided **Table 1**). This does not significantly change major element chemical compositions, but does affect some trace and minor element abundances.

(3.) The bulk chemical composition of the upper Martian crust: After carefully screening soil samples from landing site measurements, renormalizing to a S- and Cl-free composition, and adjusting for a meteoritic component, the estimate for the bulk chemistry of the upper Martian crust is listed in **Table 2**. This is the most comprehensive estimate based on all data sources available to date and updates our preliminary values reported in *Taylor and McLennan* (2009). The upper crust is of basaltic composition sitting just within the subalkaline boundary line on an igneous petrologic diagram (**Figure 2**). In addition to major element chemistry, APXS

Table 2. Estimate of the bulk composition of the upper Martian crust

SiO_2	**49.0**		
TiO_2	**0.95**		
Al_2O_3	**10.3**		
FeO	**18.8**		
Cr_2O_3	**0.40**		
MnO	**0.34**		
MgO	**9.13**		
CaO	**6.82**		
Na_2O	**2.86**		
K_2O	**0.48**		
P_2O_5	**0.90**		
Σ	***100.0***		
Na (wt%)	2.12	La (ppm)	5.3
Mg (wt%)	5.51	Ce (ppm)	13.2
Al (wt%)	5.45	Pr (ppm)	1.8
Si (wt%)	22.9	Nd (ppm)	8.9
P (ppm)	3930	Sm (ppm)	2.40
K (ppm)	3980	Eu (ppm)	0.90
Ca (wt%)	4.87	Gd (ppm)	2.9
Ti (ppm)	5700	Tb (ppm)	0.32
Cr (ppm)	2740	Dy (ppm)	3.23
Mn (ppm)	2630	Ho (ppm)	0.65
Fe (wt%)	14.6	Er (ppm)	1.81
Ni (ppm)	340	Tm (ppm)	0.24
Zn (ppm)	335	Yb (ppm)	1.78
		Lu (ppm)	0.25
Th (ppm)	0.70	Y (ppm)	17.8
U (ppm)	0.18		

Figure 2 (a; top) Petrologic diagram of Martian sediments and APXS landing site rock analyses. Calculated average upper crust plots in the basalt field just below the subalkalic fractionation line. Martian soils plot within the cluster of Martian rock measurements SNC analyses indicating they represent a physical mixture of primary sources without extreme chemical fractionation. (b; bottom) Plot of terrestrial average continental compositions, relative volumes of major terrestrial sedimentary rocks [*Taylor and McLennan,* 2009], and compositions of those specific sedimentary products with respect to bulk crustal chemistry. Unlike the Martian soils, terrestrial sediments are chemically diverse and represent products of aqueous chemical alteration resulting in considerable chemical fractionation.

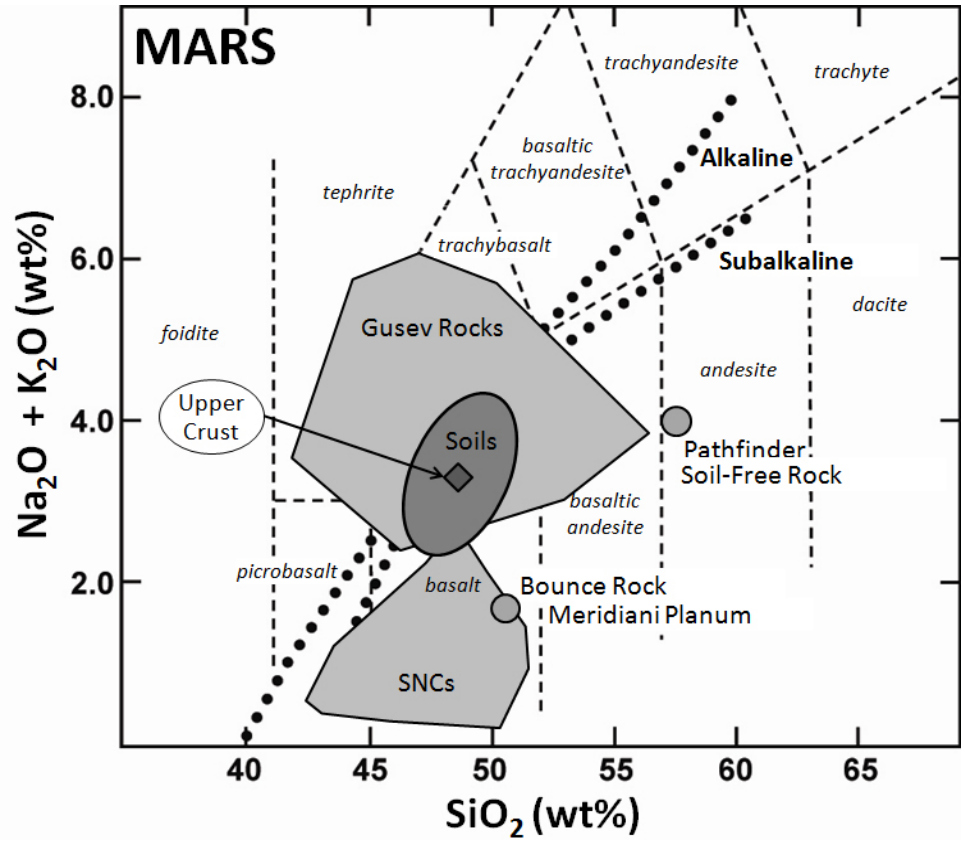
MARS
trachyandesite
trachyte
basaltic
trachyandesite
Alkaline
tephrite
trachybasalt
Subalkaline
dacite
foidite
Gusev Rocks
andesite
Upper
Crust
Soils
Pathfinder
Soil-Free Rock
basaltic
andesite
picrobasalt
basalt
Bounce Rock
Meridiani Planum
SNCs
8.0
6.0
4.0
2.0
40
45
50
55
60
65
Na2O + K2O (wt%)
SiO2 (wt%)

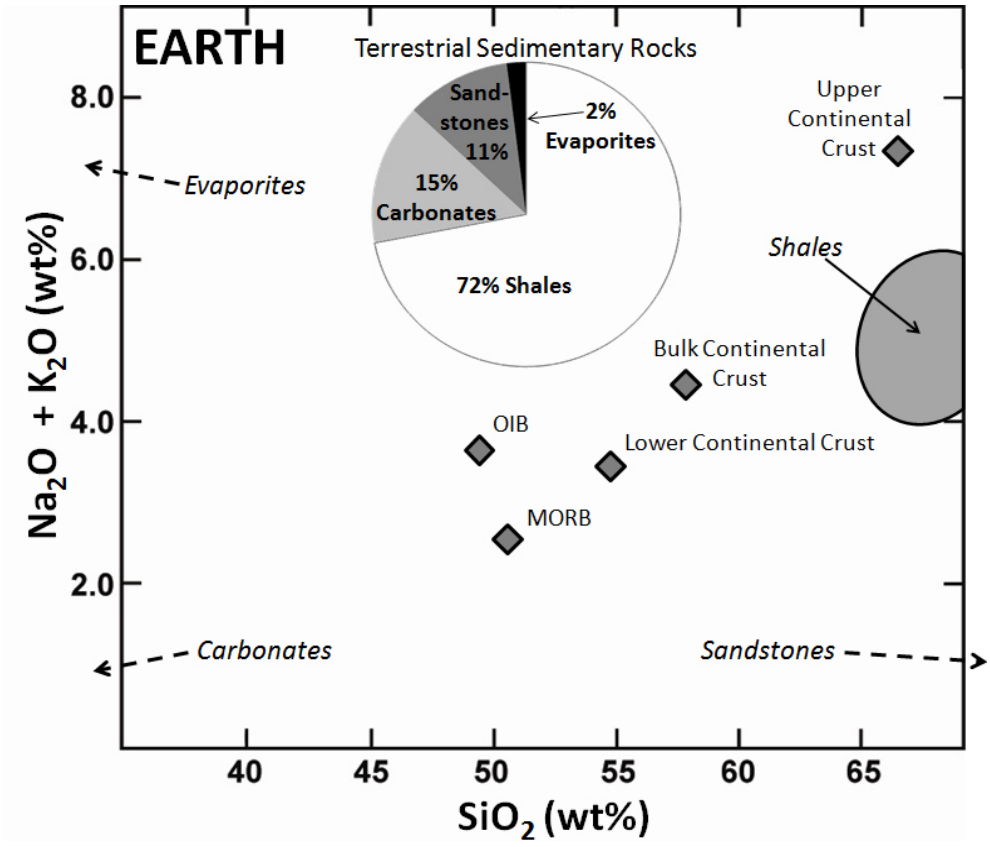
EARTH
Terrestrial Sedimentary Rocks
Sand-
stones
11%
2%
Evaporites
15%
Carbonates
72% Shales
Upper
Continental
Crust
Evaporites
Shales
Bulk Continental
Crust
OIB
Lower Continental Crust
MORB
Carbonates
Sandstones
8.0
6.0
4.0
2.0
40
45
50
55
60
65
Na2O + K2O (wt%)
SiO2 (wt%)

measurements determine Ni and Zn abundances as well; although, these abundances proportionately are more variable across samples than are the major elements and are therefore less constrained.

The GRS global averages for a suite of elements agree well with soil averages [*Karunatillake et al.*, 2007] and the bulk estimate of the upper crust derived from them. As such, Th abundances detectable by the GRS instrument but not by lander measurements are likely also representative of the bulk upper crust [*Taylor et al.*, 2006a,b]. After renormalization to a S-, Cl-, H_2O-, and meteoritic-free composition (leading to an 12% relative increase in abundance after renormalization), the GRS derived global Th average is 0.70 ppm. Th and U show similarly incompatible behavior and do not fractionate during most igneous processes. The Th/U is well-determined to be approximately 3.8 for most planetary bodies and this ratio agrees with chemical analyses of the SNC meteorites least affected by terrestrial weathering processes [*McLennan*, 2003], yielding a U abundance of 0.18 ppm. If these derived upper crustal abundances of K, Th, and U - the heat-producing, radiogenic elements (HPE) – represent the HPE distribution throughout the entire Martian crust, as much as 50% of the total budget of radiogenic heat production would be sequestered into the crust (assuming an average crustal thickness of 50 km) [*Hahn and McLennan, Chapter 4*].

McSween et al. (2009), used the GRS elemental abundance datasets, Thermal Emission Spectrometer (TES) mineralogical results, SNC chemical and mineralogical analyses and landing site soil measurements to also assess the elemental composition of the Martian crust - although the focus of *McSween at al.* (2009) is on the landing site rock

analyses instead of sediments. Their reported results generally agree with the bulk upper crustal chemistry derived in this work, although as *McSween et al.* (2009) places greater emphasis on the GRS results, which do not provide a complete list of all major element compositions, and thus they did not calculate a full bulk chemistry (nor do they make any estimates of trace element or REE abundances). Nevertheless, they also reported a generally basaltic composition with limited siliceous rocks as a main component of the crust, as we do here. Additionally, using Ca/Si-Mg/Si from the basaltic shergottites and the Ca/Si ratio determined from the GRS, they calculated a global MgO concentration of ~11.0 wt% (the GRS instrument cannot measure Mg concentrations), compared to the sediment derived MgO concentration of 9.3 wt% in this study.

Estimates for the rare earth elements are not directly constrained by soil or GRS data but some estimates can be made. If K and La are equally incompatible and do not significantly fractionate from one another during igneous processes, then a K/La ratio calculated from SNC meteorite averages should also hold for crustal abundances even though the SNCs are not a chemical representative of the Martian crust. This yields a K/La of 750 and a La concentration of 5.3 ppm. *Norman* (1999, 2002), described a method for using mass balances and the Nd isotopes of the basaltic shergottites to calculate additional REE abundances (reviewed in *Taylor and McLennan*, 2009). This method yields a Nd abundance of about 8.9 ppm; and, with a corresponding Sm/Nd of 0.25-0.27, a Sm abundance of 2.40 ppm. Also, with a La/Yb of about 3, the crustal composition of Yb is 1.78 ppm [*Norman*, 1999, 2002]. Taken together, these ratios and abundances describe a REE pattern slightly enriched in the lighter elements. *Taylor and McLennan* (2009), observe that typically there are no Eu anomalies present in SNC REE

patterns and concluded no such anomaly exists in the Martian crust or mantle. Lastly, Y ppm typically holds a value between Dy and Ho on a primitive mantle (PM)-normalized calculation – about 6.6xPM or a 17.8 ppm crustal composition or Y for a PM concentration of 2.7 ppm [*Wänke and Dreibus*, 1988]. Other elemental concentrations are very poorly constrained and are of less importance for understanding the chemical evolution of the crust and will not be speculated on here.

Figure 3 plots incompatible element abundances for Martian and terrestrial crustal types normalized to their respective primitive mantles (PM). For Mars, the primitive mantle of *Wänke and Dreibus* (1988) is adopted and for the Earth, the crustal values summarized in *Rudnick and Gao* (2003) and PM values of *Taylor* (2001) are used. The Martian crustal estimate from this study is characterized by slight enrichment in incompatible elements ranging from about 12.5xPM for Th to about 5.2xPM for Lu. In comparison, both the terrestrial upper continental crust and bulk continental crust are considerably more enriched in this suite of incompatible elements.

Although the Martian crust is significantly less enriched in incompatible elements than the terrestrial crust, it represents a proportionally larger mass of the total planet compared to the crust and mantle of Earth. As such, the Martian crust, although only modestly enriched in incompatible elements compared to the primitive mantle contains a larger proportion of the total planetary chemical budget for these elements than does the terrestrial crust. Most terrestrial crust-mantle compositional models lead to approximately 25-35% of the most incompatible elements being differentiated into the continental and oceanic crusts [*Taylor and McLennan*, 1985, 2009; *Rudnick and Gao*, 2003; *McLennan et*

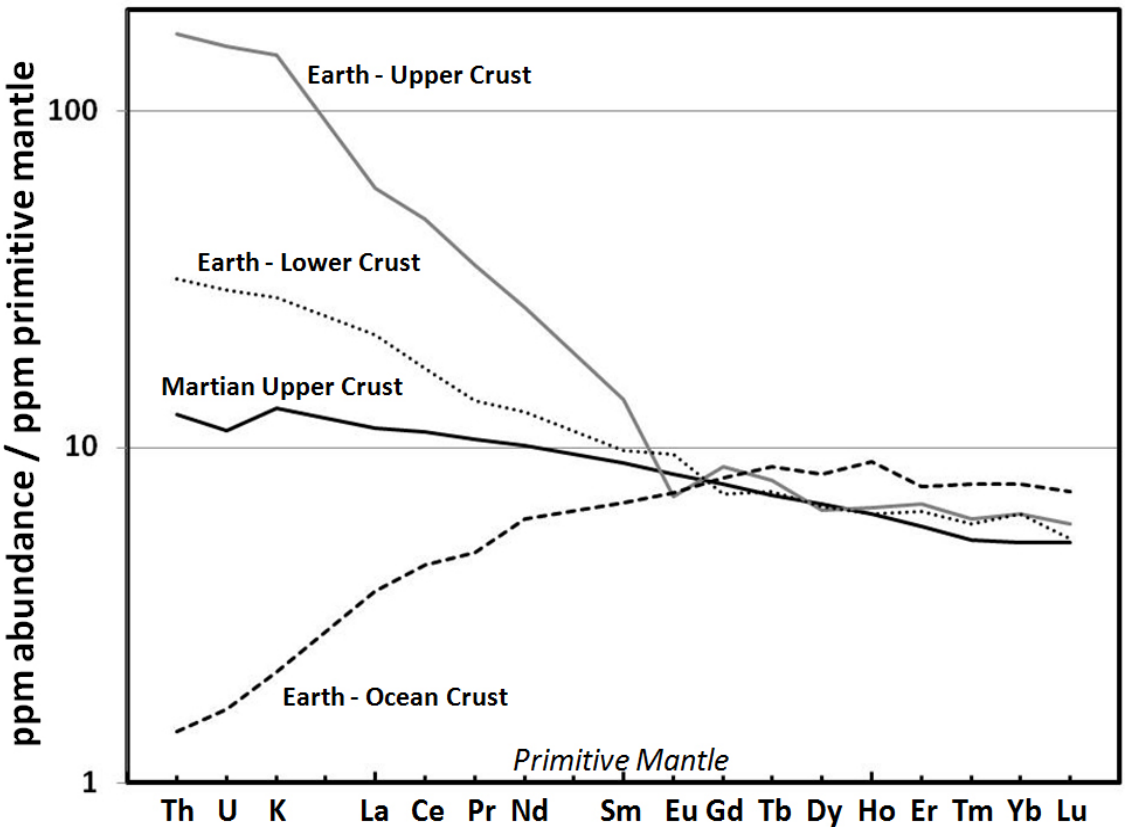

Figure 3. Incompatible elements abundances for the Martian upper crust vs. major terrestrial crustal types plotted with respect to their respective primitive mantle models [*Wänke and Dreibus*, 1988; *Taylor and McLennan*, 1985; *Taylor*, 2001]. Mars is enriched in this suite of elements, although significantly less so than the terrestrial crust (upper, lower, or total). However, while terrestrial crust is more enriched, the Martian crust is a proportionally much larger chemical reservoir with respect to total planetary mass. As such, the Martian crust sequesters a great percentage of the total planetary incompatible element budget – especially important for the HPEs K, Th, and U where as much as 50% of radiogenic heating sources could reside in the crust.

al., 2006]. This study suggests that approximately 50% or more of the incompatible elements have differentiated into the Martian crusts and consequently, the crust-mantle system of Mars is significantly more differentiated that that of the Earth.

(4.1.) Homogeneous Martian sediments vs. diverse terrestrial compositions: Loose homogeneous soils and dust are a dominant product of the Martian sedimentary cycle and formed within a weathering environment fundamentally different from the terrestrial model. While more chemically distinct sedimentary products such as evaporites, clays, and carbonates have been detected at small, areally discrete locations, their overall volumetric significance as a sedimentary component compared to general soils has yet to be established. **Figure 2 (top)** plots Martian soils and rocks from landing site measurements on a commonly used petrologic diagram of total alkalis versus silica. As stated, the estimate for upper crust plots squarely within the basalt field. The selected soils used for this study are also clustered within the basaltic field. Also shown are igneous rock analyses for the Spirit, Opportunity and Pathfinder landing sites and values for SNC meteorites. Although these various rock analyses undoubtedly do not represent all primary igneous end members on the Martian surface, they do represent the known surface rocks and rock types from which the loose Martian soils and dust may be derived. Martian soils plot in the middle of these various rock analysis fields and therefore represent a homogenized mixture of the various end members.

However, unlike Mars, terrestrial sediments are diverse (**Figure 2, bottom**) and highly fractionated. Aqueous alteration and the presence of an ocean on Earth create a weathering environment that functions as a very efficient engine for fractionating primary source rocks into chemically diverse sedimentary lithological end products. As such, rather than plotting in a cluster near primary source materials, the various terrestrial sediments plot in chemically distinct reservoirs far from the crustal averages. This important sedimentary fractionation in a water-rich environment and the lack of such apparent fractionation among the Martian sediments strongly suggests that the Martian surface has been principally dominated by an arid environment with limited global scale chemical alteration at least over the time represented by these soils (~3 Ga). As such, the chemistry of the Martian soils provides no support for the presence of a large amount of surface water, such as an ocean, during this time.

(4.2.) Upper Crust vs. Total Crust: While sediments provide a robust determination of the bulk chemistry of the upper Martian crust, it is still an unanswered question as to how representative the upper crust is chemically of the total Martian crust. The terrestrial crust is well established to be vertically chemically heterogeneous, with a lower continental crust of significantly different composition than the upper crust. Upper continental crust is significantly more felsic and enriched in incompatible elements (**Figure 3**) due to continuous reworking through plate tectonic processes and intra-crustal partial melting leading to the production of more evolved, differentiated lithologies. As

the Martian upper crust is basaltic, and clearly not highly evolved or differentiated, it is likely that the Martian crust as a whole is also less prone to vertical heterogeneity. Previous remote sensing spectroscopic studies suggesting large provinces of andesite or basaltic-andesite are inconclusive as purely surficial aqueous processes leading to thin mineralogical rinds and coatings could provide similar spectroscopic results without being volumetrically significant [*Bandfield et al., 2000*; *Wyatt and McSween*, 2002]. Also, an areally or volumetrically large, Si-enriched territory is neither detected by orbital GRS measurements nor evident as a Si-rich mixing component in the global average soil.

One mechanism that has been proposed on the basis of experiments that could result in a vertically heterogeneous Martian crust is by trapping of mantle-derived magmas at the base of the crust, where they fractionate prior to extraction of liquids that form surface magmas [*Nekvasil et al.*, 2009]. Depending on the magmatic water content, this could result in a cumulate layer below the Martian crust and could explain some of the distinctive chemical characteristics of the Martian meteorites. Even if such a process operated, it would give rise to less vertical lithological diversity than is present in the terrestrial continental crust. In any case, such a model remains to be tested by future measurements and any vertical heterogeneity of the Martian crust will likely remain an unresolved question until future missions return seismological data.

Nevertheless, the processes that have been most responsible for differentiating the terrestrial continental crust are not evident on Mars. Although some studies have suggested active plate tectonics very early in Martian history, there is no compelling evidence of plate tectonic for most of Martian history [*Breuer and Spohn*, 2003]. Most of

the Martian crust was in place by 4.0 Ga with many ancient terrains, such as the Northern lowlands, later subjected to resurfacing by relatively thin veneers of younger magma [*Frey*, 2002]. As such, the chemical composition of these younger, thin surfaces derived from more depleted mantle sources are almost certainly not be representative of the main volume of ancient crust. While GRS elemental abundances do vary to some extent with apparent surface age, the variation is subtle and muted (only 7-9% relative for K and Th) [*Hahn et al.*, 2007]. Finally, GRS chemical analyses of major deep crater ejecta do not show a statistically significant variation in chemistry with respect to the rest of the surface, suggesting that the underlying crust is chemically similar to the upper crust.

(5.) Summary: Most Martian soils are chemically similar representing an average "global" soil composition. Soils that show specific, chemically distinct signatures are explained through physical mixing between the average global sediment and local, chemically distinct lithological sources, such as the Fe-enriched hematite concretions at Meridiani Planum or the P-enriched Wishstone class outcrops in the Columbia Hills at Gusev Crater.

Like certain terrestrial sediments, Martian soils are derived from large source terrains and are the best chemical proxy for the composition of the upper Martian crust. Unlike terrestrial sediments, which can only provide insoluble trace element compositions of the upper continental crust, Martian soils are produced primarily through

physical weathering processes and, more similar to terrestrial glacial sediments, also preserve the major elemental chemical abundances of the source terrains from which they were derived.

This study uses carefully screened sediment chemical averages from all available lander mission data as well as orbital chemical abundances determined by the GRS instrument to derive the most comprehensive estimate for the bulk chemistry of the Martian crust to date. Average Martian crust is basaltic in composition and modestly enriched in the incompatible heat producing and light rare earth elements.

The diversity of terrestrial sediments results from an environment dominated by aqueous alteration in a water-rich environment and most notably the presence of an ocean which fractionates sediments into diverse chemical compositions. In contrast, the primary sedimentary products of the Martian weathering environment over at least the past 3 billion years are the Martian soils and dust that are relatively unaltered, homogeneous and chemically indistinct. This lack of compositional diversity strongly suggests an arid weathering environment with little long-term surface water and with sedimentary process dominated by physical mixing. Global sedimentary chemistry, derived from either the in situ lander experiments or GRS global elemental mapping do not appear to support the presence of a Martian ocean during this time.

Martian sediments only sample the upper crust and, as such, chemical composition estimates may not be applicable to the total Martian crust. However, unlike the terrestrial continental crust, the Martian crust is unlikely to be nearly as chemically heterogeneous vertically and there is no definitive evidence of the geologic processes that

lead to widespread continental crustal differentiation on Earth. As such, the estimate for the chemical composition of the upper Martian crust likely also represents a reasonable first-order approximation to the chemical composition of the bulk total crust.

Supplementary Table 1. Summary of screened soil samples used for determining the global average soil composition.

Mission	*Sample Name*	*Na_2O*	*MgO*	*Al_2O_3*	*SiO_2*	*P_2O_5*	*SO_3*	*Cl*	*K_2O*	*CaO*	*TiO_2*	*Cr_2O_3*	*MnO*	*FeO*
Spirit	Gusev_Soil	2.76	8.34	9.89	46.32	0.87	6.61	0.78	0.48	6.36	0.86	0.31	0.33	15.96
Spirit	Crest_morning	2.80	8.67	10.02	46.05	0.80	5.26	0.69	0.43	6.98	0.72	0.49	0.36	16.61
Spirit	Track	2.88	8.45	10.30	46.77	0.81	5.00	0.60	0.45	6.52	0.91	0.41	0.36	16.45
Spirit	Rampflats	2.54	8.69	10.23	46.30	0.87	6.06	0.71	0.43	6.58	0.77	0.26	0.29	16.16
Spirit	Angelflats	3.09	8.59	9.96	45.51	0.78	6.19	0.78	0.48	6.69	0.68	0.38	0.30	16.48
Spirit	Grandeflats	3.13	8.41	10.05	45.98	0.86	6.33	0.73	0.44	6.32	0.89	0.33	0.34	16.09
Spirit	Road Cut_Floor3_	2.44	8.90	9.83	46.17	0.68	6.11	0.69	0.38	6.14	1.00	0.43	0.34	16.77
Spirit	Road Cut_WallMIonl	2.65	8.77	9.96	46.13	0.73	5.69	0.77	0.37	6.24	1.02	0.40	0.35	16.77
Spirit	Sugar_T1	3.18	8.47	9.67	45.63	0.83	6.10	0.80	0.41	6.60	0.81	0.37	0.34	16.68
Spirit	SugarLoafFlats_soi	3.20	8.57	9.86	45.94	0.81	6.76	0.84	0.47	6.04	0.83	0.31	0.31	15.91
Spirit	Gobi1_soil	2.91	8.25	9.56	45.01	0.91	7.61	0.88	0.49	6.17	0.89	0.31	0.31	16.55
Spirit	Serpent_Scuffed	2.89	8.86	10.12	46.71	0.66	4.39	0.54	0.40	6.57	0.94	0.46	0.36	17.02
Spirit	Bear_Island	3.12	9.54	10.38	46.60	0.88	4.57	0.58	0.84	5.86	0.80	0.32	0.31	16.05
Spirit	Bitterrootflats_flats1	3.01	8.43	9.68	46.35	0.79	6.67	0.72	0.44	6.45	0.89	0.32	0.34	15.82
Spirit	Bighole_Mayfly_surface	3.10	8.39	9.92	46.13	0.88	6.37	0.79	0.47	6.07	1.00	0.37	0.31	16.08
Spirit	Bighole_RS2	2.51	9.19	9.06	43.69	0.80	9.13	1.00	0.35	5.74	0.87	0.36	0.34	16.84
Spirit	Bighole_Trico	2.47	9.04	9.08	44.23	0.74	8.37	1.00	0.34	5.86	0.89	0.43	0.34	17.08
Spirit	Owens_soil_Track	3.07	8.41	10.65	47.01	0.95	5.45	0.63	0.47	6.38	0.88	0.33	0.28	15.41
Spirit	Calibrationsoil	3.20	8.49	11.12	48.29	0.83	4.11	0.53	0.44	6.45	0.77	0.33	0.31	15.00
Spirit	EileenDean	0.92	16.46	5.60	49.95	0.65	3.05	1.88	0.43	3.61	0.47	0.54	0.21	16.02
Spirit	EileenDean2	1.79	15.05	6.56	49.11	0.68	3.23	1.44	0.41	4.03	0.54	0.52	0.27	16.15
Spirit	Accelerator_Soil	3.06	8.15	10.02	46.25	0.83	6.40	0.77	0.45	6.50	0.96	0.29	0.32	15.87
Spirit	Santa_Anita_trench_surface	3.04	8.73	10.71	46.96	0.77	4.67	0.54	0.42	6.27	0.89	0.42	0.34	16.13
Spirit	PumpkinPie_Track	3.14	8.92	10.43	46.55	0.79	4.39	0.50	0.37	6.28	0.87	0.44	0.37	16.82

Mission	*Sample Name*	*Na_2O*	*MgO*	*Al_2O_3*	*SiO_2*	*P_2O_5*	*SO_3*	*Cl*	*K_2O*	*CaO*	*TiO_2*	*Cr_2O_3*	*MnO*	*FeO*
Spirit	Boroughs_Mills_bottom	2.36	9.82	8.47	41.36	0.71	11.19	0.68	0.35	5.77	0.90	0.39	0.36	17.53
Spirit	Boroughs_Hellskitchen_side	2.53	10.48	7.85	39.25	0.80	14.06	0.73	0.36	5.76	0.85	0.39	0.34	16.50
Spirit	ArthurCHarmon	3.54	8.49	9.60	44.82	0.98	7.47	0.86	0.46	6.12	0.88	0.29	0.31	16.05
Spirit	Shredded_dark4_soil	3.25	8.73	11.29	47.82	0.75	4.10	0.52	0.45	6.31	0.67	0.36	0.33	15.30
Spirit	Goldfinger_Jaws_soil	3.31	9.84	10.08	46.30	0.80	5.26	0.62	0.41	5.90	0.73	0.27	0.32	16.02
Spirit	Kilmary_soil	2.77	8.42	9.59	45.72	0.87	7.50	0.94	0.49	5.88	0.84	0.28	0.31	16.25
Spirit	Greeneyes_soilTG	2.91	8.39	9.85	45.81	0.95	7.44	0.85	0.44	6.17	0.82	0.21	0.29	15.75
Spirit	Disturbance_soil	3.21	8.42	10.13	46.38	0.90	6.65	0.76	0.46	6.22	0.84	0.29	0.30	15.34
Spirit	Tofurkey_disturbedsoil	3.37	8.68	10.31	46.90	0.88	5.82	0.68	0.43	6.24	0.84	0.31	0.32	15.12
Spirit	Penny_dist_soil	3.45	9.42	10.63	46.75	0.84	4.80	0.57	0.40	6.20	0.70	0.33	0.31	15.48
Spirit	Paso_dark	3.24	8.74	10.44	46.11	0.96	5.68	0.55	0.39	6.25	0.89	0.38	0.33	15.94
Spirit	Bell	3.09	8.58	10.78	47.72	0.83	4.75	0.55	0.43	6.37	0.83	0.34	0.33	15.31
Spirit	Whymper	3.18	8.61	9.79	45.43	0.93	7.42	0.83	0.45	6.08	0.86	0.26	0.31	15.72
Spirit	Lambert_Couzy_mod	3.17	8.84	9.86	45.63	0.93	6.95	0.76	0.43	6.10	0.87	0.28	0.31	15.78
Spirit	ElDorado_Scuff_Shadow	3.01	11.31	10.74	46.91	0.81	3.06	0.38	0.31	6.10	0.62	0.32	0.31	15.96
Spirit	ElDorado_Scuff_Edgar	3.17	10.04	10.93	47.53	0.75	3.26	0.42	0.37	6.28	0.73	0.34	0.31	15.76
Spirit	Mawson	3.06	8.98	10.44	47.05	0.87	4.53	0.57	0.44	6.41	0.79	0.36	0.33	16.05
Spirit	Progress	2.87	8.14	10.30	47.23	0.97	5.52	0.64	0.48	6.50	0.87	0.34	0.32	15.73
Spirit	Progress 1 brushed	2.83	7.94	10.36	47.08	0.98	5.76	0.66	0.50	6.52	0.82	0.32	0.33	15.78
Spirit	Progress 2 brushed	3.34	8.51	10.47	46.59	0.90	5.43	0.61	0.44	6.31	0.82	0.34	0.32	15.80
Opportunity	Tarmac	1.83	7.58	9.26	46.34	0.83	4.99	0.63	0.47	7.31	1.04	0.45	0.37	18.80
Opportunity	Hematite_Slope_Hema2	2.12	7.50	8.59	42.66	0.81	4.77	0.68	0.43	6.13	0.78	0.30	0.31	24.80
Opportunity	Trench_floor	2.03	7.49	9.21	45.88	0.80	6.96	0.70	0.49	6.69	1.13	0.40	0.35	17.72
Opportunity	Trench_sidewall	1.92	7.42	9.05	45.29	0.75	5.69	0.59	0.45	6.72	1.24	0.46	0.36	19.90
Opportunity	MontBlanc_LeHauches	2.24	7.63	9.22	45.34	0.94	7.34	0.79	0.48	6.59	1.02	0.33	0.34	17.62
Opportunity	BeagleBurrow_Trench	2.34	7.59	9.88	47.14	0.74	4.57	0.49	0.41	6.73	1.23	0.48	0.36	17.89

Mission	*Sample Name*	*Na_2O*	*MgO*	*Al_2O_3*	*SiO_2*	*P_2O_5*	*SO_3*	*Cl*	*K_2O*	*CaO*	*TiO_2*	*Cr_2O_3*	*MnO*	*FeO*
Opportunity	Scuff_Nougat	2.35	7.78	9.25	45.63	0.86	5.81	0.60	0.44	6.70	1.09	0.46	0.38	18.52
Opportunity	Alicante	1.31	6.75	7.83	41.94	0.88	4.58	0.62	0.48	6.67	0.87	0.42	0.30	27.25
Opportunity	Alicante2	1.97	7.38	7.88	42.36	0.79	4.50	0.60	0.44	6.64	0.89	0.46	0.37	25.59
Opportunity	HillTop_Wilson	2.38	7.61	9.21	45.33	0.87	7.12	0.84	0.51	6.73	0.97	0.36	0.37	17.56
Opportunity	Soil_Millstone_Dahlia	2.40	7.14	10.04	47.66	0.81	5.19	0.64	0.55	7.32	0.85	0.34	0.39	16.60
Opportunity	Auk_RAT	2.39	6.90	10.41	48.83	0.84	4.56	0.58	0.59	7.38	0.85	0.28	0.35	15.93
Opportunity	Rocknest_void_soil	2.39	7.65	9.59	46.70	0.85	4.62	0.59	0.48	7.30	0.91	0.45	0.40	17.98
Opportunity	Left_of_peanut_TrenchFloor	2.20	7.13	8.98	44.55	0.84	6.58	0.50	0.45	6.75	1.17	0.46	0.39	19.85
Opportunity	Scuff_Srcuffy	2.11	7.20	9.10	45.27	0.88	6.06	0.52	0.44	6.87	1.25	0.46	0.39	19.31
Opportunity	Mobarek_undist_soil	2.21	6.75	8.19	41.55	0.86	5.21	0.67	0.42	6.17	0.85	0.33	0.33	26.32
Opportunity	NorthDune_New_Track	2.32	7.05	8.74	44.78	0.91	6.59	0.72	0.47	7.06	1.02	0.41	0.39	19.44
Opportunity	Purgatory_Track2.	2.13	7.02	8.70	44.15	0.94	7.36	0.76	0.50	6.75	1.05	0.35	0.37	19.79
Opportunity	Fala	2.17	7.46	8.89	45.57	0.85	4.95	0.62	0.47	7.50	0.94	0.46	0.43	19.60
Opportunity	Alamogordo_Creek	2.23	6.48	8.25	41.15	0.79	5.43	0.65	0.41	5.98	0.77	0.30	0.30	27.14
Opportunity	Westport	2.30	7.18	8.84	45.15	0.91	6.72	0.65	0.47	6.87	1.14	0.41	0.36	18.87
Opportunity	Powells_Brother	2.33	7.25	8.49	42.97	0.85	5.79	0.60	0.41	6.57	1.12	0.47	0.39	22.62
Pathfinder	A-4	0.94	9.95	8.31	42.57	1.83	7.49	0.57	0.60	6.02	1.00	0.15	0.77	19.59
Pathfinder	A-5	1.08	9.29	8.69	40.85	1.60	6.49	0.55	0.52	6.58	0.83	0.44	0.39	23.02
Pathfinder	A-10	1.35	8.13	7.37	41.71	0.92	6.99	0.53	0.45	6.86	1.00	0.29	0.52	23.59
Pathfinder	A-15	0.94	7.46	7.56	43.85	0.92	5.99	0.54	0.87	6.58	1.17	0.29	0.52	23.02
Pathfinder	A-8	1.62	7.30	9.07	45.56	0.69	6.24	0.55	0.78	8.12	1.17	0.00	0.52	18.73

Chapter 3: Mars Odyssey Gamma-Ray Spectrometer Elemental Abundances and Apparent Relative Surface Age: Implications for Martian Crustal Evolution

Published in the Journal of Geophysical Research - Planets

B. C. Hahn, S. M. McLennan, G. J. Taylor, W. V. Boynton, J. M. Dohm, M. J. Finch, D. K. Hamara, D. M. Janes, S. Karunatillake, J. M. Keller, K. E. Kerry, R. M. S. Williams, and The Odyssey GRS Science Team, Mars Odyssey Gamma-Ray Spectrometer Elemental Abundances and Apparent Relative Surface Age: Implications for Martian Crustal Evolution, J. Geophys. Res. 112 (2007) doi:10.1029/2006JE002821.

(1.) Introduction: Secular changes in element abundances, as recorded in age-specific provinces, reveal significant information about planetary crustal formation and evolution. Therefore, relating the age of a planetary crust to its chemical composition is of great geologic importance. On Earth, it is a relatively straightforward task to sample geographically wide-spread crustal materials, perform detailed chemical analyses of major and trace element abundances, and reliably date samples through a variety of field and laboratory methods. The relationship of age to chemistry has been used for decades to better understand the nature and evolution of the continental and oceanic crust [*Armstrong*, 1981; *Taylor and McLennan*, 1985], the reservoirs of heat producing elements throughout the crust-mantle system [*Taylor*, 2001], magmatic resurfacing histories [*Jerram and Widdowson*, 2005], sedimentary processes and recycling [*Veizer and Jansen*, 1985; *Taylor and McLennan*, 1985], plate tectonics [*Richter et al.*, 1992],

and a wide array of other important geologic questions. Likewise, lunar samples returned by the Apollo missions, while more limited in sampling diversity, have been well characterized for chemistry and age and consequently, lunar science has made great progress (see reviews in *Taylor,* 1982, 2001). However, for planetary bodies outside the immediate terrestrial neighborhood, these data are difficult to obtain. Here, we report the first results of correlations between element abundances determined by GRS and the apparent relative surface age of the Martian upper crust as determined by existing geologic mapping and explore some of the potential implications for better understanding Martian crustal evolution and global scale surficial processes.

For Mars, chemical and isotopic analyses, including radiometric dating [*Jagoutz*, 1991; *Nyquist et al.,* 2001], have been performed on the Martian meteorites (SNCs) – the only samples available for detailed laboratory study. However, it is a matter of ongoing discussion as to how fully and accurately the SNCs represent the overall Martian crust [*McSween,* 2002]. Additionally, we cannot determine their geographic origin with any confidence, as they were removed by impact from unknown Martian provinces and attempts to constrain these locations using orbital data have been only partially successful [*Hamilton et al.*, 2003]. The successful lander missions (Viking 1 and 2, Pathfinder, and Spirit and Opportunity), measured in situ elemental chemistry for a variety of surface samples; however, no landers have been equipped with instrumentation necessary for determining rock ages. Also, the landing sites do not entirely represent geographic diversity, both due to the limited number of successful landings (five, to date) and an understandable site selection bias that favors specific scientific goals and a maximum probability of safe landing [*Golombek et al.*, 1997; *Golombek et al.*, 2003]. Previous

works have examined relationships between variations in Martian crustal mineralogy derived from the Thermal Emission Spectrometer (TES) and crustal age [*McSween et al.*, 2003].

The 2001 Mars Odyssey orbiter began its primary mapping mission in February 2002 and the Gamma Subsystem of the Gamma-Ray Spectrometer (GRS) instrument suite has since determined statistically reliable elemental abundance maps for H, Si, Fe, Cl, K, and Th (see reviews of instrumentation and summary of primary scientific results in *Boynton et al.,* 2004 and *Boynton et al.,* 2007, respectively). The GRS instrument is limited by a surface penetration depth of only a few tens of centimeters and an areally extensive resolution footprint of approximately 270 km radius. However, while being an inherently low-resolution observational tool, GRS has provided the first detailed global maps of elemental abundances, has proven to be especially valuable for distinguishing the broad-scale variations in elemental compositions across the Martian surface [*Karunatillake et al.*, 2006; *Keller et al.*, 2006; *Taylor et al.*, 2006a,b], and is largely unencumbered by thin surface dust layers that obscure most other spectroscopic methods (e.g., TES – on board the Mars Global Surveyor; THEMIS – on board the 2001 Mars Odyssey; and OMEGA – on board the European Space Agency's Mars Express spacecraft [*Christensen et al.*, 2001, 2003; *Bibring et al.*, 2005]). The GRS elemental abundance maps provide the chemical data used in this study.

Currently, the only means of constraining Martian surface age is through the analysis of crater count statistics, cross-cutting relationships, and stratigraphic position. Since the first orbital images of the Martian surface were returned, the USGS and other

groups have been reliably mapping the geology of Mars. We have adapted a suite of these maps [*Scott and Tanaka*, 1986; *Greeley and Guest,* 1987; *Tanaka and Scott*, 1987] to create a global apparent relative surface age dataset of the Martian surface for comparison to GRS determined elemental abundances (see Methods below). Discussion continues about the uncertainties attached to relative ages derived by these methods; however, while absolute surface ages may not be well-constrained, relative ages between geologic provinces at regional scales are likely quite robust [*Dohm et al.*, 2001]. We examine chemical variations with respect to the three primary Martian age epochs from the formal stratigraphic systems devised by *Scott and Carr*, 1978: Noachian, Hesperian and Amazonian.

(2.1) Methods – GRS Elemental Abundances: Details as to the specific manner in which the GRS data have been collected, reduced, and processed can be found in *Boynton et al.*, 2007 and *Evans et al.*, 2006. Portions of this study use element abundance datasets derived from a 2-degree base map and smoothed with a 10-degree arc-radius mean filter - 5-degree for K (see histograms in **Figures 3-7**). These are then re-binned into datasets consisting of 5ºx5º bins, which have good counting statistics and provide the large number of bins necessary for improving the confidence of our age specific averages.

Note that individual 5ºx5º bins for each chemical dataset are not entirely computationally independent of one another due to significant spatial autocorrelation effects inherent to all non-imaging remote sensing observations and the data reduction methods used specifically for generating GRS datasets [*Haining*, 2003]. The 10-degree arc-radius mean filter (5-degree for K), areally large spacecraft footprint, neutron capture correction factors (for Cl, Fe, and H), and neutron scatter correction factors (for Si) [*Boynton et al.*, 2007; *Evans et al.*, 2006], coupled with inherent compositional variation in the Martian regolith, all cause some degree of autocorrelation between geographically proximate 5ºx5º bins.

Element abundance averages for each primary age category (**Figure 1** and see Methods – Apparent Relative Surface Age below) and the associated standard errors of the calculated means were produced by summing the individual spectra acquired over the geographic range covered by a particular age category (**Table 1**). All errors reported throughout this text, table, and figures are the calculated standard errors of the reported means. The summation process for regional data is reviewed in *Boynton et al.*, 2007 and *Evans et al.*, 2006. Gamma ray spectra were collected during the primary mapping period from June 8, 2002 through April 3, 2005.

Hydrogen abundance increases dramatically pole-ward of about ±45º latitude corresponding to the inferred higher concentration of near-surface ice. H concentrations have a strong influence on the correction techniques used for determining Fe, Si and Cl abundances. To compensate, we have excluded Fe, Si, H and Cl data pole-ward of ~45º-60º latitude in both hemispheres using a cut-off based upon water equivalent hydrogen

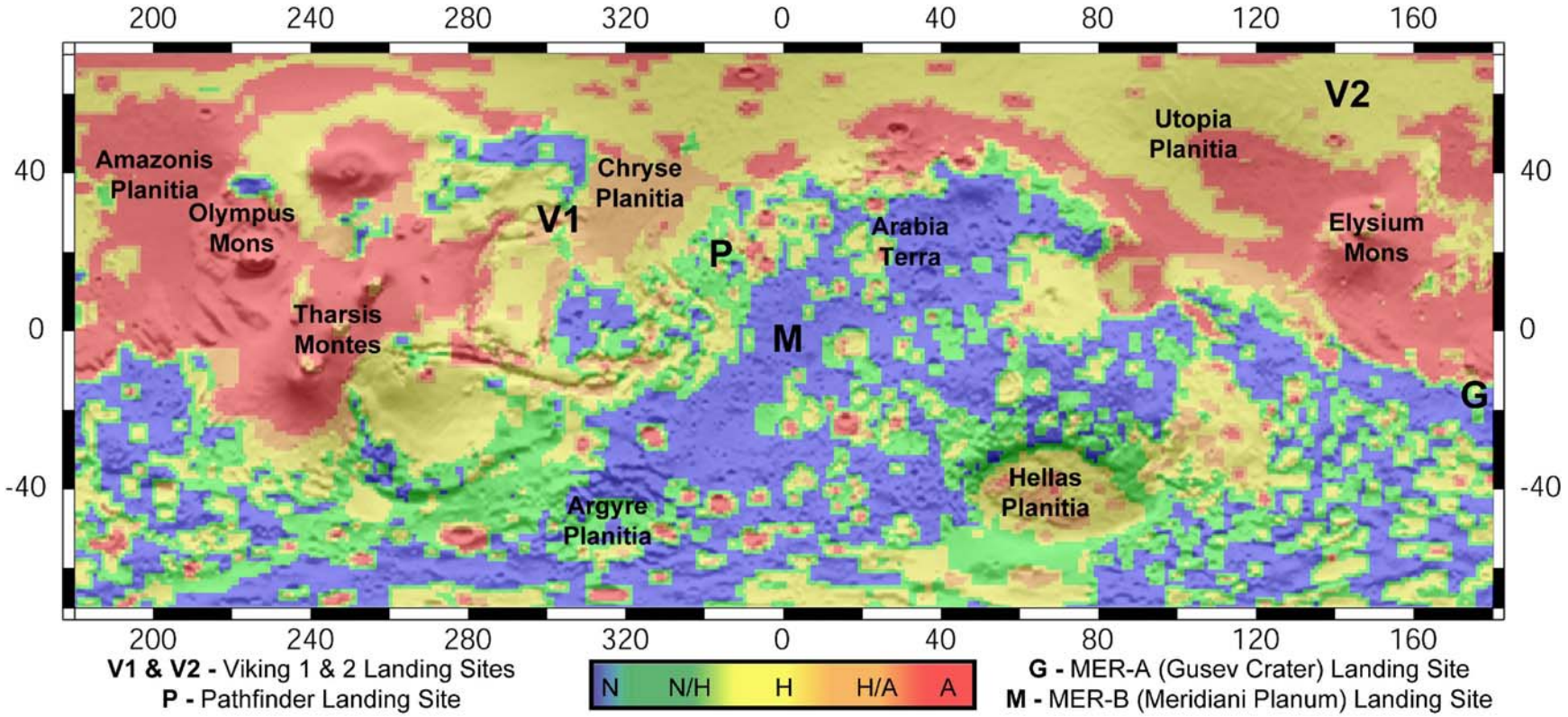

Figure 1. Global map of apparent surface age used in this study. Ages were adapted from the USGS Martian Geologic Investigations Series I-1802 (ABC) [*Scott and Tanaka*, 1986; *Greeley and Guest,* 1987; *Tanaka and Scott*, 1987], and binned into a 1ºx1º resolution grid. Three primary age categories have been assigned (N-Noachian, H-Hesperian, and A-Amazonian); as well as two, less areally extensive transitional age categories (N/H-Noachian-Hesperian and H/A-Hesperian-Amazonian). A gray-scale MOLA topography base-map and labels of prominent geologic features and landing sites have been provided for reference. For comparison to GRS element abundance datasets, we further re-binned age data to a 5ºx5º resolution.

Table 1. Summary of Elemental Abundance Averages for Each Primary Apparent Relative Age

	Age Category		
Element	Noachian	Hesperian	Amazonian
K			
ppm ± S.E.	3260 ± 10	3340 ± 20	3070 ± 20
Number of bins[a]	867	660	470
Number of spectra	1,029,800	758,700	582,450
Th			
ppm ± S.E.	0.65 ± 0.02	0.64 ± 0.03	0.61 ± 0.03
Number of bins[a]	867	660	470
Number of spectra	1,029,800	758,700	582,450
Fe			
wt% ± S.E.	13.6 ± 0.8	15.3 ± 0.9	14.6 ± 0.9
Number of bins[b]	657	377	341
Number of spectra	905,500	481,810	453,180
Cl			
wt% ± S.E.	0.48 ± 0.03	0.47 ± 0.03	0.56 ± 0.04
Number of bins[b]	657	377	341
Number of spectra	905,500	481,810	453,180
Si			
wt% ± S.E.	20.7 ± 0.3	20.9 ± 0.4	20.1 ± 0.4
Number of bins[b]	657	377	341
Number of spectra	905,500	481,810	453,180
H_2O			
wt% ± S.E.	4.04 ± 0.24	3.49 ± 0.23	4.14 ± 0.27
Number of bins[b]	657	377	341
Number of spectra	905,500	481,810	453,180

[a]Data set includes all bins up to ±75° latitude to exclude pole-ward values that show dilution effects from large amounts of near-surface water ice.

[b]Data set includes all bins up to the "H-mask" (Boynton et al., submitted manuscript, 2006) to exclude pole-ward values where correction techniques for Fe, Cl, and Si are influenced by high H abundances.

concentration – the H-mask – described in *Boynton et al.*, 2007. Elemental concentrations for K and Th are not similarly affected by H concentrations and, therefore, K and Th abundance maps extend to both poles and the standard H-mask is not warranted. However, extremely high concentrations of water ice (e.g., very near the poles) dilute these elemental signatures. Consequently, data for K and Th have been excluded in the pole-ward regions (75º+ latitude in both hemispheres). Choosing a slightly different polar cutoff for these data (±5º) does not significantly change our values or uncertainties.

(2.2.) Methods – Apparent Relative Surface Age: Geologic maps provide, in a historical context, fundamental syntheses of information of the materials, landforms, and processes that characterize planetary surfaces and the basis for assessing the geologic, paleohydrologic, and paleoclimatic histories at local to global scales. For Mars, the first global geologic map was produced on a photo-mosaic of 1-2 km/pixel Mariner 9 images at 1:25,000,000 scale [*Scott and Carr*, 1978]. Next, Viking orbiter data with resolutions of 100 to 300 m/pixel were used to generate a series of three 1:15,000,000-scale maps, covering the western [*Scott and Tanaka*, 1986], eastern [*Greeley and Guest*, 1987], and polar [*Tanaka and Scott*, 1987] regions, all of which have been the standards for Mars geology [*Tanaka*, 1986]. Stratigraphic relations and morphologic characteristics form the basis for geologic unit assignment for these maps, while relative ages were assigned based on crater densities and stratigraphic and structural relations. We digitized print versions of these maps into a 1ºx1º data grid. Each cell was assigned the single geologic

unit that represented the most areally dominant mapping unit within that particular cell. As examples, a 1ºx1º cell areally composed of approximately 75% Hesperian Ridged Plains Material (**Hr**) and 25% Amazonian Knobby Plains Material (**Apk**) would be assigned the **Hr** designation, as would a 1ºx1º cell composed of approximately 45% **Hr**, 30% **Apk,** and 25% Noachian plateau ridged unit (**Nplr**), since the **Hr** unit is dominant in both these cases. Cells were then given a specific age value based on the assigned geologic unit – Noachian, Hesperian, or Amazonian (**Figure 1**). The USGS geologic maps include some geologic units that do not conform to a single stratigraphic system, straddling system boundaries. For example, the **HNu** unit of the "Plateau and high plains assemblage – Undivided Material" for the Eastern Equatorial region of Mars [*Greeley and Guest*, 1987] is shown to straddle both the Noachian and Hesperian systems. Such single units that cross the boundary between two stratigraphic systems were assigned to one of two intermediate age categories: Noachian-Hesperian and Hesperian-Amazonian. No geologic units on any maps considered in this study cross into all three primary stratigraphic systems. For the Martian surface, these apparent age categories areally represent approximately: 37% Noachian; <7% Noachian-Hesperian; 27% Hesperian; <4% Hesperian-Amazonian; and 25% Amazonian – in general agreement with areal extents determined in previous studies [*Tanaka et al.*, 1992; *Nimmo and Tanaka,* 2005].

For comparison with the GRS element abundance datasets and to conform more closely with the instrument's areally-large ~5º-radius footprint, our apparent relative age dataset was further smoothed by re-binning cells into aggregate 5ºx5º bins. This was done by assigning to the 5ºx5º bin the most areally dominant apparent relative surface age for

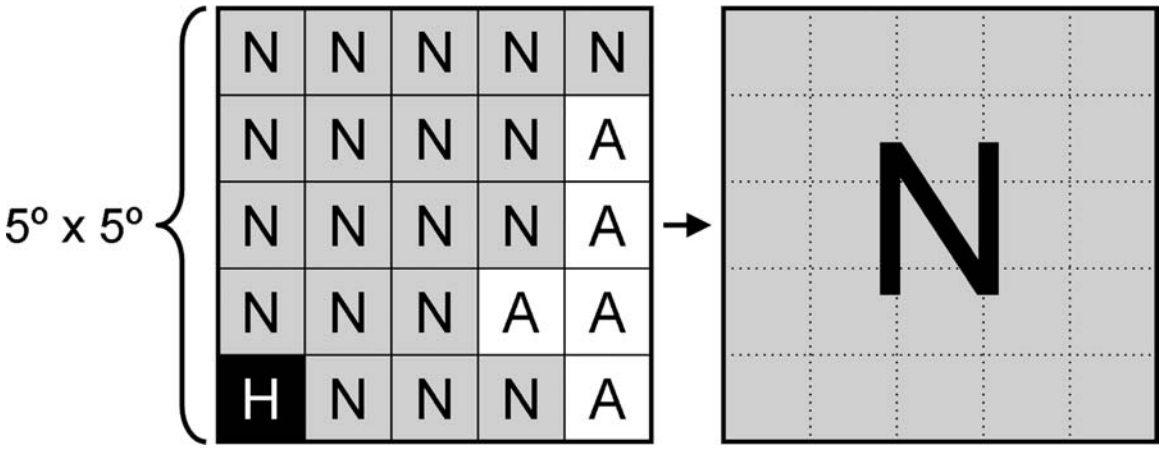

Figure 2. Graphical representation of the method used for assigning a single apparent surface age (N-Noachian; H-Hesperian; A-Amazonian) to a 5ºx5º bin from the originally compiled 1ºx1º resolution map. The age assigned to a 5ºx5º bin is the mode of the included cells, thus the dominant age category for the 5ºx5º bin. On average, the dominant age category for a given 5ºx5º bin makes up approximately 80% of the areal extent of the included cells.

the included 1ºx1º cells (illustrated in **Figure 2**). While most 5ºx5º bins were not entirely age-homogeneous, on average, the age category considered dominant for any given 5ºx5º bin made up more than 80% of the areal extent of the included cells. Further, re-binning the apparent relative surface age dataset into a 5ºx5º resolution does not significantly change the areal distributions of our age categories. Age categories must be areally large to allow for higher confidence of our calculated averages and thus for the purposes of this study, we have excluded the less areally extensive intermediate age categories (i.e., Noachian-Hesperian and Hesperian-Amazonian). The remaining bins were grouped into the three main age regions (Noachian, Hesperian, and Amazonian) and elemental abundances were determined by summing all gamma-ray spectra collected for the individual regions. We do not subdivide these three main regions (e.g., Early Hesperian and Late Hesperian) both because we wish to keep our age provinces areally large and finer age resolutions based on crater count statistics and geologic interpretation add additional uncertainty (See Section 2.3 below). Areally small, geographically separate outliers of the three main age regions (<10ºx10º) were excluded from the spectral summation process as they are smaller than the instrument footprint and would therefore suffer interference from adjoining regions.

Note that we refer to these assigned values as "apparent relative" surface ages. Absolute dating of the Martian surface is not yet possible and the surface ages used in this study are based on the geologic mapping investigations noted above. See below for discussion of several factors that may mask the "true" age of certain geologic provinces and the implications for interpreting age-concentration relationships.

(2.3.) Methods - Sources of Uncertainty for Apparent Surface Age: The only means presently available for constraining Martian surface age is through the analysis of crater count statistics, cross-cutting relationships, and stratigraphic position. Carefully crafted global geologic mapping based upon long established stratigraphic relationships were produced first from Mariner 9 orbital photography and later from Viking Orbiter images [see reviews in *Tanaka*, 1986; *Tanaka et al*., 1992]. While the dataset used in this study is derived from the USGS global maps of *Scott and Tanaka*, 1986, *Greeley and Guest,* 1987, and *Tanaka and Scott*, 1987, even more recent, highly detailed geologic mapping was made possible by images returned from the Mars Orbital Camera (MOC) with support from the Mars Orbital Laser Altimeter (MOLA) aboard the Mars Global Surveyor (MSG) spacecraft [*Tanaka et al*., 2003, 2005]. Thus, it is generally agreed that the stratigraphy of Mars, especially in terms of broad-scale geologic features, is well understood.

However, assigning reliable dates for stratigraphic units is more problematic. While crater counting has proven reliable for lunar surface dating, there are considerable sources of uncertainty and caveats when applied to the more-complex Martian surface [*Ivanov*, 2001; *Hartmann and Neukum*, 2001; *Neukum et al*., 2001]. Alone, isochrons determined by crater count statistics can only provide rough age estimates – perhaps as imprecise as 1 Gyr or more [*Hartmann and Neukum*, 2001]. Crater counts, along with stratigraphic superposition and cross-cutting relationships, can yield relative surface ages between geologic provinces [*Scott and Tanaka*, 1986; *Dohm et al.*, 2001, 2005; *Anderson et al.*, 2001]; however, ground sampling and isotopic dating are required to determine an absolute surface age. For the Moon, datable samples were returned via the Apollo

missions (see reviews in *Taylor*, 1982, 2001), but no such sample return has yet been attempted for Mars. As a result, although relative surface ages between Martian provinces are believed to be well-constrained, absolute ages are uncertain.

Discussions continue about additional sources of uncertainty regarding crater count derived surface ages. Martian isochrons are calibrated using similar, better-constrained, isochrons determined for the Moon. However, fundamental differences affecting the formation, evolution, and bombardment history of these very different terrestrial planets require the application of a number of correction factors. Also, possible secondary craters (those formed by ejecta from an initial primary impact) and non-impact craters, particularly at smaller diameters, may skew count statistics [*McEwen et al.*, 2005]. There are certain morphological indicators that allow secondaries to largely be screened out; however, debate persists in their effect on calculated surface ages.

Recent work using high-resolution topography has shown definitive evidence of "ghost" cratering or "quasi-circular depressions" – large impacts lacking obvious morphological distinctions, but preserved as subtle, circular topographic basins [*Frey at al*., 2002; *Buczkowski et al.*, 2005]. A new population of heretofore unknown large impacts has important implications for apparent surface ages and it has been suggested that the Northern Plains may in fact be an ancient surface covered by a thin, relatively young veneer. Additionally, and perhaps most significantly, the crater count method of dating implicitly assumes the long-term preservation of the crater record on the surface. The Moon's surface records a pristine cratering history. However, it is becoming increasing clear that Mars has long experienced a complex history of weathering and

resurfacing and its crater record is far from pristine. For example, detailed geologic mapping investigations have reported that geologic processes such as erosion, deposition, lava emplacement, and tectonism have caused degraded and/or embayed craters, as well as inflections and roll-offs in crater-size distributions due to crater obliteration [*Scott and Tanaka*, 1986; *Dohm et al.*, 2001; *Tanaka et al.,* 2006]. In addition, orbital and lander observations suggest crater infilling and degradation is common [*Hartmann and Neukum*, 2001; *Golombek et al.*, 2006; *Grant et al.*, 2006].

Despite these possible problems with surface dating, general stratigraphy and the relative formation ages of significant features on Mars such as distinct geologic provinces will be improved upon in the future, but not totally revised. Current understanding of absolute ages and durations of geologic periods, however, may be significantly modified (e.g., there may be more Periods, Epochs, Eras, etc.) [*Fairén and Dohm*, 2004]. Since rocks have not been returned from known locations for absolute age determinations, geologic mapping combined with assessment of mission data, which includes impact crater statistics, cross-cutting relationships, and stratigraphic positions, collectively afford best estimates of the relative ages of geologic provinces. Therefore, the areal binning of our apparent surface age categories is considered robust and the GRS-based chemical averages for these categories are unlikely to change significantly with future work.

(2.4.) Methods – Statistical Approach Comparing Means: The summation of gamma-ray spectra provides mean elemental abundances and the associated standard errors of those means for each age category. We performed z-statistic tests when comparing differences in element abundance averages across age categories. Abundances for all elements conform to an approximately standard normal distribution. Comparisons that reject the null hypothesis are reported as "statistically significant" with the respective confidence interval for that determination. Note however, that small statistically significant differences in calculated means may not be significant or interpretable geologically (see Discussion below).

The large number of bins used in this study allow for good precision for the calculated averages. Note, that there exists the possibility that future data calibration issues for the GRS instrument may revise certain global element abundance maps. However, while any such revisions may affect absolute abundances, relative abundances are less likely to change. Therefore, the relative elemental abundance differences across stratigraphic systems reported here are likely quite robust.

(3.) Results: The sections below detail the reported results of this study. Results by element are subdivided into three categories: elements with decreasing abundance with younger surface age (K and Th); elements with increasing abundance with younger surface age (Fe and Cl); and elements that show no statistically reliable relation with surface age or a relationship not readily explained by geologic controls (Si and H). A compiled summary of results is provided in **Table 1** along with listings of the included number of 5ºx5º bins used to determine the averages of each age category and the

approximate number of individual spectra used for determining regional sums. Results are also plotted in **Figures 3-7** along with histograms of the 5ºx5º bin frequency. Note that for the histograms, individual 5ºx5º bins are not of equal weight due to an areal dependence on latitude and may not properly represent age category means precisely. All errors reported are the calculated standard errors of the reported means.

(3.1.) Results – K and Th: As discussed in *Taylor et al.,* 2006a,b, K and Th elemental abundances are not uniform across the Martian surface. Both K and Th abundances show a subtle but significant decrease with younger apparent relative surface age (**Figures 3, 4**). K and Th abundances decrease most significantly from the Hesperian to the Amazonian age categories, with an approximate 9% decrease in K (from 3340±20 ppm to 3070±20 ppm) and 7% decrease in Th (from 0.64±0.03 ppm to 0.61±0.03 ppm). These differences in mean abundances are statistically significant (i.e., they fail the null hypothesis for a z-statistic test) at 99.9% confidence for K and 85% confidence for Th. From the Noachian to the Hesperian age categories, there is a small statistically significant increase in K abundance (from 3260±10 ppm to 3340±20 ppm) and a statistically insignificant decrease in Th (from 0.65±0.02 ppm to 0.64±0.03 ppm). The implications of these results are discussed below.

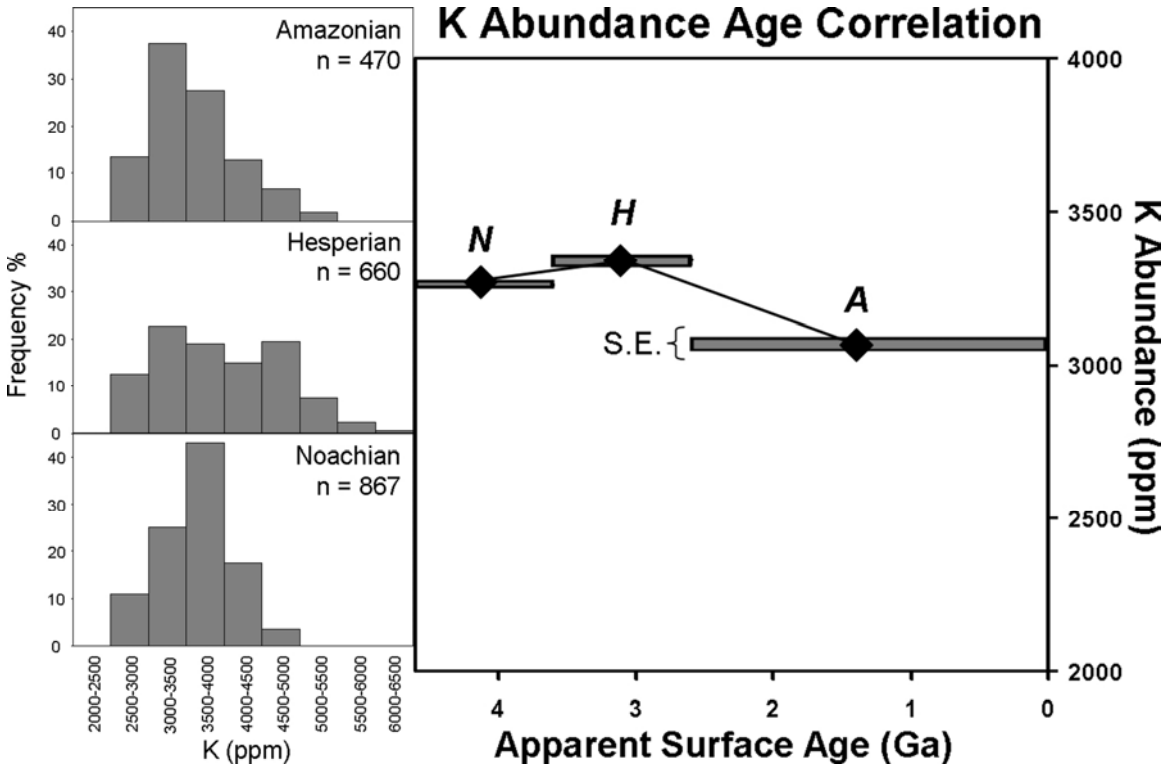

Figure 3. (left) Histograms of percentages of total 5ºx5º bins versus age category. (right) Plot of average K abundance versus apparent relative surface age with the calculated standard errors of the means represented by the thickness of the lines. The most significant feature is the 10% decrease in K abundance between the Hesperian and Amazonian age categories (age boundaries from *Hartmann*, 2005).

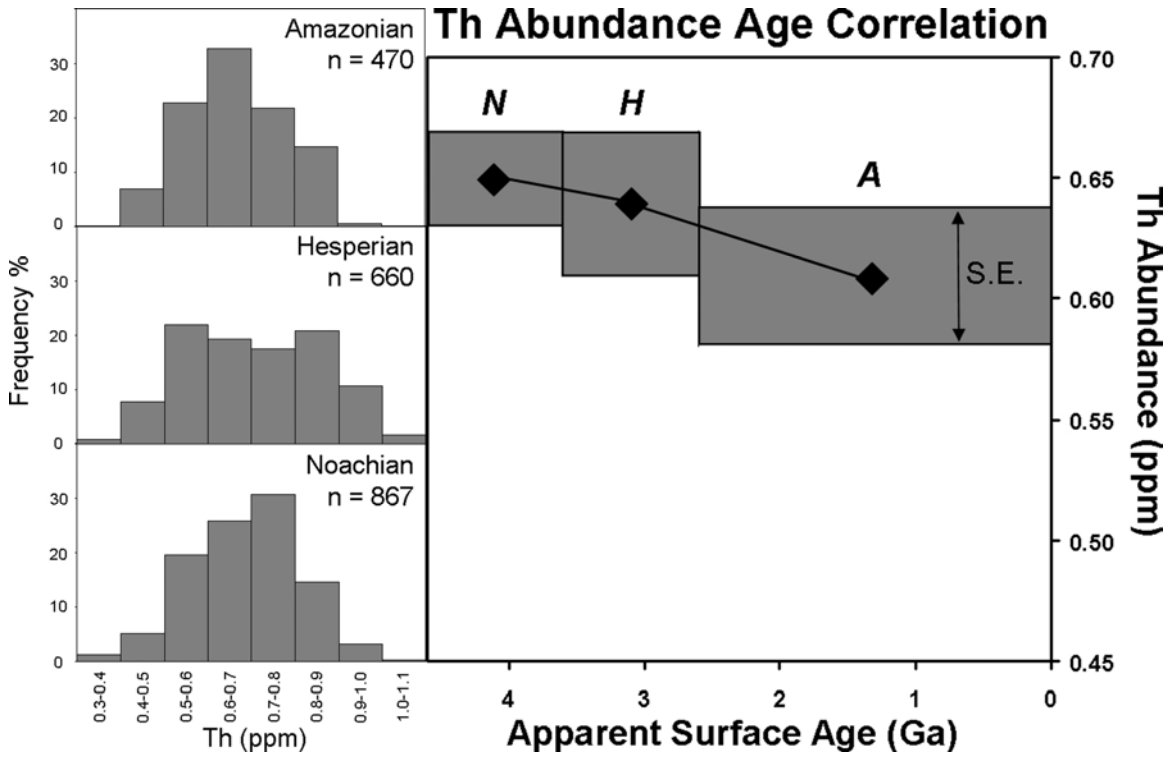

Figure 4. (left) Histograms of percentages of total 5ºx5º bins versus age category. (right) Plot of average Th abundance versus apparent relative surface age with the calculated standard errors of the means represented by the thickness of the lines. The most significant feature is the 7% decrease in Th abundance between the Hesperian and Amazonian age categories (age boundaries from *Hartmann*, 2005).

(3.2.) Results – Fe and Cl: Detailed discussions about the global distributions of Fe and Cl can be found in *Taylor et al.*, 2006b and *Keller et al.*, 2006, respectively. Both Fe and Cl abundances show a subtle but significant increase with younger relative apparent surface age (**Figure 5, 6**). Fe abundance increases most significantly from the Noachian to the Hesperian age categories, with an approximate 12% increase in Fe (from 13.6±0.8 wt% to 15.3±0.9 wt%). This difference is statistically significant (i.e., it fails the null hypothesis for a z-statistic test) at 90% confidence. From the Hesperian to the Amazonian age categories, there is a statistically insignificant decrease in Fe (from 15.3±0.9 wt% to 14.6±0.9 wt%). Cl abundances increase most significantly from the Hesperian to the Amazonian age categories, with an approximate 19% increase in Cl (from 0.47±0.03 wt% to 0.56±0.04 wt%). This difference is statistically significant (i.e., it fails the null hypothesis for a z-statistic test) at 95% confidence. From the Noachian to the Hesperian age categories, there is a very minor statistically insignificant decrease in Cl (from 0.48±0.03 wt% to 0.47±0.03 wt%). The implications of these results are discussed below.

(3.3.) Results – Si and H: There are no geologically significant relations between apparent relative surface age and Si and H element abundances. Although GRS has determined some geographic variations in Si abundance [*Boynton et al.*, 2007], the full range over which Si varies is relatively small and a correlation, if any, may be difficult to discern by this method. There are notable changes in H abundance (reported

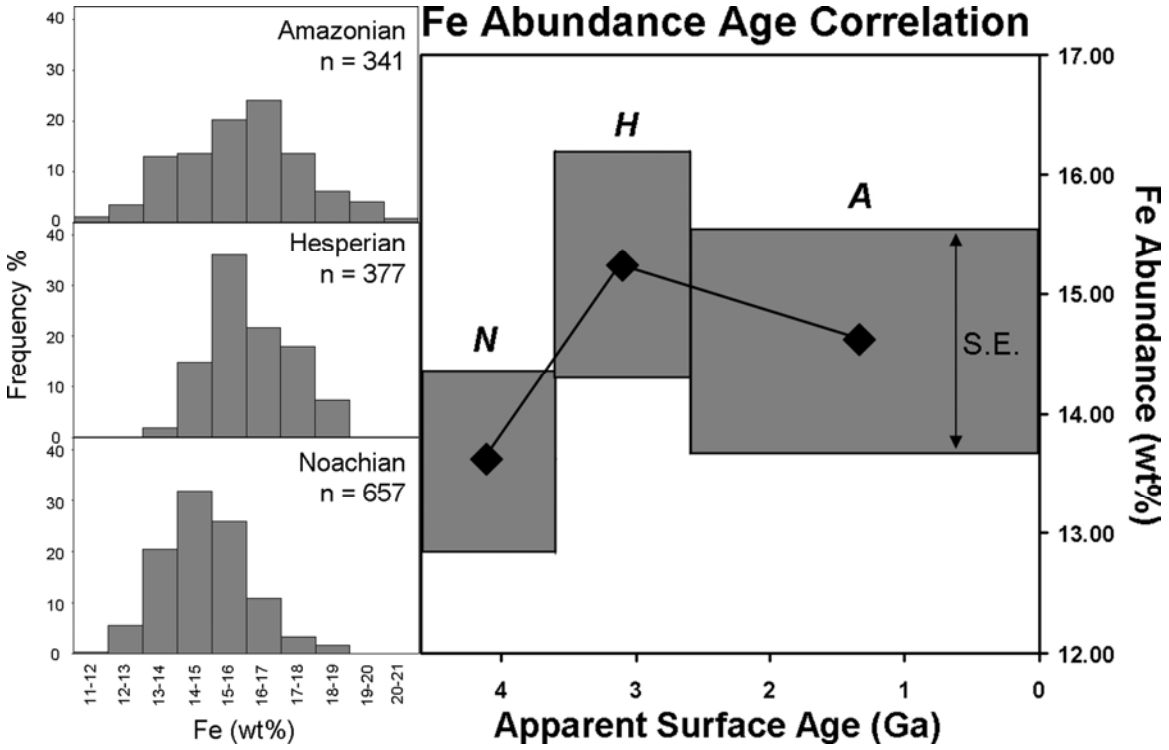

Figure 5. (left) Histograms of percentages of total 5ºx5º bins versus age category. (right) Plot of average Fe abundance versus apparent relative surface age with the calculated standard errors of the means represented by the thickness of the lines. The most significant feature is the 12% increase in Fe abundance between the Noachian and Hesperian age categories (age boundaries from *Hartmann*, 2005).

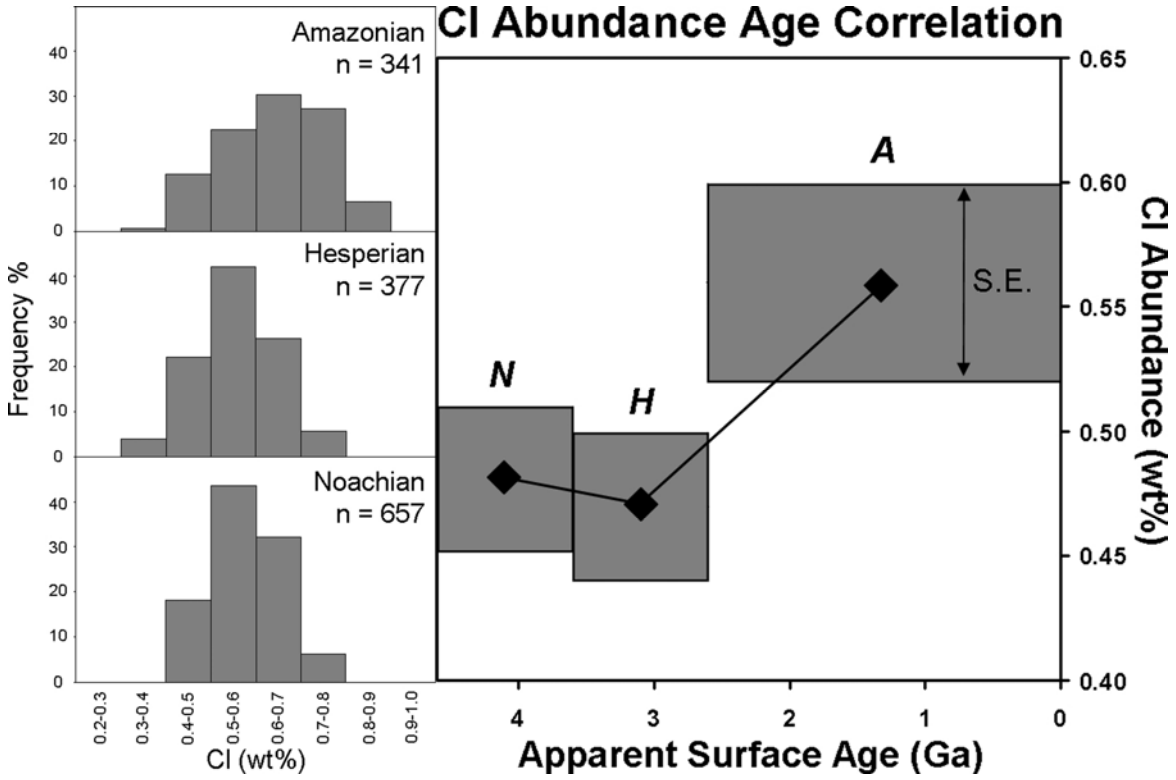

Figure 6. (left) Histograms of percentages of total 5ºx5º bins versus age category. (right) Plot of average Cl abundance versus apparent relative surface age with the calculated standard errors of the means represented by the thickness of the lines. The most significant feature is the 19% increase in Cl abundance between the Hesperian and Amazonian age categories (age boundaries from *Hartmann*, 2005).

as water equivalent hydrogen; **Figure 7**) across age categories. However, we interpret these changes as coincidental and not representative of a geologic process. The observed H age-relationship is more a function of the latitudinal distribution of the age regions. Among other factors [*Baker*, 2001], H (in the form of water ice or hydrated mineral phases) has likely been transferred to different regions of the planet by a variable climate caused primarily by changes in planetary obliquity [*Kieffer and Zent*, 1992]. As obliquity varies on a timescale shorter than the stratigraphic systems defined for this study, a true H versus surface age relation is not expected.

(4.1.) Discussion – Secular variations in K and Th: As detailed in *Taylor et al.*, 2006a and *Karunatillake et al.*, 2006, K, Th and the K/Th ratio do vary across the surface of Mars. K and Th are positively correlated with each other and the areal fraction of Surface type 2 determined with the Mars Global Surveyor Thermal Emission Spectrometer (MGS-TES) [*Karunatillake et al.*, 2006]. However, GRS observations show that these variations are muted when compared to K and Th variations measured on Earth or in lunar samples. The K/Th ratio varies subtly; primarily a response to varying Th and broadly independent of K abundance which has less variance globally. Although outlier regions exist, for most measured elements, GRS observations generally show Mars to be a fairly chemically homogeneous planet compared to the Earth or the Moon, despite obvious geologic and morphologic surface diversity. This lack of chemical diversity has been attributed to a number of factors. First, the long-term, broad-scale

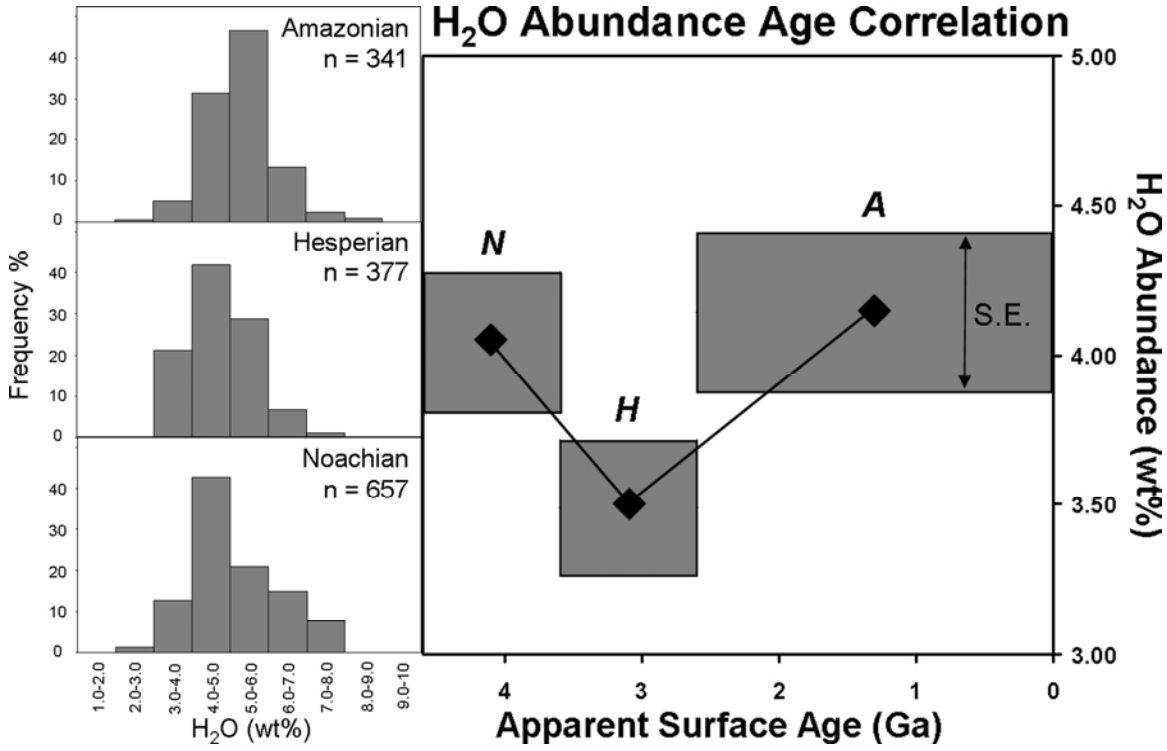

Figure 7. (left) Histograms of percentages of total 5ºx5º bins versus age category. (right) Plot of average H (as water equivalent hydrogen) abundance versus apparent relative surface age with the calculated standard errors of the means represented by the thickness of the lines. While H abundance does change across age categories, it is unlikely that such variation represents a true geologic process (age boundaries from *Hartmann*, 2005).

mixing of Martian surface components through a combination of aqueous and eolian transport and impact gardening would buffer chemical variations [*Greeley et al.*, 1992; *Hartmann et al.*, 2001]. Also, the absence of active plate tectonic processes prevents the continued recycling, fractionation, and evolution of crustal material typically seen in subduction and collision zone environments on Earth. The global component of air fall dust transported around the planet by frequent dust storm events also contributes to surface chemical homogeneity [*Kahn et al.*, 1992]. This GRS globally-observed, chemical homogeneity supports landing site chemical analyses of Martian soils. While some concentration variation in certain elements can be found among landing sites (e.g., K concentrations), in situ measured soils are generally indistinct despite considerable geographic landing site separation [*Clark et al.*, 1982; *Brückner et al.*, 2003; *Gellert et al.*, 2004; *Rieder et al.*, 2004; *Yen et al.*, 2005] and most variation is believed to result from local chemical contributions. Consequently, observed secular variations in elemental abundances are expected to be subtle.

The K and Th abundances and their relationship provide a great deal of information about the formation and evolution of a terrestrial planetary body. Both are highly incompatible large ion lithophile elements. Because of their similar high degree of incompatibility, they generally do not fractionate significantly from one another through purely igneous processes. However, while K is a moderately volatile element, Th is refractory. Therefore, the K/Th ratio has been used as a proxy for the loss of volatile elements during planetary accretion and early development [*Taylor*, 2001; *McLennan*, 2003]. Previous models of bulk planetary composition are supported by the GRS derived globally averaged K/Th ratio suggesting Mars is a volatile rich planet compared to Earth

(i.e., crustal K/Th of ~5500 for Mars; crustal K/Th of ~2600 for Earth) [*Taylor et al.*, 2006b; *McLennan* 2003; *Wänke and Dreibus*, 1988, 1994].

A variety of models predict various and differing behavior for the suite of incompatible elements during early planetary evolution [*Borg and Draper*, 2003; *Elkins-Tanton et al.*, 2003, 2005]. The possible overturn of an early magma ocean may complicate lateral and vertical variations in elemental abundances throughout the mantle and subsequently, the crust. However, it is generally believed that incompatible elements such as K and Th ($D<<1$) are preferentially sequestered into crustal materials during planetary differentiation and mantle melting; resulting in an enriched crust and depleted upper mantle [*McLennan*, 2003]. Consequently, planetary crusts derived from older, primitive mantle sources will have chemical compositions highly enriched in incompatible elements. Conversely, younger crusts are usually produced from more evolved upper mantle sources already stripped of much of their incompatible element budget. Therefore, younger crustal material will typically be depleted in incompatible elements relative to older crusts, but still enriched with respect to the bulk planet. This expected secular variation in K and Th is supported by GRS observations (**Figures 3, 4**). Variations in both K and Th abundance between the Noachian and Hesperian age categories are small (with the Th variation between these age categories being statistically insignificant – see Results, above) and we do not interpret any geologic significance. However, there is a statistically significant variation across the Hesperian and Amazonian age boundary with abundances decreasing for both elements. This result, showing both elements decreasing together with younger ages, broadly supports the hypothesis of a primarily igneous origin as the cause of K and Th variations, with

younger crustal terrains derived from a more depleted mantle rock source.

It has been suggested that K and Th variations could be due to aqueous weathering and transport and it has been further noted that K and Th can and do fractionate from one another through certain aqueous alteration processes [*Taylor et al.*, 2006a]. In most terrestrial weathering situations, K is more mobile than Th and a vigorous alteration environment should result in a significant variation in the K/Th ratio – a result not generally observed by the GRS instrument. However, several recent studies have suggested that the Martian surface, far from experiencing generally neutral pH conditions such as those found most frequently on Earth, may have been subjected to highly acidic weathering environments in the past [*Tosca et al.*, 2004, 2005; *Hurowitz et al.*, 2006]. Although the solution chemistry is complex and will not be described here; typically, Th becomes far more soluble with decreasing pH [*Taylor et al.*, 2006a]. This implies that for an acidic Mars, the K/Th ratio may be less affected in response to aqueous processes. Note however, that the most likely result of broad scale aqueous alteration could be the gradual depletion of K and Th in the older terrains. Noachian and Hesperian provinces would have been subjected to both a longer duration of aqueous alteration, as well as the more active weathering environment reported for the Noachian [*Fairén et al.*, 2003]. The secular variations observed in this study (higher K and Th concentrations in older terrains) therefore do not readily support aqueous alteration as the sole cause of global variations in K and Th (**Figure 3, 4**). While regional exceptions exist, planet-wide, weathering is likely a second order cause of K and Th variation (see also *Karunatillake et al.*, 2006).

As has been reported elsewhere, the K and Th concentrations for almost all the SNC meteorite samples for which reliable chemical analyses have been performed are substantially lower than the global and regional abundance averages reported by GRS [*Meyer*, 2003; *Taylor et al*., 2006a,b]. Clearly then, at least for the heat producing elements, the SNCs are not representative of the bulk crust or any specific age province and appear to be derived from an extremely depleted source. K and Th abundances for SNCs with published age analyses are plotted on **Figure 8** along with system age abundance averages. By Martian standards, the SNC meteorites are quite young. All, save one, have isotopically determined ages younger than 1.3 Ga (the ancient ALH84001 is the sole reliable exception – dated between 4.5 and 4.0 Ga) [*Jagoutz,* 1991; *Nyquist et al.,* 2001].

(4.2.) Discussion – Secular variations in Fe: *Boynton et al.*, 2007 and *Taylor et al.*, 2006b described the Fe abundance distribution across the Martian surface. They report a Fe concentration dichotomy, with higher Fe abundances in the northern lowlands and lower Fe abundances in the southern highlands. Also, GRS observations are consistent with previous models of bulk chemistry suggesting Mars is a Fe-rich planet compared to Earth [*Wänke and Dreibus*, 1992].

The Fe concentration difference between the Hesperian and Amazonian age categories is statistically insignificant; however, there is a statistically significant increase

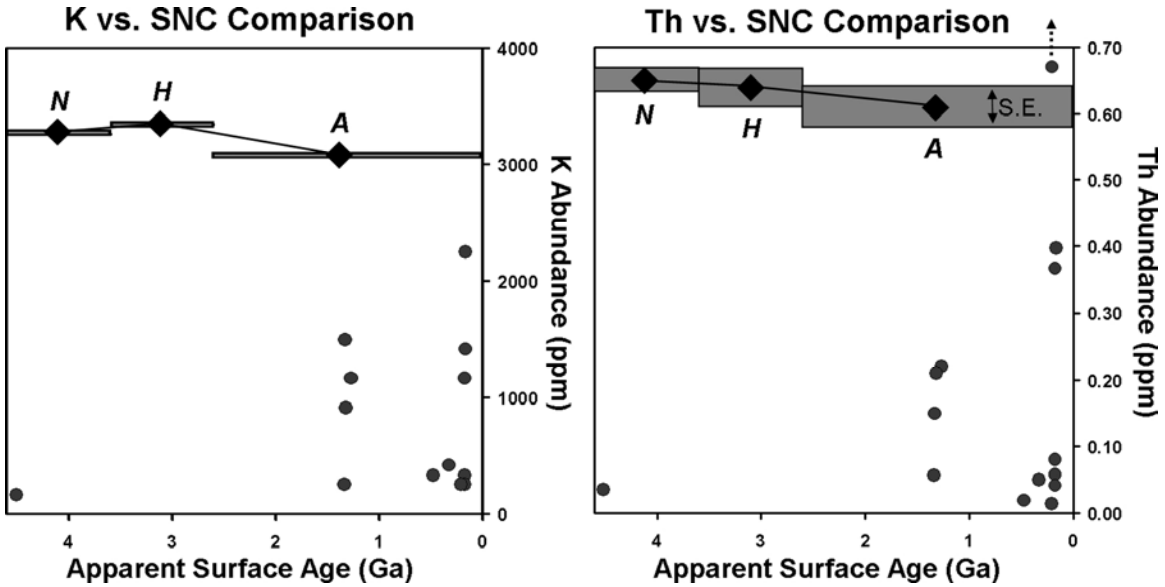

Figure 8. Expanded plots of K and Th abundances with the calculated standard errors of the means represented by the thickness of the lines as well as elemental abundances of the Martian meteorites with reliable published dating and chemical analyses (see compilation in *Meyer*, 2003). Note that irrespective of the ages of the meteorites, all (save the Los Angeles meteorite with a non-characteristic high Th value) show significantly lower K and Th abundances than the broad-scale averages reported by the GRS instrument (age boundaries from *Hartmann*, 2005).

in Fe concentration of ~12% between the Noachian and Hesperian (**Figure 5**). Is this change a result of primary igneous origin, surface alteration processes, or a combination of both? Our analysis of apparent surface age versus Fe abundance is ambiguous. The Fe increase, while statistically real, cannot be reliably attributed to a purely igneous or sedimentary process.

A relatively modest compositional change in a parent magma could explain the Fe abundance different between the Noachian and Hesperian surfaces. However, in younger, more evolved magmas, we would expect a positive correlation between Fe and Si. As mentioned above, Si appears largely invariant across age categories and id a correlation exists, it may be too subtle to discern by this method. As such, a purely igneous origin for such a subtle secular variation in Fe abundance may be unrelated to larger issues regarding planetary crustal evolution.

The processes affecting the weathering and mobility of Fe on the Martian surface are very different from those normally seen in terrestrial environments. As mentioned above, Mars may have experienced a far more acidic weathering environment [*Tosca et al.*, 2004, 2005; *Hurowitz et al.*, 2006], implying several complications for iron solubility and secondary mineralogy. With lower pH and increased solubility, Fe could have been leached out of the southern highlands and been deposited onto the northern lowlands through long-term, aqueous transport [*Scott et al.*, 1995; *Fairén et al.*, 2003, 2004; *Tanaka et al.*, 2003, 2005]. However, global transport of the kind necessary to cause broad-scale stripping of Fe from the Southern Highlands would have required significant long-term circulation of water no matter what the pH of the interacting fluids. Evidence

of periodic surface water flow on the Martian surface has been documented [*Fairén et al.*, 2003]; however, it is unclear if even a warmer, wetter ancient Mars was hydrological active enough to support such a vigorous aqueous transport system. Also, acidic weathering and transport of Fe and subsequent enrichment in younger terrains is not directly supported by the K and Th data which shows the opposite and argues against leaching.

(4.3.) Discussion – Secular variations in Cl: *Keller et al.*, 2006 documents the GRS-determined heterogeneous distribution of Cl across the Martian surface and explores in detail the geologic mechanisms that might lead to such a variation. They report that Cl abundances vary by a factor greater than 4 and conclude that Cl and H have the strongest positive correlation of any elements studied and Cl correlates negatively with Si abundance and thermal inertia. Cl accounts for a significant amount of the observed total global chemical variation [*Gasnault*, 2006]. Geologic processes that may govern the Cl surface distribution include: eolian transport of a Cl-rich globally ubiquitous dust component; aqueous leaching and transport of Cl through groundwater systems; acid-fog reactions of volcanic materials; and hydrothermal alteration. In light of the degree of Cl variation, it is likely that combinations of these processes were at work across the Martian surface in various regions and at various times. The strong correlation between Cl and H implies that Cl is involved in the Martian hydrologic cycle. Furthermore, a region of anomalously elevated chlorine centered over Medusa Fossae

records a long-lived history of magmatism, tectonism, and paleohydrologic activity which is reported to be often linked in space and time [*Keller et al.*, 2006]. Also, in situ soil measurements by lander and rover missions generally show correlations between Cl and S concentrations, again supporting a hydrologic control [*Wang et al.*, 2006].

Of the elements studied, Cl shows the strongest variation with apparent surface age (**Figure 6**). Amazonian terrains have an average Cl abundance ~19% higher than older terrains. The very small decrease in Cl abundance between the Noachian and Hesperian age categories is not statistically significant. The marked increase in Cl with younger surfaces provides support for a number of hypotheses, although no process can be uniquely determined as the primary cause of the age correlation and combinations of processes are likely. Younger terrains with more recent active volcanism would likely be a significant source of Cl in the near-surface environment, whereas ancient, more heavily weathered surfaces may have been stripped over time of their Cl through aqueous processes prevalent during warmer and wetter periods of Martian history.

To put Cl age category abundances in context with other observations, **Figure 9** shows the Cl abundance averages for each age category in relation to average Cl concentrations in soils measured by the successful lander missions – Viking 1, Pathfinder, Spirit, and Opportunity [*Clark et al.*, 1982; *Brückner et al.*, 2003; *Gellert et al.*, 2004; *Rieder et al.*, 2004]. Also plotted is the Cl concentration for the average Gusev Plains basalt derived from samples that have been abraded by the Spirit Rock Abrasion Tool (RAT) and thus presumably represents an igneous composition without surface alteration effects [*Gellert et al.*, 2005]. Note that Cl concentrations for all soil averages

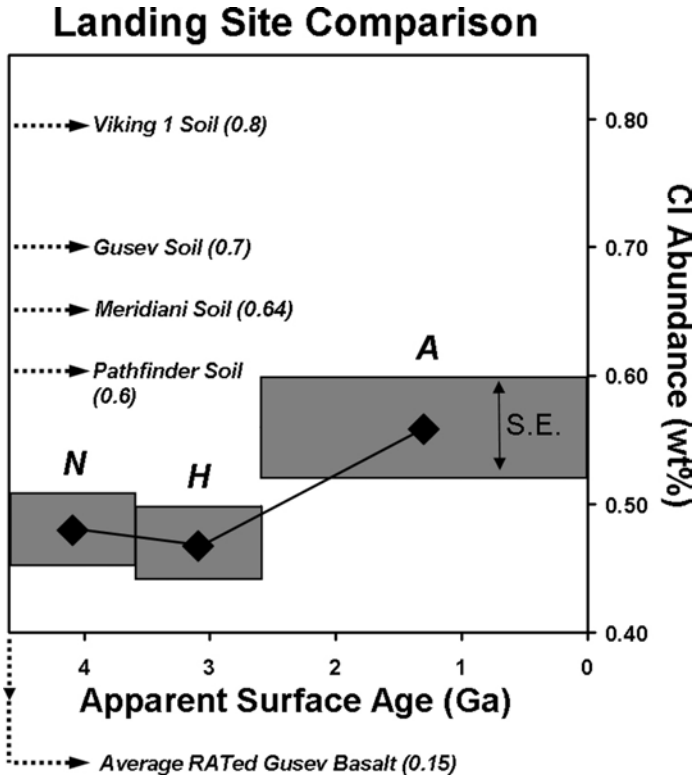

Figure 9. Expanded plot including average soil Cl abundances from landing site analyses. Note that irrespective of the age category, all landing site average soil abundances plot above the broad-scale averages reported by the GRS instrument. Also plotted below, the Cl abundance for average Gusev Plains basalts determined from in situ APXS measurements of rocks abraded by the Spirit Rock Abrasion Tool (RAT) [*Clark et al.*, 1982; *Brückner et al.*, 2003; *Gellert et al.*, 2004; *Rieder et al.*, 2004].

are higher than any of the age category averages, while the average Gusev Plains basalt plots significantly lower than the age category averages.

We expect Cl measurements for soils to be generally higher than GRS averages. First, the areally large resolution footprint of the GRS instruments and superior penetration depth of tens of centimeters measures a mixture of both soils and rocks (generally Cl-poor) [*Keller et al.*, 2006]. Also, the Spirit and Opportunity rovers have observed concentrations of subsurface salts in the uppermost soil layers [*Haskin et al.*, 2005; *Clark et al.*, 2005; *Wang et al.*, 2006]. The GRS penetration depth is deeper than the sampling depths of all surface soil or trench observation on any lander or rover to date. Landers may be preferentially sampling salt-rich soils, yielding higher measured Cl concentrations. To achieve a Cl concentration on the order of the age category averages only requires an approximate 0.5 wt% addition of a Cl-bearing salt (e.g., halite) to an average Gusev Plains basalt starting composition. The ~19% difference in Cl abundance averages between the older and younger age categories (0.47-0.48 wt% for Noachian and Hesperian; 0.56 wt% for Amazonian) can be achieved with the addition of only ~0.1-0.2 wt% of a Cl-bearing salt phase. Note also the Martian landing site selection bias which maximizes the probability of locating signs of liquid surface water. As Cl and H (in the form of hydrated mineral phases or sub-surface ice) show strong positive correlations, it is probable that landing sites selected for water enrichment will also be enriched in Cl.

(5.) Summary: The data reported and analyzed here support several important conclusions about the nature of the Martian crust. K and Th abundances both show significant decreases with younger apparent surface age. Although weathering and broad-scale transport in an acidic environment could cause some of the variation in these elemental abundances, the age relationship suggests an igneous origin. Younger resurfacing magmas were likely derived from a more evolved, depleted mantle source when compared to the older terrains derived from a more primitive mantle. All abundance averages for all age categories are higher than those determined for the SNC meteorites suggesting that, in this respect, the SNCs are not representative of the bulk Martian crust. Fe abundances show an increase with younger apparent surface age. However, the cause of this increase cannot be uniquely interpreted as igneous, alteration and weathering, or a combination of both. In a generally acidic Martian surface environment, Fe would be far more mobile than in typical terrestrial weathering scenarios. Alternately, a relatively modest change in primary igneous magma composition could lead to the abundance increase seen in the GRS data. Cl abundances increase with younger surface age, possibly the result of volcanic activity in younger provinces and the leaching of Cl from older, weathered terrains. The involvement of Cl in the Martian hydrologic cycle is supported by the close correlation between GRS determined Cl and H abundances. The global Cl averages determined for all age categories are lower than average soil compositions sampled at landing sites. However, given the site selection bias of landed missions and the disparate sampling depths of GRS versus in situ lander observations, higher Cl in individual measured soils is not unexpected. No statistically or geologically significant correlation was found between

elemental abundance and apparent surface age for Si or H, nor was a correlation expected as Si varies little over the planet and H re-distribution occurs at faster timescales.

While this study examines the relationships between Martian crustal chemistry and apparent surface age, uncertainties in both datasets allow us to make only first order observations. Surface samples, with well determined laboratory analyzed dating will help constrain the absolute ages of geologic provinces on Mars. With improving counting statistics, other elemental datasets may become available. For example, regional data for U can help constrain the K/Th system, and maps of S would greatly improve our understanding of the global weathering environment.

Chapter 4: Martian Surface Heat Production and Crustal Heat Flow from Mars Odyssey Gamma-Ray Spectrometry

To Be Submitted to Geophysical Research Letters

B. C. Hahn, S. M. McLennan, and E. C. Klein

(1) Introduction: Martian thermal state and evolution depend principally on the heat-producing element (HPE) distributions in the planet's crust and mantle, specifically the incompatible radiogenic isotopes of K, Th, and U. Normally these elements are preferentially sequestered into a planet's crust during differentiation [*Taylor and McLennan*, 2009], and this is especially true for Mars, which possesses a thick and mostly ancient crust that is proportionally large with respect to the planet's total volume. The Gamma-Ray Spectrometer (GRS) instrument on board the 2001 Mars Odyssey spacecraft can detect all three of these elements and has been used to map the K and Th abundances across nearly the entire Martian surface [*Boynton et al.*, 2007]. Here we present the first detailed Martian surface heat production and crustal heat flow maps based on unambiguous orbital geochemical measurements that show significant geographic variation in the crustal thermal reservoir. As the crust is a repository for approximately 50% of the radiogenic elements on Mars, these models provide important, directly measurable constraints on Martian thermal behavior. These results are valuable for better understanding Martian geodynamics, crust-mantle evolution, the cryosphere,

formation and history of geologic provinces, and many other varied applications. Our calculations show considerable geographic and temporal variations in crustal heat flow, and demonstrate the existence of anomalous heat flow provinces.

Orbital GRS data are of lower spatial resolution than most other orbital remote sensing instruments and, accordingly, are best suited for global or large, regional-scale studies, rather than detailed, local analyses of geographically small features and landforms. Elemental abundance data for K and Th have been compiled into smoothed maps with 5°x5° per pixel resolution [*Boynton et al.*, 2007; *Taylor et al.*, 2006a,b]. At this time, it is not possible to generate a useful map of U abundances at comparable resolution (due to low U concentrations). Fifty percent of incident photons collected by the GRS are from a footprint of 440 km diameter. The penetration depth is on the order of a few tens of centimeters, depending on the density of the underlying material (see *Boynton et al.*, for technical specifications). Data spectra were collected and summed over 2 mapping periods from June 2002 through April 2005 and from April 2005 through March 2006. Although the GRS instrument can determine K and Th abundances at high latitudes, extremely high concentrations of water ice (e.g., very near the poles) dilute these elemental signatures. Also, H concentrations have a strong influence on the correction techniques used for determining other elemental abundances. To compensate for these complexities, we have excluded data pole-ward of ~45º-60º latitude in both hemispheres using a cut-off based upon water equivalent hydrogen concentration – the H-mask described in *Boynton et al*., 2007.

(2) Surface Heat Production: Using smoothed GRS global K and Th maps where the data have been binned into 5°x5° pixels, we determined the radiogenic ^{40}K and ^{232}Th surface abundances for each GRS pixel based on well-determined isotopic fractions. Currently, ^{232}Th is 100% of total Th abundance with a heat release constant of $2.64x10^{-5}$ $W \cdot kg^{-1}$; ^{235}U and ^{238}U are 0.7204% and 99.2742% of total U abundance with heat release constants of $5.69x10^{-4}$ $W \cdot kg^{-1}$ and $9.46x10^{-5}$ $W \cdot kg^{-1}$, respectively; and ^{40}K is 0.012% of total K abundance with a heat release constant of $2.92x10^{-5}$ $W \cdot kg^{-1}$ [*Turcotte and Schubert*, 2001]. Uranium abundances (^{235}U and ^{238}U) were calculated using an assumed Th/U ratio of 3.8; a canonical cosmochemical value thought to be representative of most planetary bodies and that also agrees with analyses of most Martian meteorites [*Meyers*, 2006]. The GRS instrument measures elemental abundances in the top-most tens of centimeters of the Martian surface, and accordingly is strongly influenced by near-surface soils, ice and dust deposits. These sediments broadly represent the bulk chemistry of the Martian upper crust when renormalized to a volatile-free basis [*Taylor and McLennan*, 2009] and as such, K and Th values must be renormalized to a H_2O-, S-, and Cl-free basis to better reflect bulk crustal values. H_2O and Cl surface abundances are obtained by using smoothed 5°x5° GRS maps. Although the GRS instrument has not yet mapped surface S abundances at the required resolution, we use preliminary GRS estimates of a global S/Cl weight ratio of 5 to calculate the S content of each individual pixel. This ratio is also within the range of values measured in Martian soils at various landing site locations [*Bruckner et al.*, 2003; *Rieder et al.*, 2004; *Gellert et al.*, 2004]. These renormalizations are modest and equate to a 7-14% correction to the K, Th, and U abundances.

We calculate a present day average surface heat production of 4.87×10^{-11} $W \cdot kg^{-1}$. Heat production varies significantly across the Martian surface (**Figure 1**), ranging from 2.52×10^{-11} $W \cdot kg^{-1}$ in the Hellas Basin and Solis Planum regions to 7.52×10^{-11} $W \cdot kg^{-1}$ in the Acidalia Planum region. Of all the GRS measured elemental abundances, K and Th most closely correlate with one another [*Taylor et al.*, 2006b]. In addition, Th is presently the largest heat source among the radiogenic isotopes (**Figure 2**). Consequently, present-day surface heat production closely correlates with Th surface abundances measured by the GRS (as U is also a function of Th abundance).

(3) Crustal Heat Flow: Using the crustal thickness model of *Neumann et al.*, 2004, smoothed to agree with the GRS 5°x5° pixel resolution, and an average uniform crustal density of 2,900 $kg \cdot m^{-3}$ [*Zuber*, 2001; *Spohn et al.*, 2001], we calculate the average crustal component of heat flow of 6.43 $mW \cdot m^{-2}$ and ranging from <1 $mW \cdot m^{-2}$ in the Hellas Basin and Utopia Planitia regions to 12.6 $mW \cdot m^{-2}$ in the Sirenum Fossae region (**Figure 3**). Crustal thicknesses proportionately vary more across Mars than do heat producing elemental abundances. Therefore, although there are some significant deviations, the crustal component of heat flow generally correlates with crustal thickness – i.e., a thicker crust represents higher crustal heat flow. It has been estimated that as much as 50% or more of the Martian planetary budget of heat producing elements has seen sequestered into the crust during planetary differentiation due to their incompatibility in igneous processes [*Taylor et al.*, 2006b; *McLennan*, 2001]; a process

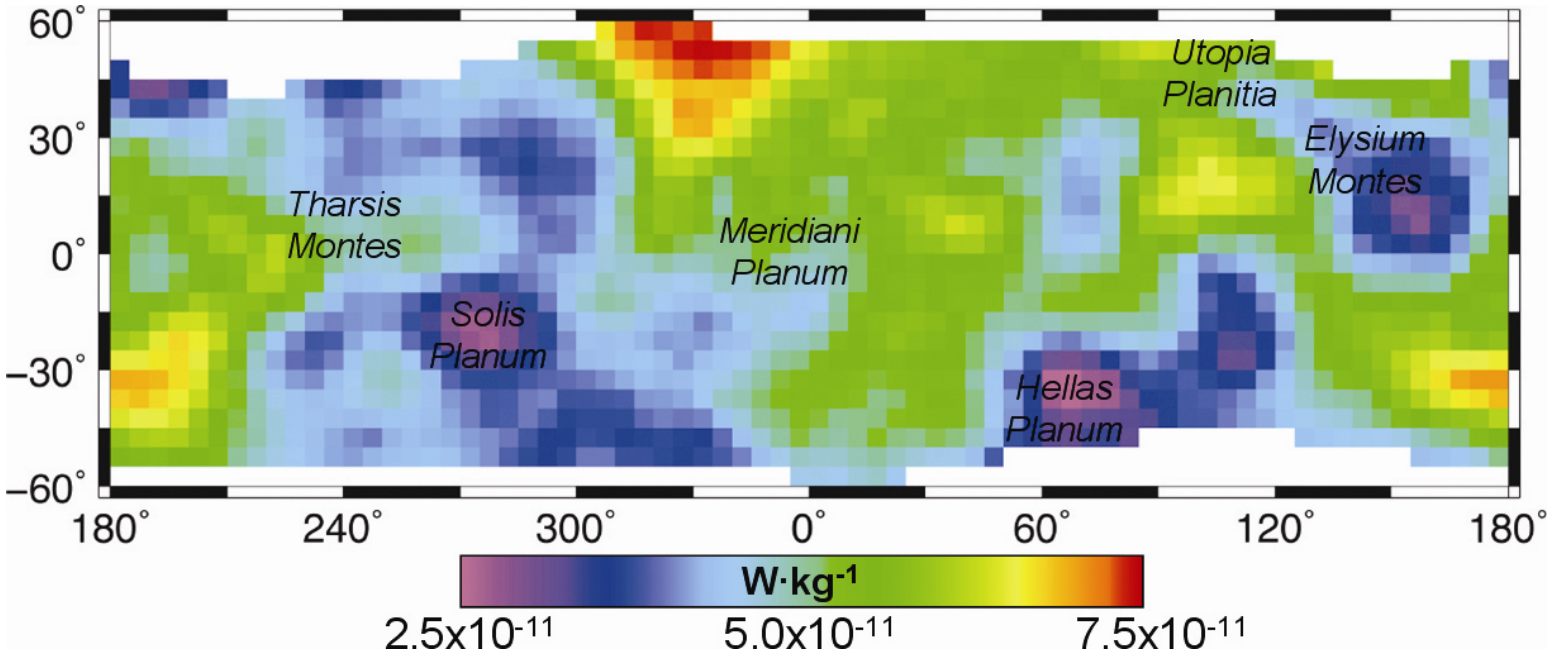

Figure 1: Surface heat production on Mars based on 5x5 smoothed re-binned global GRS K and Th abundance maps renormalized to an H_2O-, S-, and Cl-free basis and assuming Th/U=3.8.

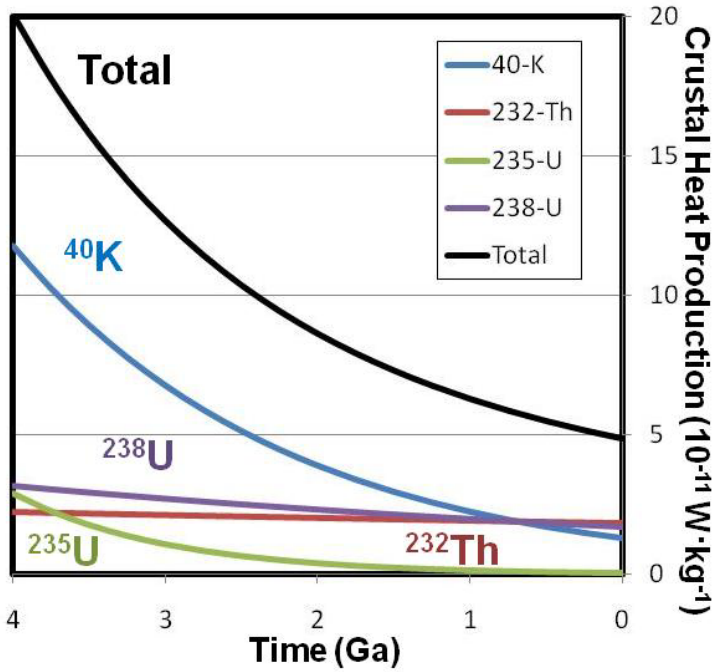

Figure 2: Average Martian crustal heat production through time based on current surface observations from the GRS instrument and established cosmochemical ratios. The present day average is 4.87×10^{-11} W·kg^{-1}. Thorium-232 is currently the major radiogenic heat source with ^{238}U being only slightly less assuming Th/U of 3.8. However, the K/Th (and K/U) ratios of Martian crustal rocks are approximately twice those typically observed on Earth [*Taylor et al.*, 2006a,b] leading to ^{40}K dominating surface heat production prior to about 3.0 Ga.

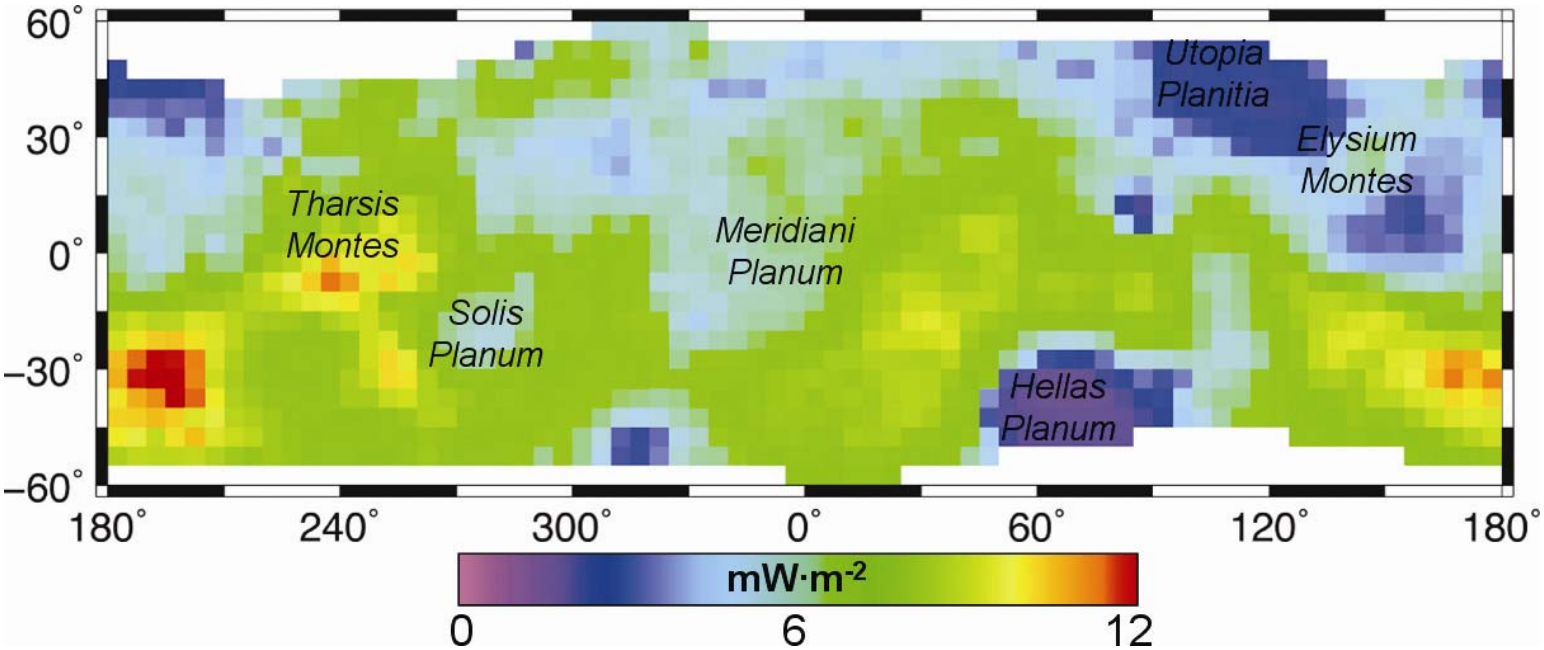

Figure 3: Crustal heat flow for low- and mid-latitudes based on 5x5 smoothed re-binned global GRS elemental abundances, an assumed average uniform crustal density of 2,900 kg·m^{-3} [*Spohn et al.,* 2001; *McLennan*, 2001], and the crustal thickness model of Neumann et al., 2004. Note that these heat flow calculations assume that the GRS-measured surface abundances of the radiogenic elements represent average crust.

that mostly took place very early in Martian geological history. As such, the crustal component of heat flow represents as much as half of the total planetary output of radiogenic heat, which we estimate to be ~13 $mW \cdot m^{-2}$. This value agrees well with estimates from previous works based on separate and independent cosmochemical or lithospheric cooling models which range from approximately 8-18 $mW \cdot m^{-2}$ [*Montési and Zuber*, 2003]. For comparison, in the terrestrial continental crust, average heat flow is 65 $mW \cdot m^{-2}$ and 48 $mW \cdot m^{-2}$ from tectonically stabilized crust with the crustal radiogenic component estimated to be in the range of 25-35 $mW \cdot m^{-2}$ [*Taylor and McLennan*, 2009; *Jaupart and Mareschal*, 2006; *McLennan et al.*, 2006].

(4) Discussion: These calculations assume a vertically homogeneous crust with no vertical change in the concentrations of K, Th and U with crustal depth. This is in contrast to the Earth's continental crust that typically exhibits an approximately exponential decrease in the abundances of the heat producing elements with depth. This is due to intracrustal melting and tectonic processes that further concentrate the incompatible elements into the more-evolved, upper crust [*Taylor and McLennan*, 2009]. However, these processes of intracrustal differentiation that so affect the terrestrial continental crust are unlikely to be active on Mars to any significant degree. There is no definitive evidence for current or past plate tectonic processes, nor have orbital remote sensing instruments detected any major provinces of the highly-evolved crustal products that we see on Earth. Geochemical mapping by the GRS reveals no suggestion that ejecta

from the largest (and deepest) impact basins have compositions that differ from surrounding areas [*Boynton et al.*, 2007]. Although there are localized regions of quartz-bearing igneous rocks [*Christensen et al.*, 2005], previously observed regions of high-silica, igneous "andesite" (Surface Type 2) have been more recently reinterpreted to reflect surface coatings of a silica-bearing secondary mineral phase [*Wyatt and McSween*, 2002]. Also, extensive impact gardening is thought to have vertically homogenized a significant portion of the Martian crust, so measured surface abundances can be reasonably inferred to be representative of concentrations from lower depths [*Hartmann et al.*, 2001]. However, if Mars has a vertically heterogeneous crustal chemistry with upward enrichment of incompatible elements, our calculations for heat flow would represent an upper limit.

It is beyond the scope of this report to describe in detail the implications of regional-scale variations in heat production and heat flow. However, below we discuss two examples that serve to illustrate such approaches.

A number of regions of Mars show anomalous crustal heat flow (**Figure 3**). Despite having a relatively thick crust, the Solis Planum region is unusually depleted in K and Th, resulting in an anomalously low crustal heat flow compared to surrounding terrains. Thus earlier suggestions that the crust at Solis Planum had unusually high heat flow [*Ruiz et al.*, 2006] are in error because they were based on the great crustal thickness and a heat production assumed to be equivalent to a global average. These chemical anomalies are not well understood for Solis Planum, a large terrain with unusual

geophysical and morphological characteristics associated with the Tharsis formation [*Carr*, 2006].

Conversely, regions in the Northern Plains are highly enriched in K and Th (and Fe) with respect to the planetary average and thus yield a high surface heat production. Most workers attribute incompatible element enrichment to primary igneous composition and not to near-surface secondary sedimentary processes [*Taylor et al.*, 2006b; *Karunatillake et al.*, 2006; *Hahn et al.*, 2007]. Despite high abundances of heat producing elements, these regions show very low crustal heat flow due to a thin crust. Consequently, future studies concerned with the thermal or geodynamic properties of a particular Martian geologic province should take care to use more geographically refined estimates of heat flow, such as those mapped and reported here, for modeling purposes, rather than previously reported global or large-scale regional averages.

Because the respective half-lives of ^{40}K, ^{232}Th, ^{235}U, and ^{238}U are well-known, we can calculate the average crustal component of heat flow over geologic time (**Figure 2**). Furthermore, temporal regressions of the mapped data show crustal heat flow evolution. **Figure 4** shows such evolution by mapping the global Martian crustal component of heat flow for the present and for 1 Ga intervals to 4 Ga. Crustal heat flow increases back through time and most dramatically before 2 Ga when the decay of ^{40}K becomes the dominant source of radiogenic heat. Average crustal heat flow at 4 Ga is almost five times that of present day (~28 $mW \cdot m^{-2}$), with some regions, specifically in some sections of the Southern Highlands, showing crustal heat flow of over 50 $mW \cdot m^{-2}$. Note, that these heat production and heat flow regression calculations assume that the K and Th

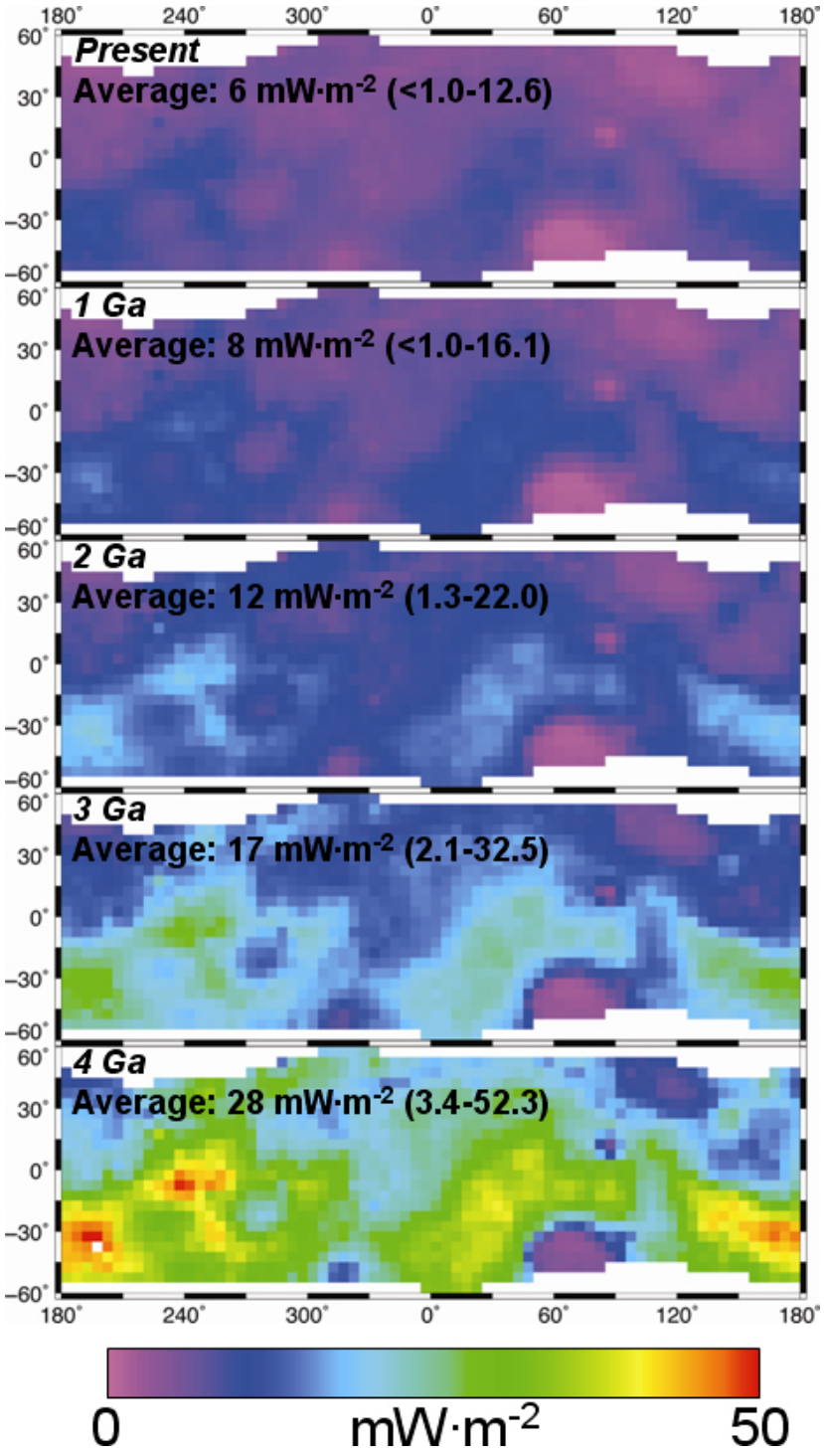

Figure 4: GRS-derived crustal component of Martian heat flow for the present and regressed through time at 1 Ga intervals. Note that these heat flow calculations assume that the GRS-measured surface abundances of the radiogenic elements represent average crust and that crustal thickness has remained constant over the past 4.0 Ga.

abundances in the Martian crust have not been significantly modified due to past igneous processes. Although not an entirely realistic assumption (e.g., the formation of Tharsis), *Hahn et al.* showed that K and Th vary only subtly with apparent surface age indicating that past crustal resurfacing and the formation of past geologic provinces, on average did not form with dramatically different K and Th and, therefore, heat production values. This also assumes no significant change in crustal thickness; a reasonable assumption, as it is estimated that 80±10% of the Martian crust has been in place since ~4 Ga [*Taylor and McLennan*, 2008].

Previously, total surface heat flow has been calculated from estimates of the thickness of the mechanical lithosphere based on gravity and topography data and estimates of the depth to the brittle-ductile transition using wrinkle ridge morphologies to constrain fault depths [*McGovern et al.*, 2004]. Such calculations provide heat flow estimates at the time of formation of features being considered. Since the age of a particular geologic province can be roughly determined from cratering history; the results of this study can also be used to determine the crustal thermal characteristics of these geologic regions at the time of formation. For example, Solis Planum, with a present day crustal heat flow range of 4.8-5.2 $mW \cdot m^{-2}$, would have had a crustal heat flow range of approximately 8.8-9.8 $mW \cdot m^{-2}$ at time of formation in the late Hesperian [*Tanaka et al.*, 1992]; a lower value than previous estimates [*Ruiz et al.*, 2006]. Similarly, the Opportunity rover landing site at Meridiani Planum, with a present day crustal heat flow value of 5.6 $mW \cdot m^{-2}$, would have had a crustal heat flow of approximately 19.2 $mW \cdot m^{-2}$ at time of formation in the late Noachian or early Hesperian [*Hynek et al.*, 2002].

The maps produced here show the considerable variation and complexity of radiogenic crustal heat flow across the present day Martian surface and through geologic time. As a direct orbital instrument observation, these heat production and crustal heat flow values support previous heat flow estimates produced by different methodology, but are better constrained and less model dependent. The specific thermal histories for individual locations that can be calculated with these data will be a valuable aide for landing site selections, refining geologic timelines, and understanding the evolution of buried sedimentary deposits.

Chapter 5: Regional Martian Crustal Heat Flow from Mars Odyssey Gamma-Ray Spectrometry

To Be Submitted to the Journal of Geophysical Research - Planets

B. C. Hahn and S. M. McLennan

(1.) Introduction: The incompatible, heat producing elements (K, Th, and U) are the primary sources of radiogenic heat in the Martian crust and all three can be measured in the upper few decimeters of the Martian surface from orbit by remote sensing, with K and Th mapped in detail. Using elemental abundances measured by the Gamma-Ray Spectrometer (GRS) instrument suite onboard the 2001 Mars Odyssey spacecraft, *Hahn et al.* (Chapter 4) calculated and mapped the global distribution of the crustal component of Martian surface heat production and crustal heat flow. Evident from these maps are specific regions of anomalous heat flow, showing significant geographic variation in the crustal thermal reservoir. In this study, we explore in greater depth these specific regions of anomalous heat flow as well as report on the present crustal heat flow and heat flow at the time of formation for certain geologically important terrains.

A number of previous studies have attempted to constrain Martian heat flow, primarily through geophysical methods [*Zuber et al.*, 2000]. For example, *McGovern et al.* (2002, 2004) estimated heat flow for specific geologic regions and features using

models determining the elastic or mechanical thickness of the Martian lithosphere [*McNutt*, 1984]. *Ruiz et al.* (2006) used similar methods to argue for a differentiated (i.e., geochemically layered) Martian crust at Solis Planum. *Montesi and Zuber* (2003) used the distribution and horizontal length scale of wrinkle ridges in tectonic zones on the Martian surface to deduce flexural response to deformation and thus constrain heat flow. More recently, the results of the Shallow Radar (SHARAD) instrument onboard the Mars Reconnaissance Orbiter (MRO) have vertically mapped layered deposits, specifically in the Polar Regions. The amounts of downward deflection these loads incur also provide constraints on the rheology and thermal properties of the underlying lithosphere [*Phillips et al.,* 2008; *Nunes and Phillips*, 2006].

Most of these previous studies were primarily interested in mantle heat flow as it relates to mantle convection or surface deformation. These studies estimated total heat flow; combining both mantle and crustal components of heat flow due to the inability to distinguish between the two thermal reservoirs using existing methods. However, as the radiogenic heat-producing isotopes are preferentially sequestered into planetary crusts during differentiation, the crustal component of heat flow is especially important [*Taylor and McLennan*, 2009; *McLennan*, 2001; *Hahn and McLennan*, Chapter 2; *Norman*, 1999, 2002]. *Hahn et al.* (Chapter 4) and this follow-up regional study are the first to use elemental abundances, directly measured from recent orbital remote sensing, combined with independent estimates of crustal thickness, to constrain crustal heat flow in the mid- and low-latitudes (**Figure 1**) [*Hahn and McLennan*, 2008]. These results generally agree well with past geophysical studies with a few notable exceptions to be detailed below.

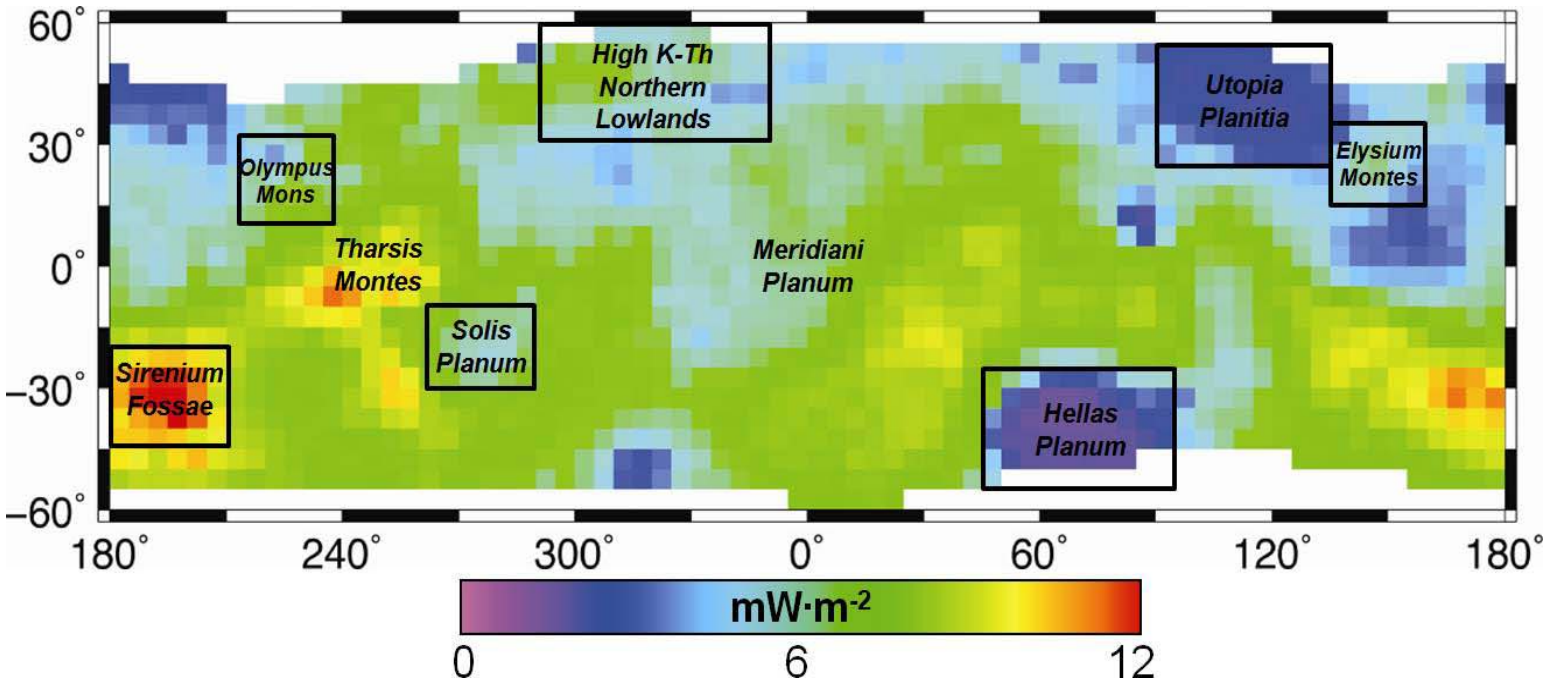

Figure 1: Crustal heat flow for low- and mid-latitudes based on 5x5 smoothed re-binned global GRS elemental abundances adapted from *Hahn et al.* (Chapter 4) [*Hahn and McLennan*, 2008]. Also indicated are the specific geological regions and features detailed in this study. Because of the areally large GRS footprint, only relatively large regions or features can be measured with statistical reliability (several GRS pixels or more) [*Boynton et al.,* 2007].

(1.1) Radiogenic element distribution from gamma-ray spectrometry – background: GRS coverage for K and Th extends to both poles. However, at high latitudes, extremely high concentrations of water ice (e.g., very near the poles) dilute these elemental signatures reducing effective coverage for these elements to between latitudes of ±75º [*Boynton et al.*, 2007; *Taylor et al.*, 2006a]. Additionally, high H concentrations have a strong influence on the correction techniques used for determining other elemental abundances that further reduces the GRS effective coverage considerably. To compensate, we have excluded data using the "H-mask" for high water equivalent hydrogen concentrations described in *Boynton et al.* (2007). This limits GRS coverage to regions in the mid- and low-latitudes between the equator and ~45º-60º in both hemispheres – the same coverage restrictions applied for *Hahn et al.* (Chapter 4). Data spectra were collected and summed over 2 mapping periods from June 2002 through April 2005 and from April 2005 through March 2006.

The GRS instrument is limited by a surface penetration depth of only a few tens of centimeters. However, this is considerably greater than the penetration depths of other remote sensing instruments and GRS measurements are largely unencumbered by thin surface dust layers that obscure most other spectroscopic methods (e.g., TES – on board the Mars Global Surveyor; THEMIS – on board the 2001 Mars Odyssey; and OMEGA – on board the European Space Agency's Mars Express spacecraft [*Christensen et al.*, 2001, 2003; *Bibring et al.*, 2005]). Note however, that extensive, thicker layers of mantled dust may affect results in certain regions [*Newsom et al*., 2007].

GRS also has a spatially-large, areally extensive resolution footprint of approximately 270 km radius. While being a low-resolution remote sensing tool, GRS has provided the first detailed global maps of elemental abundances, and has proven to be especially valuable for distinguishing the broad-scale variations in elemental compositions across the Martian surface [*Boynton et al.*, 2007; *Hahn et al.*, 2007; *Karunatillake et al.*, 2006; *Keller et al.*, 2006; *Taylor et al.*, 2006a, 2006b]. However, chemical abundances can only be accurately reported for areally large regions and major geologic provinces where GRS counting statistics reduce uncertainty. GRS data are not well suited for small surface features, or minor geologic terrains smaller than a few GRS pixels. Consequently, for this study, we have limited our examination to nine large areas representing volcanic provinces, major impact basins, and large geologic features or regions with heat flow anomalies within the GRS special coverage range (See **Section 3, below**).

(1.2) Determining Martian crustal heat flow from radiogenic isotopes: Using these 5ºx5º pixel resolution maps, we calculate the radiogenic abundances of K and Th for each pixel and using well-established isotopic fractions (see **Table 1**) [*Turcotte and Schubert*, 2001]. Although GRS can detect and measure U abundances, the element is not in high enough concentration to be mapped reliably at a similar resolution to other measured elements (although global and large regional estimates may be possible in the future with additional observation time). In terrestrial weathering environments, Th and

Table 1: Global HPE abundances, radiogenic isotopic fractions, and heat constants

Element	*Elemental Average Abundance (ppm)*[†]	*Isotope (percent of total)*[‡]	*Isotopic Average Abundance (ppm)*	*Heat Release Constant ($W \cdot kg^{-1}$)*[‡]
K	3980	^{40}**K** (0.012%)	0.48	2.92×10^{-5}
Th	0.70	^{232}**Th** (100%)	0.70	2.64×10^{-5}
U[*]	0.18	^{235}**U** (0.7204%)	0.001	5.69×10^{-4}
		^{238}**U** (99.2742%)	0.179	9.46×10^{-5}

[†] [*Hahn et al.*, Chapter 2; *Hahn and McLennan*, 2008; *Taylor and McLennan*, 2009; *Taylor et al.*, 2006a]
[‡] [*Turcotte and Schubert*, 2001]
[*] Calculated using Th/U = 3.8 [*McLennan*, 2003]

U are subject to considerable fractionation. However, these elements show similarly incompatible behavior and do not appear to fractionate during most known igneous processes on Mars [*McLennan*, 2003; *Hahn and McLennan*, Chapter 2]. Given the generally basaltic nature of the Martian surface [*McSween et al.*, 2009] and considerable evidence of an arid weathering environment with little long-term surface water and with sedimentary process dominated by physical mixing [*Hurowitz et al.*, 2006, 2007; *Hahn and McLennan*, Chapter 2] these elements are far less likely to fractionate in the Martian weathering environment, especially over the large geographic scale of a GRS footprint. Therefore, uranium abundances (^{235}U and ^{238}U) were calculated using the assumed Th/U ratio of 3.8; a canonical igneous cosmochemical value thought to be representative of most planetary bodies and that also agrees with analyses of most Martian meteorites [*Meyers*, 2006] and with preliminary GRS global measurements [*GRS Team, personal communication*]. The U concentration so determined results in a near-surface K/U ratio of 22,000, a value consistent with the factor of two enrichment, compared to the Earth, of moderately volatile elements in the Martian primitive mantle [*Dreibus and Wänke*, 1985; *Wänke and Dreibus*, 1988; *Wänke*, 2001].

As the GRS instrument only measures elemental abundances in the top tens of centimeters of the Martian surface, it is influenced by surface soils and near-surface ice, as well as bedrock. Landing site measurements at all locations show various levels of enrichment in volatile and mobile elements, such as S and Cl, through the addition of certain evaporite salts that are either detrital deposits or products formed from local aqueous processes (or both) [*Brückner et al.*, 2003; *Rieder et al.*, 2004; *Gellert et al.,* 2004]. GRS measurements agree well with landing site chemical analyses and global

elemental abundances show similar volatile element levels, indicating that these enrichments are present globally at varied concentrations [*Karunatillake et al.*, 2007]. Both the GRS and Neutron Spectrometer on the Odyssey spacecraft have also detected the presence of near surface hydrogen, believed to be either in the form of mineralogically bound water at lower latitudes or as subsurface ice closer to the poles [*Feldman et al.*, 2004; *Boynton et al.*, 2007].

These volatile element enrichments are caused by surficial and near-surface processes and are not representative of the total crustal chemistry that governs crustal heat flow. Therefore, each GRS pixel has been renormalized to a S-, Cl-, and H_2O free basis to better reflect a bulk crustal chemistry. H_2O and Cl surface abundances, both mapped by the GRS instrument, are obtained by using the smoothed 5°x5° GRS maps. Although the GRS instrument has not yet mapped surface S abundances at the required resolution, we use preliminary GRS estimates of a global S/Cl weight ratio of 5 to calculate the S content of each individual pixel. This ratio is also within the range of values measured in Martian soils at various landing site locations [*Bruckner et al.*, 2003; *Rieder et al.*, 2004; *Gellert et al.*, 2004]. These renormalizations are modest and equate to a 7-14% correction to the K, Th, and U abundances. The question of whether GRS surficial measurements accurately reflect the underlying crustal elemental abundances as a whole is addressed in **Section 4**, below.

With radiogenic abundances renormalized to a volatile-free composition, and using the methods detailed in *Turcotte and Schubert* (2001) and *Hahn et al.* (Chapter 4), we calculated the surface heat production for each 5ºx5º GRS pixel and averages for the

Martian geologic regions detailed below. The global crustal thickness estimates of *Neumann et al.,* 2004 are smoothed to the GRS equivalent resolution of 5ºx5º and, assuming an average uniform crustal density of 2,900 $kg \cdot m^{-3}$ [*Zuber*, 2001; *Spohn et al.*, 2001], we calculate the present-day crustal component of heat flow for each pixel. Further, given the relative decay rates for each radiogenic isotope, and using surface ages and formation ages from a variety of cited sources, it is possible to estimate the crustal component of heat flow at the time of formation for each of the selected geologic features, geographic regions, or formations. A list of these regions and features, the average crustal thickness, apparent surface age or age of formation, as well as estimates of present day crustal heat flow and crustal heat flow at time of formation is provided in **Table 2**.

(2.) Heat flow variations: *Hahn et al.* (Chapter 4) mapped the surface heat production and crustal heat flow from GRS-determined radiogenic isotopes. Present day, of the HPEs, ^{232}Th is the largest single contributor of radiogenic heating; although, prior to about 1 Ga, the shorter half-life ^{40}K becomes the dominant heat producer. Also, of all the GRS measured elemental abundances, K and Th most closely correlate with one another, with over 95% of the surface having a K/Th ratio between 4000 and 7000 [*Taylor et al.*, 2006b]. Further, for this study, U is calculated directly from measured Th concentrations using a Th/U ratio of 3.8. Consequently, variations in surface heat production (2.52×10^{-11} - 7.52×10^{-11} $W \cdot kg^{-1}$), which is the sum of radiogenic heating

Table 2: Geologic regions and approximate ages, GRS derived elemental abundances, and present and past heat flow

Geologic Feature/Region	Feature Age[†]	Average Crustal Thickness (km)[‡]	GRS Average Abundances		Crustal Heat Flow ($mW \cdot m^{-2}$)	
			K (ppm)	*Th (ppm)*	*Present*	*At Formation*
Olympus Mons	Amazonian	65	3340	0.67	8.9	~10-20
Elysium Mons	Late Hesperian, Early Amazonian	55	2900	0.53	5.9	~16
Tharsis Montes	Noachian and younger	60-65	3300-3700	0.55-0.73	8.4 (6.3-10.0)	~28-36
Solis Planum	Late Hesperian	65	2320	0.37	5.0	~12-14
Meridiani Planum *(Opportunity Landing Site)*	Late Noachian, Early Hesperian	40	3790	0.66	5.6	~20
High K-Th Northern Plains	Late Hesperian	25	6130	1.02	5.4	~16
Sirenum Fossae	Early-Mid Noachian	65	4340	0.98	11.9	~45-50
Hellas Basin	Early Noachian (Hesperian Sediments)	10	2830	0.34	0.9	~6
Utopia Planitia	Early Noachian (Hesperian Sediments)	15	4000	0.71	2.2	~12
Northern Lowlands[*]	N/A	30	4250	0.71	4.5	N/A
Southern Highlands[*]	N/A	60	3990	0.70	8.8	N/A
Global Average	**N/A**	**~50**	**3980**	**0.70**	**6.43**	**N/A**

[†][*Hahn et al.,* 2007; *Scott and Tanaka*, 1986; *Greeley and Guest*, 1987; *Tanaka and Scott*, 1987; *Carr and Head*, 2009; *Hynek et al.*, 2002]
[‡][*Neumann et al.*, 2004]
[*]**[***Taylor et al.,* 2006b**]**

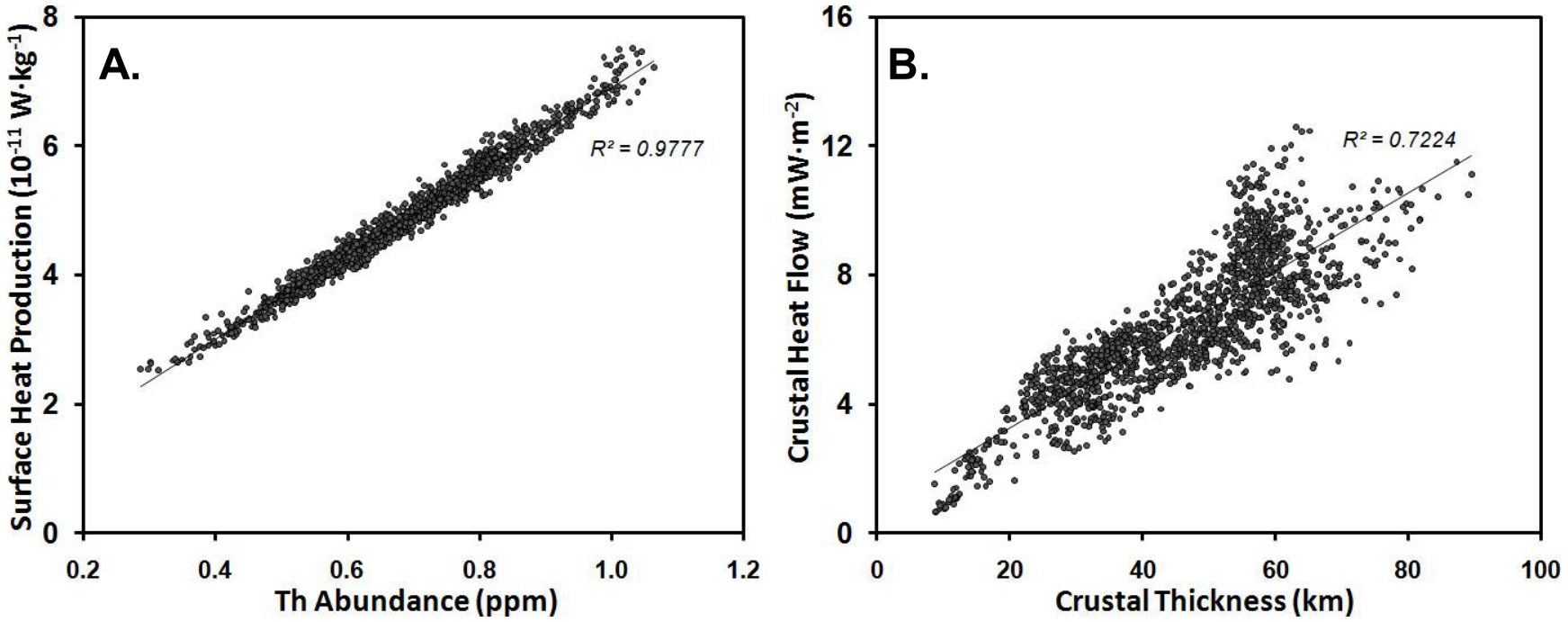

Figure 2: Correlation diagrams for Martian surface heat production and crustal heat flow. **A.** GRS derived K and Th abundances are closely correlated across the Martian surface with relatively modest geographic variations in K/Th [*Taylor et al.,* 2006a]. U concentrations are calculated directly from measured Th abundances using a Th/U = 3.8. Therefore, surface heat production strongly correlates with Th concentration. **B.** Crustal heat flow most strongly correlates with crustal thickness as the magnitude of variation in Martian crustal thickness is larger than the magnitude of variation in K or Th abundances [*Neumann et al.,* 2004].

based on surface measurements and does not take into account crustal thickness, are strongly dependent on variations in surface Th abundance (**Figure 2a**). Although Th variations range from about 0.3-1.1 ppm with an average of 0.70±0.14 ppm, this is less variation than seen on a comparable scale on either the Moon, based on orbital GRS mapping, or in the terrestrial crust, based on large-scale regional averages [*Prettyman et al.,* 2002; *Lucey et al.*, 2006; *Taylor and McLennan*, 1985].

Crustal heat flow is calculated using the crustal thickness model of *Neumann et al.* (2004) smoothed and registered to agree with the GRS 5°x5° pixel resolution maps. Additionally, calculations assume a vertically constant crustal density of 2,900 $kg \cdot m^{-3}$ [*Zuber*, 2001; *Spohn et al.*, 2001]. Crustal thicknesses proportionately vary more across Mars than do heat producing elemental abundances with 5°x5° averages ranging from 9-90 km. Therefore, although there are some significant deviations, the crustal component of heat flow generally correlates rather strongly with crustal thickness – i.e., a thicker crust represents higher crustal heat flow, although the correlation is not as strong as the Th - surface heat production relationship (**Figure 2a**). The present-day radiogenic crustal component of Martian heat flow ranges from <1 $mW \cdot m^{-2}$ - 12.6 $mW \cdot m^{-}2$, with a global average of 6.4±0.1 $mW \cdot m^{-2}$ (95% confidence level based on a standard deviation of 2.0 $mW \cdot m^{-2}$ and 1,507 5°x5° pixels). As the radiogenic abundances in the Martian crust likely represent 50% or more of the total radiogenic budget for the planet, total heat flow derived from radioactive decay should be approximately twice the crustal value estimated here, or approximately 12-13 $mW \cdot m^{-2}$ (i.e., neglecting any potential additional heat derived from planetary secular cooling, core crystallization, etc.). Previous works based on separate and independent cosmochemical or lithospheric cooling models determined

average total heat flow ranging from approximately 8-18 $mW \cdot m^{-2}$ [*Montési and Zuber*, 2003; *Treiman et al*., 1986; *Laul et al.*, 1986].

Crustal heat flow is not uniform across the Martian surface. The crustal dichotomy represents the largest, first-order variation in crustal heat flow due to the significant difference in average crustal thicknesses (**Figure 1; Table 2**), with lower heat flow in the Northern lowlands (average crustal thickness of 30 km and crustal heat flow of 4.5 $mW \cdot m^{-2}$) and significantly higher heat flow in the Southern highlands (average crustal thickness of 60 km and crustal heat flow of 8.8 $mW \cdot m^{-2}$). In contrast, the average surface heat production for the Northern lowlands averages 5.2×10^{-11} $W \cdot kg^{-1}$ and compares to the Southern highland average of 5.1×10^{-11} $W \cdot kg^{-1}$. Therefore, while the averages for surface heat production are essentially equivalent in the northern and southern hemispheres, the averages for crustal heat flow differ by close to a factor of two – due solely to the significant differences in crustal thickness. **Figure 3** plots a histogram of 5°x5° pixel crustal heat flow values. The crustal dichotomy is the primary cause of the deviation from a normal distribution due to the bimodal nature of heat flow values in the northern or southern hemispheres. Second order variations in heat flow associated with specific geologic features and provinces or measured surface chemical anomalies are detailed in **Section 3**, below.

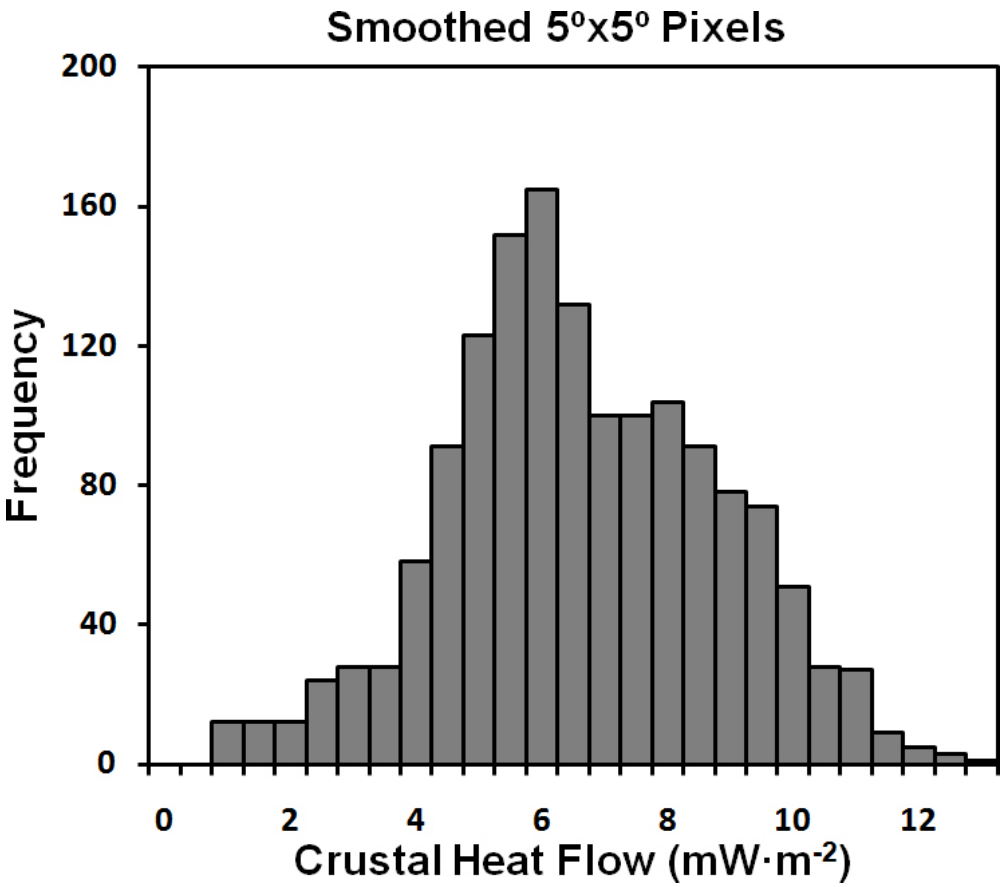

Figure 3: Histogram of heat flow for each 5ºx5º GRS pixel. Heat flow does not follow a normal distribution across the Martian surface. The deviation from a normal distribution seen above is most likely primarily due to the Martian dichotomy, where most of the Northern Lowland Plains show lower heat flow, while the Southern Highlands have high heat flow.

(3.) Regional crustal heat flow for selected geologic provinces and features: Due to the spatially large GRS footprint and coverage limitations detailed in **Section 1.1** above, regional analyses are limited to areally large geologic provinces and features in the low- and mid-latitudes of Mars (**Figure 1**). Here we examine nine such regions (**Table 2**): the volcanic provinces of Olympus Mons, Elysium Mons, and Tharsis Montes; Solis Planum and Meridiani Planum; regions displaying GRS chemical anomalies in the High K-Th Northern Pains and the region around Sirenum Fossae, and the Hellas and Utopia impact basins. Present day heat flow for each region was determined using averages of specific subsets of the 5°x5° GRS pixels for radiogenic abundances overlaying that region. Unless otherwise specified, the average crustal thickness of each region was calculated from the *Neumann et al.* (2004) model.

An important factor for any geologic region is the heat flow conditions that contribute to the thermal behavior of that feature at the time of formation. Given the measured present-day abundances of heat producing elements and an estimated age of formation for a geologic region, it is possible to calculate the crustal component of heat flow at the time of formation using the respective half-lives of the heat contributing isotopes (**Table 2**). Apparent surface ages for geologic features on Mars are estimated using crater count statistics and cross-cutting relationships; however, formation ages are only loosely constrained with high uncertainties. Unless otherwise indicated, geologic ages are from the *USGS Atlas of Mars* geological mapping series [*Scott and Tanaka*, 1986; *Greeley and Guest*, 1987; *Tanaka and Scott*, 1987].

(3.1) Olympus Mons and Elysium Mons: Olympus Mons is the largest shield volcano on the Martian surface. A relatively young formation, Olympus Mons has likely experienced intermittent activity throughout the Amazonian that is believed to have continued until very recently (10-200 Ma) [*Hartmann*, 2005]. While the volcano is geographically proximate to the Tharsis volcanic formation, orbital mapping of the Martian geoid (i.e., surface gravity field) shows the two formations have separate gravity anomalies and may not share the same magmatic sources [*Lemoine et al.*, 2001]. Although slightly depleted in K compared to the global average, the formation has a thick crust (~65 km using the averaged crustal thicknesses for a 5°x5°) which yields a corresponding crustal heat flow slightly higher than the global average. Elysium Mons is a large shield volcano that is part of the Elysium rise volcanic complex. Like Olympus Mons (and Tharsis, see below), Elysium formed through episodic growth, mostly in the Late Hesperian and Early Amazonian. It is a chemically anomalous region substantially depleted in both K and Th, making it one of the lowest present-day surface heat production regions. This chemical anomaly of low elemental abundances is geographically discrete to the formation and does not extend beyond the Elysium Mons. When integrated over crustal thickness, these abundances yield a crustal heat flow value somewhat lower than the global average (5.9 $mW \cdot m^{-2}$).

McGovern et al. (2002, 2004) estimated total heat flux (crust plus mantle component) at the time of formation for Olympus Mons to be <24 $mW \cdot m^{-2}$ based on estimates of lithospheric thickness from topography and a total heat flow between 15-45 $mW \cdot m^{-2}$ for the total Elysium rise. This study calculates an approximate crustal heat flow at formation of 10-20 $mW \cdot m^{-2}$ for Olympus Mons and ~16 $mW \cdot m^{-2}$ for Elysium Mons,

based on the estimated formation ages. If the distribution of radiogenic elements throughout the Martian crust and mantle imply that approximately half of radiogenic heating comes from the crust (see Section 2, above), then these crustal heat flow values correspond to approximately 20-40 $mW \cdot m^{-2}$ and ~32 $mW \cdot m^{-2}$ for Olympus and Elysium Montes, respectively.

(3.2) Tharsis Montes: Volcanism at the Tharsis bulge has likely continued intermittently over most of Martian geologic history and several young lava flows show few craters indicating a relatively fresh surface. However, the bulk of the Tharsis super-formation was likely in place by 4 Ga [*Phillips et al.*, 2001; *Nimmo and Tanaka*, 2005]. The formation and growth of Tharsis has also had considerable effect on nearby geologic provinces causing episodic faulting and deformation [*Anderson et al*., 2001]. Surface concentrations of K, Th, and U vary across this geographically large region (ranges provided in **Table 2**; also see **Figure 1**).

We estimate an average present-day crustal heat flow of 8.4 $mW \cdot m^{-2}$ for the entire Tharsis plateau; however, values range from ~6.3-10.0 $mW \cdot m^{-2}$, moderately higher than the global average. As most of Tharsis was in place by the mid- to late Noachian, we use this as the principle formation age. Note that the surfaces sampled by the GRS are considerably younger than the bulk of Tharsis. These younger flows (mostly Amazonian with some late Hesperian flows on the formation's flanks) also represent a small portion

of the total mass of the total formation. Therefore, measured K, Th, and U abundances may not be completely representative of the generally older Tharsis Plateau as a whole. However, *Hahn et al.* (2007) demonstrated that while there are statistically significant variations in elemental abundances with surface age, variations in K and Th are muted and vary only on the order of ~10%. As such, elemental abundances measured from the younger, overlying layers of Tharsis may have abundances that are not readily distinguishable from the bulk, older Tharsis formation. This can not be constrained, but we will make such an assumption for the purposes of calculating a crustal heat flow for Tharsis during its formation period. We therefore estimate a crustal heat flow at the time of Tharsis formation in the range of ~28-36 $mW \cdot m^{-2}$.

(3.3) Solis Planum: This Late Hesperian formation is notable as a region of anomalously low crustal heat flow. However, as Solis Planum has a thick crust, this is due to unusually low crustal concentrations of K and Th specific to the region (**Figure 1**) – some of the lowest for both elements measured on the planet. Like the chemical anomaly at Elysium Mons, the low abundances of K and Th are geographically limited specifically to Solis Planum.

We estimate a lower than average present day crustal heat flow of ~5 $mW \cdot m^{-2}$ and approximately 12-14 $mW \cdot m^{-2}$ at the time of formation in the Late Hesperian. *Montesi and Zuber* (2003) estimated a total heat flow (crust and mantle) of 27-47 $mW \cdot m^{-2}$, which is

somewhat higher than our estimate if we assume our crustal heat flow value represents half of total heat flow. However, *McGovern et al.* (2002, 2004) report corrected heat flow values that more closely agree with the radiogenic element-derived values from this study. Wrinkle ridges located throughout Solis Planum suggest subsurface faulting associated with episodic stages of deformation from the nearby Tharsis plateau [*Golombek et al.,* 2001; *Anderson et al.,* 2001]. It is possible that while Solis Planum may have relatively modest crustal heat flow, there is a corresponding larger contribution from mantle heating given its proximity of the Tharsis volcanic bulge.

(3.4) Meridiani Planum: Meridiani Planum is covered by Early Hesperian deposits of sediments that are believed to be several hundred meters thick overlaying a Noachian aged subsurface [*Hynek et al*., 2002]. Orbital remote sensing detected crystalline hematite, suggesting the possibility of an aqueous environment [*Christensen et al.*, 2000]. At the Mars Exploration Rover (MER) *Opportunity* landing site, these deposits were discovered to be reworked evaporitic sandstones with a significant intermixed component of weathered basaltic debris [*McLennan et al.,* 2005; *Grotzinger et al.,* 2005; *Squyres et al.,* 2004, 2006]. The overall bulk composition of these mixed sedimentary deposits, on a S- and Cl-free basis, also approximates to typical Martian basalt.

This region was selected since chemical analyses of soils from the Opportunity landing site agree well with the GRS measurements of the surrounding area [*Hahn and*

McLennan, Chapter 2]; although it is unclear as to what degree the soils are representative of the underlying Noachian terrain. K and Th abundances are close to global averages. With the average crustal thickness of the region measuring ~40 km; present day crustal heat flow is estimated at ~5.6 $mW \cdot m^{-2}$ or ~20 $mW \cdot m^{-2}$ at the time of formation in the Late Noachian-Early Hesperian.

(3.5) High K-Th Northern Plains: The highest concentrations of K and Th, and therefore surface heat production, are found in the Northern plains, close to the H-mask boundary on the edge of GRS coverage [*Hahn et al.*, Chapter 4]. This region closely corresponds to the "Surface Type 2" terrain – a region identified by orbital thermal emission remote sensing methods as having unusual spectral characteristics. This chemical anomaly does not conform to an obvious separately defined geologic formation within the Northern Lowlands (for example, as the chemical anomalies detailed above at Solis Planum and Elysium Mons conform to those specific geologic features). Initially identified as an "andesite" mineralogy, more recent studies have suggested that the particular spectral characteristics were the result of thin, surface rinds or coatings that formed from minor amounts of chemical alteration [*Karunatillake et al.,* 2006, 2009; *Bandfield et al.,* 2000; *Wyatt and McSween*, 2002]. This enrichment in HPEs yield surface heat production values for the region as high as 7.5×10^{-11} $W \cdot kg^{-1}$ (compared to the global average of 4.89×10^{-11} $W \cdot kg^{-1}$). However, due to an average crustal thickness for the region of only ~25 km, present-day crustal heat flow is only 5.4 $mW \cdot m^{-2}$ and

estimated crustal heat flow of formation during the Late Hesperian is only ~16 $mW \cdot m^{-2}$. As such, this region illustrates the importance of crustal thickness in heat flow calculations, since the significant chemical anomalies for the High K-Th Northern Plains do not equate to any significant crustal heat flow anomaly with respect to the global average – in fact, this region shows a slightly lower calculated present-day crustal heat flow than average.

(3.6) Sirenum Fossae: This terrain, among the most ancient of the surviving Martian crust (Early to Mid-Noachian), has the highest calculated crustal heat flow of anywhere on the Martian surface due to relative enrichment in both K and Th as well as, unlike the High K-Th Northern Plains detailed in **Section 3.5** above, possessing a very thick crust. The actual region of high heat flow extends to cover an area larger than Sirenum Fossae specifically, but does not conform to a specific single geologic unit. This ancient region is also part of the highly magnetized crust detected by the Mars Global Surveyor [*Mitchell et al.*, 2007; *Acuna et al.,* 2001]. Present day crustal heat flow for the region is ~12 $mW \cdot m^{-2}$ - almost twice the global average. At the time of formation in the early to mid-Noachian, crustal heat flow for the region could have been as high as 45-50 $mW \cdot m^{-2}$, almost 8 times the present global average.

(3.7) Hellas Basin and Utopia Planitia: Large impact basins present two unique problems for estimating crustal heat flow from GRS measurements of K, Th and U. We calculate extremely low values for present day crustal heat flow for both the Hellas Basin and Utopia Planitia that do not agree with any heat flow estimates from geophysical studies or with models of secular cooling from radiogenic decay.

First, both impact basins selected here are Early Noachian (Hellas, 4.1 Ga; Utopia, 4.12 Ga [*Frey*, 2006]), but have considerable infill of Hesperian and younger age sediments. Based on GRS, Hellas is relatively depleted in K and Th. However, it remains inconclusive as to whether these low abundances are measurements of an underlying lower crust exposed by the impact process. Although K and Th are anomalously low at Hellas, similarly low values can be seen at non-impact related regions elsewhere (i.e., Solis Planum and Elysium Mons, see above). Although the site of an ancient impact, Utopia has been filled with sediment. Most of this sediment was likely deposited shortly after formation [*Searls et al.*, 2006], with only the top-most layers and thin surface veneer from the mid- to late-Hesperian [*Frey et al.,* 2002]. The source terrains for these deposited sediments may have been geographically large enough that any chemical distinctions were homogenized by mixing during transport and deposition since the K and Th abundances for Utopia are almost identical to the globally averaged composition [*Hahn and McLennan*, Chapter 2]. As with Hellas, the sedimentary infill is not representative of the terrain at formation.

A second difficulty is that calculations of crustal heat flow using this method require the inclusion of a crustal thickness estimate. However, the impact process has

removed much of the crust – the reason why the crustal heat flow estimates here are so low. For example, *McGovern et al.* (2004) estimates a minimum total heat flow for Hellas at formation of at least 35 $mW \cdot m^{-2}$, compared to our estimate of the crustal component of only 6 $mW \cdot m^{-2}$ (and assuming half the heat is from the mantle, about 12 $mW \cdot m^{-2}$ total heat flow) . As such, while crustal heat flow estimates using this method agree well with many of the heat flow estimates from other geophysical studies, it is not effective for modeling ancient heat flow in the vicinity of large Martian impact basins.

(4.) Discussion and Conclusions: Formation ages for geologic features coupled with estimates of crustal heat flow can provide a great deal of information about the thermal history of the Martian crust. **Figure 4** (after *Montesi and Zuber*, 2003) plots the estimate for the global average of crustal heat flow and crustal heat flow at age of formation for selected regions back through geologic time. Most geologic regions fit reasonably well with the expected thermal evolution curve based on radiogenic decay rates of global average near-surface heat production and mean crustal thickness. Older provinces show higher crustal heat flow at their age of formation than younger regions, as would be expected for a cooling planet with diminishing heat flux. This is trend agrees with other geophysical models assuming that the crust contributes approximately half of the total radiogenic heat flow [*Montesi and Zuber*, 2003]. This estimate of total heat flow from radiogenic sources is plotted as the solid black line. The exception is the impact

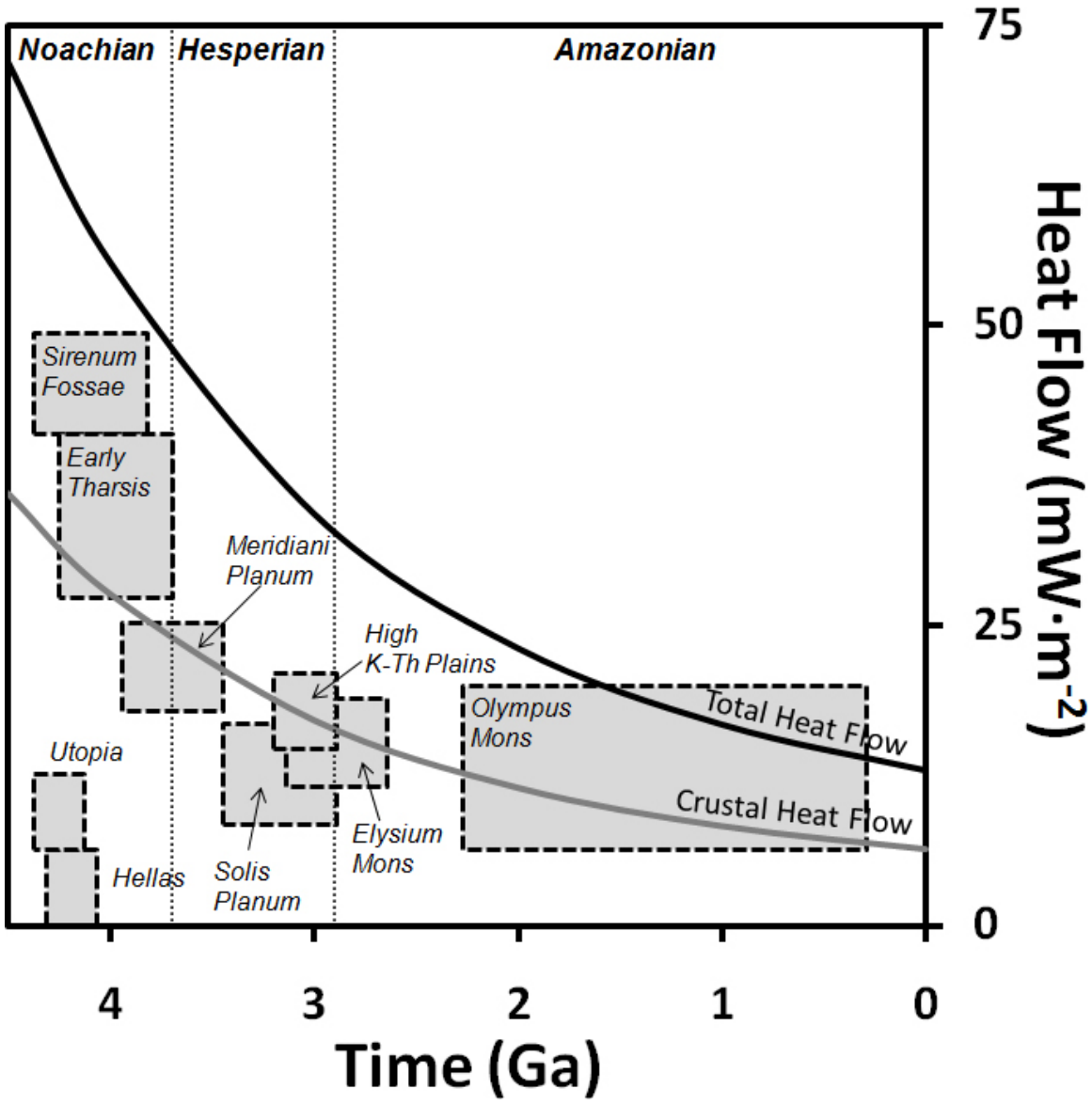

Figure 4: Heat flow modeled through Martian geologic history. The gray curve indicates the crustal component of heat flow from this study and *Hahn et al.* (Chapter 4). Gray boxes indicate the formation age and crustal component of heat flow for each geologic region or formation calculated at the age of formation. Many geologic regions fit reasonably well, with older features showing higher crustal heat flow at formation. However, some features, such as the Hellas and Utopia impact crater basins are clearly anomalous. Total radiogenic heat flow (black line) is calculated assuming the crustal component represents 50% of total heat flow due to the preferential sequestering of 50% of radiogenic elements into the crust [*Taylor et al.*, 2006ab]. Note that additional sources of heat, such as planetary secular cooling and core crystallization, are neglected. Age boundaries are from *Hartmann* (2005) and *Head et al.* (2001). After *Montesi and Zuber* (2003).

basins which are not expected to conform to a heat flow evolution model calculated using this method for the reasons detailed in **Section 3.7**, above.

An important result of this regional study and the global result presented in *Hahn et al.* (Chapter 4) is the general agreement between heat flow modeled from geophysical methods in previous studies and the crustal heat flow modeled in this study for most of the individual geologic regions examined (excluding impact basins) and for globally averaged heat flow.

One of the lingering unanswered questions from the GRS dataset is to what degree the elemental abundances measured in the upper tens of centimeters of the surface correctly reflect the underlying crust. GRS elemental compositions also agree well with sediment averages determined from landing site measurements, which likely represent a good chemical proxy for the Martian upper crust [*Hahn and McLennan*, Chapter 2]. While GRS has a greater penetration depth compared to other remote sensing instruments, the data still only reflect the upper-most tens of centimeters of the surface. Are GRS measurements heavily influenced or dominated by purely surficial and near-surficial processes and thus not representative of the crust as a whole?

For terrestrial continental crust, radiogenic isotope concentrations decrease with depth (approximately exponentially but with considerable variability) due to intracrustal melting, high grade metamorphism and tectonic processes that concentrate the incompatible heat producing elements into the more geochemically and petrologically evolved upper crust [*McLennan and Taylor,* 1996; *Taylor and McLennan*, 2009; *Nyblade and Pollack*, 1993]. However, these intracrustal differentiation processes are unlikely to

be active on Mars to any significant degree – especially on the scale of GRS pixel resolution. Orbital remote sensing instruments have not detected any major provinces of the highly-evolved igneous products that we see on Earth (i.e., granites and related rocks), and estimates of crustal composition based on sediment averages do not suggest an obvious contribution from an evolved crustal end member [*Hahn and McLennan,* Chapter 2; *Taylor and McLennan*, 2009]. There is also no definitive evidence for current or past plate tectonic processes [*Breuer and Spohn*, 2003] and geochemical mapping by the GRS reveals no statistically significant difference between the compositions of ejecta from the largest and deepest impact basins and the surrounding areas [*Boynton et al.*, 2007].

The crustal heat flow model presented here assumes that lacking terrestrial style intracrustal differentiation, the surface abundances for the radiogenic elements are near-constant vertically through the total thickness of the Martian crust. This interpretation also leads to the conclusion that approximately 50% or more of the total planetary budget of K, Th, and U have been sequestered into the crust [*Taylor et al*., 2006b; *Dreibus and Wanke,* 1985; *Wanke and Dreibus*, 1988; *Wänke*, 2001]. This assumption is supported by the agreement with previous geophysical estimates of heat flow, which have been calculated independently of radiogenic isotope abundances [*McGovern et al*., 2002, 2004; *McNutt, 1984*; *Montesi and Zuber*, 2003]. Furthermore, the heat producing elements are highly incompatible and would likely be most sensitive to fractionation from crustal processes that produce vertical chemical heterogeneity. Therefore, if this suite of incompatible heat producing elements is homogeneously distributed vertically through the crust, it is very likely that other, less-incompatible lithophile elements are similarly

distributed. We can therefore further conclude that surface abundances of the non-mobile elements measured by the GRS instrument (i.e., Si, Fe, Al, Ca, K, Th, and U, but excluding S, Cl, H) are generally representative of the underlying crust, at least over the spatially large scale of a GRS footprint.

The regional crustal heat flow estimates calculated for this study are based on the crustal abundances of radiogenic isotopes detected by GRS orbital mapping and provide valuable constraints on the thermal evolution of the Martian crust. Previous independent measurements of total crustal heat flow made by purely geophysical methods – with some notable exceptions discussed above – agree reasonably well with the results of this study. The Martian crust is an extremely important reservoir for heat production. Therefore, the results of this study will provide useful additional information for future models attempting to determine the thermal regime for volcanic provinces, deformation styles and rates, crustal dynamics, and crust-mantle interactions.

References:

Acuna, M. H., J. E. P. Connerney, P. Wasilewski, R. P. Lin, D. Mitchell, K. A. Anderson, C. W. Carlson, J. McFadden, H. Reme, C. Mazelle, D. Vignes, S. J. Bauer, P. Cloutier, and N. F. Ness (2001), Magnetic field of Mars: Summary of results from the aerobraking and mapping orbits, *J. Geophys. Res*., *106*, 23,403-23,417.

Anders, E., and N. Grevesse (1989), Abundances of the elements – Meteoritic and Solar, *Geochim. Cosmochim. Acta, 53*, 197-214.

Anderson, R. C., J. M. Dohm, M. P. Golombek, A. F. C. Haldemann, B. J. Franklin, K. L. Tanaka, J. Lias, and B. Peer (2001), Primary centers and secondary concentrations of tectonic activity through time in the western hemisphere of Mars, *J. Geophys. Res., 106*, 20563-20585.

Armstrong, R. L. (1981), Radiogenic isotopes: the case for crustal recycling on a near-steady-state no-continental-growth Earth, *Phil. Trans. Roy. Soc. Lond., A301*, 443-472.

Arvidson, R. E., S. W. Ruff, R. V. morris, D. W. Ming, L. S. Crumpler, A. S. Yen, S. W. Squyres, R. J. Sullivan, J. F. Bell, N. A. Cabrol, B. C. Clark, W. H. Farrand, R. Gellert, R. Greenberger, J. A. Grant, E. A. Guinness, K. E. Herkenhoff, J. A. Hurowitz, J. R. Johnson, G. Klingelhofer, K. W. Lewis, R. Li, T. J. McCoy, J. Moesch, H. Y. McSween, S. L. Murchie, M. Schmidt, C. Schroder, A. Wang, S. Wiseman, M. B. Madsen, W. Goetz, and S. M. McLennan (2008), Spirit Mars Rover Mission to the Columbia Hills, Gusev Crater: Mission overview and selected results from the Cumberland Ridge to Home Plate, *J. Geophys. Res., 113*, doi:10.1029/2008JE003183.

Baker, V. R. (2001), Water and the Martian landscape, *Nature, 412*, 228-236.

Bandfield, J. L., V. E. Hamilton, and P. R. Christensen (2000), A Global View of Martian Surface Compositions from MGS-TES, *Science, 287*, 1626-1630.

Banin, A., B. C. Clark, and H. Wänke (1992), Surface Chemistry and Mineralogy, in *Mars*, edited by H. H. Kieffer, B. M. Jakosky, C. W. Snyder, M. S. Matthews, pp. 594-625, University of Arizona Press, Tucson.

Bibring, J. P., Y. Langevin, A. Gendrin, B. Gondet, F. Poulet, M. Berthé, A. Soufflot, R. Arvidson, N. Mangold, J. Mustard, P. Drossart, and the OMEGA Team (2005), Mars Surface Diversity as Revealed by the OMEGA/Mars Express Observations, *Science, 307*, 1576-1581.

Bibring, J.-P., and Y. Langevin (2008), Mineralogy of the Martian surface from Mars Express OMEGA observations, in: The Martian Surface, Composition, Mineralogy, and Physical Properties, edited by J. F. Bell III, *Cambridge Univ. Press*, pp. 153-168.

Bishop, J. L., E. Z. N. Dobrea, N. K. McKeown, M. Parente, B. L. Ehlmann, J. R. Michalski, R. E. Milliken, F. Poulet, G. A. Swayze, J. F. Mustard, S. L. Murchie, and J.-P. Bibring (2008), Phyllosilicate diversity and past aqueous activity revealed at Mawrth Vallis, Mars, *Science, 321*, 830-833.

Borg, L.E., and D. S. Draper (2003), A petrogenetic model for the origin and compositional variation of the martian basaltic meteorites, *Meteorit. Planet. Sci., 38*, 1713-1731.

Boynton, W. V., G. J. Taylor, L. G. Evans, R. C. Reedy, R. Starr, D. M. Janes, K. Kerry, D. M. Drake, K. J. Kim, R. M. S. Williams, K. Crombie, J. M. Dohm, V. Baker, A. E. Metzger, S. Karunatillake, J. Keller, H. E. Newsom, J. R. Arnold, J. Brckner, P. A. J. Englert, O. Gasnault, A. L. Sprague, I. Mitrofanov, S. W. Squyres, J. I. Trombka, L. d'Uston, and H. Wanke, D. K. Hamara (2007), Concentration of H, Si, Cl, K, Fe, and Th in the low and mid latitude regions of Mars, *J. Geophys. Res*., *112*, doi: 10.1029/2007JE002887.

Boynton, W.V., W. C. Feldman, I. G. Mitrofanov, L. G. Evans, R. C. Reedy, S. W. Squyres, R. D. Starr, J. I. Trombka, C. d'Uston, J. R. Arnold, P. A. Englert, A. E. Metzger, H. Wänke, J. Brückner, D. M. Drake, C. Shinohara, C. Fellows, D. K. Hamara, K. Harshman, K. E. Kerry, C. Turner, M. Ward, H. Barthe, K. R. Fuller, S. A., Storms, G. W. Thornton, J. L. Longmire, M. L. Litvak and A. K. Ton'chev (2004) The Mars Odyssey Gamma-Ray Spectrometer Instrument Suite, *Space Sci. Rev., 10*, 37-83.

Breuer, D., and T. Spohn (2003), Early plate tectonics versus single-plate tectonics on Mars: Evidence from magnetic field history and crust evolution, *J. Geophys. Res., 108*, doi:10.1029/2002JE001999.

Brückner, J., G. Dreibus, R. Reider, and H. Wänke (2003), Refined data of Alpha Proton X-ray Spectrometer analyses of soils and rocks at the Mars Pathfinder site: Implications for surface chemistry, *J. Geophys. Res., 108*, doi:10.1029/2003JE002060.

Buczkowski, D. L., H. V. Frey, J. H. Roark, and G. E. McGill (2005), Buried impact craters: A topographic analysis of quasi-circular depressions, Utopia Basin, Mars, *J. Geophys. Res*., *110*, doi:10.1029/2004JE002324.

Carr, M. H. (2006), *The Surface of Mars,* Cambridge University Press, Cambridge, UK, p. 93.

Carr, M. H., and J. W. Head (2009), Geologic history of Mars, *Earth Planet. Sci. Lett., in press*, doi:10.1016/j.epsl.2009.06.042.

Christensen, P. R., H. Y. McSween, J. L. Bandfield, S. W. Ruff, A. D. Rogers, V. E. Hamilton, N. Gorelick, M. B. Wyatt, B. M. Jakosky, H. H. Kieffer, M. C. Malin, and J. E. Moersch (2005), Evidence for magmatic evolution and diversity on Mars from infrared observations. *Nature, 436*, 504-509.

Christensen, P. R., J. L. Bandfield, R. N. Clark, K. S. Edgett, V. E. Hamilton, T. Hoefen, H .H. Kieffer, R. O. Kuzmin, M. D. Lane, M. C. Malin, R. V. Morris, J. C. Pearl, R. Pearson, T. L. Roush, S. W. Ruff, and M. D. Smith (2000), Detection of crystalline hematite mineralization on Mars by the Thermal Emission Spectrometer: Evidence for near-surface water, *J. Geophys. Res*., *105*, 9623-9642.

Christensen, P. R., J. L. Bandfield, V. E. Hamilton, S. W. Ruff, H. H. Kieffer, T. N. Titus, M. C Malin, R. V. Morris, M. D. Lane, R. L. Clark, B. M. Jakosky, M. . Mellon, J. C. Pearl, B. J. Conrath, M. D. Smith, R. T. Clancy, R. O. Kuzmin, T. Roush, G. L. Mehall, N. Gorelick, K. Bender, K. Murray, S. Dason, E. Greene, S. Silverman, and M. Greenfield (2001), Mars Global Surveyor Thermal Emission Spectrometer experiment: Investigation, description, and surface science results, *J. Geophys. Res., 106*, 23823-23871.

Christensen, P. R., J. L. Banfield, J. F. Bell, N. Gorelick, V. E. Hamilton, A. Ivanov, B. M. Jakosky, H. H. Kieffer, M. D. Lane, M. C. Malin, T. McConnochie, A. S. McEwen, H. Y. McSween, G. L. Mehall, J. E. Moersch, K. H. Nealson, J. W. Rice, M. I. Richardson, S. W. Ruff, M .D. Smith, T. N. Titus, and M .B. Wyatt (2003), Morphology and composition of the surface of Mars: Mars Odyssey THEMIS results, *Science, 300*, 2056-2061.

Clark, B. C., A. K. Baird, R. J. Weldon, D. M. Tsusaki, L. Schnabel, and M. P. Candelaria (1982), Chemical Composition of Martian Fines, *J. Geophys. Res., 87*, 10059-10067.

Clark, B. C., R. V. Morris, S. M. McLennan, R. Gellert, B. Jolliff, A. H. Knoll, S. W. Squyres, T. K. Lowenstein, D. W. Ming, N. J. Tosca, A. Yen, P. R. Christensen, S. Gorevan, J. Brückner, W. Calvin, G. Dreibus, W. Farrand, G. Klingelhoefer, H. Wänke, J. Zipfel, J. F. Bell, J. Grotzinger, H. Y. McSween, and R. Rieder (2005), Chemistry and mineralogy of outcrops at Meridiani Planum, *Earth Planet. Sci. Lett., 240,* 73-94.

Condie, K. C. (1993), Chemical composition and evolution of the upper continental crust: Contrasting results from surface samples and shales, *Chem. Geol., 104*, 1-37.

Dohm, J. M., K. E. Kerry, J. M. Keller, V. R. Baker, W. V. Boynton, S. Maruyama, and R. C. Anderson (2005), Mars Geological province designations for the interpretation of GRS data. *Lunar Planet. Sci. XXXVII*, abstract #1567.

Dohm, J. M., K. L. Tanaka, and T. M. Hare (2001), Geologic map of the Thaumasia region of Mars, *USGS Atlas of Mars – Geologic Series I-2650*.

Dreibus, G., and H. Wänke (1985), Mars, a Volatile-Rich Planet, *Meteor. Planet. Sci., 20*, 367-381.

Elkins-Tanton, L. T., E. M. Parmentier, and P. C. Hess (2003), Magma ocean fractional crystallization and cumulate overturn in terrestrial planets: Implications for Mars, *Meteorit. Planet. Sci., 38*, 1753-1771.

Elkins-Tanton, L. T., E. M. Parmentier, and P. C. Hess (2005), Possible formation of ancient crust on Mars through magma ocean processes, *J. Geophys. Res., 110*, doi:10.1029/2005JE002480.

Eugster, O., A. Weigel, and E. Polnau (1997), Ejection times of Martian meteorites, *Geochim. Cosmochim. Acta, 61*, 2749-2757.

Evans, L. G., R. C. Reedy, R. D. Starr, K. E. Kerry, and W. V. Boynton (2006), Analysis of gamma ray spectra measured by Mars Odyssey, *J. Geophys. Res., 111,* doi:10.1029/2005JE002657.

Fairén, A. G. and J. M. Dohm (2004), Age and origin of the lowlands of Mars, *Icarus, 168*, 277-284.

Fairén, A. G., D. Fernández-Remolar, J. M. Dohm, V. R. Baker, and R. Amils (2004), Inhibition of carbonate synthesis in acidic oceans on early Mars, *Nature, 431*, 423-426.

Fairén, A.G., J. M. Dohm, V. R. Baker, M. A. de Pablo, J. Ruiz, J. C. Ferris, and R. C. Anderson (2003), Episodic flood inundations of the northern plains of Mars, *Icarus, 165*, 53-67.

Feldman, W. C., T. H. Prettyman, S. Maurice, J. J. Plaut, D. L. Bish, D. T. Vaniman, M. T. Mellon, A. E. Metzger, S. W. Squyres, S. Karunatillake, W. V. Boynton, R. C. Elphic, H. O. Funsten, D. J. Lawrence, and R. L. Tokar (2004), Global distribution of near-surface hydrogen on Mars, *J. Geophys. Res., 106*, doi: 10.1029/2003JE002160.

Frey, H. V. (2006), Impact constraints on, and a chronology for, major events in early Mars history, *J. Geophys. Res., 111*, doi: 10.1029/2005JE002449.

Frey, H. V., J. H. Roark, K. M. Shockey, E. L. Frey, and S. E. H. Sakimoto (2002), Ancient lowlands on Mars, *Geophys. Res. Lett., 29*, doi:10.1029/2001GL013832

Gasnault, O. (2006), Unsupervised Definition of Chemically Distinct Provinces at Mars, *Lunar Planet. Sci. XXXVII*, abstract #2328.

Gellert, R., R. Rieder, R. C. Anderson, J. Brückner, B. C. Clark, G. Dreibus, T. Economou, G. Klingelhöfer, G. W. Lugmair, D. W. Ming, S. W. Squyres, C. d'Uston, H. Wänke, A. Yen, and J. Zipfel (2004), Chemistry of Rocks and Soils in Gusev Crater from the Alpha Particle X-ray Spectrometer, *Science, 305*, 829-832.

Gillis, J. J., B. L. Jolliff, and R. L. Korotev (2004), Lunar surface geochemistry: Global concentrations of Th, K, and FeO as derived from lunar prospector and Clementine data, *Geochim. Cosmochim. Acta, 68*, 3791-3805.

Goetz, W., S. F. Hviid, K. M. Kinch, and M. B. Madsen (2008), Magnetic properties of Martian surface materials, in *The Martian Surface: Composition, Mineralogy, and Physical Properties*, edited by J. Bell, pp. 366-380, Cambridge University Press, Cambridge.

Golombek, M. P., F. S. Andersen, and M. T. Zuber (2001), Martian wrinkle ridge topography: Evidence for subsurface faults from MOLA, *J. Geophys. Res., 106*, 23,811-23,821.

Golombek, M. P., J. A. Grant, L. S. Crumpler, R. Greeley, R. E. Arvidson, J. F. Bell, C. M. Weitz, R. Sullivan, P. R. Christensen, L. A. Soderblom, and S. W. Squyres (2006), Erosion rates at the Mars Exploration Rover landing sites and long-term climate change on Mars, *J. Geophys. Res., 111*, doi:10.1029/2006JE002754.

Golombek, M. P., J. A. Grant, T. J. Parker, D. M. Kass, J. A. Crisp, S. W. Squyres, A. F. C. Haldemann, M. Adler, W. J. Lee, N. T. Bridges, R. E. Arvidson, M. H. Carr, R. L. Kirk, P. C. Knocke, R. B. Roncoli, C. M. Weitz, J. T. Schofield, R. W. Zurek, P. R. Christensen, R. L. Fergason, F. S. Anderson, and J. W. Rice (2003), Selection of the Mars Exploration Rover landing sites, *J. Geophys. Res., 108*, doi:10.1029/2003JE002074.

Golombek, M. P., L. S. Crumpler, J. A. Grant, R. Greeley, N. A. Cabrol, T. J. Parker, J. W. Rice, J. G. Ward, R. E. Arvidson, J. E. Moersch, R. L. Fergason, P. R. Christensen, A. Castaño, R. Castaño, A. F. C. Haldemann, R. Li, J. F. Bell III, and S. W. Squyres (2006), Geology of the Gusev cratered plains from the Spirit rover transverse, *J. Geophys. Res., 111*, doi:10.1029/2005JE002503.

Golombek, M. P., R. A. Cook, H. J. Moore, and T. J. Parker (1997), Selection of the Mars Pathfinder landing site, *J. Geophys. Res., 102*, 3967-3988.

Golombek, M. P., R. C. Anderson, J. R. Barnes, J. F. Bell, N. T. Bridges, D. T. Britt, J. Bruckner, R. A. Cook, D. Crisp, J. A. Crisp, T. Economou, W. M. Folkner, R. Greeley, R. M. Haberle, R. B. Hargraves, J. A. Harris, A. F.C. Haldemann, K. E. Herkenhoff, S. F. Hviid, R. Jaumann, J. R. Johnson, P. H. Kallemeyn, H. U. Keller, R. L. Kirk, J. M. Knudsen, S. Larsen, M. T. Lemmon, M. B. Madsen, J. A. Magalhaes, J. N. Maki, M. C. Malin, R. M. Manning, J. Matijevic, H. Y. McSween, H. J. Moore, S. L. Murchie, J. R. Murphy, T. J. Parker, R. Rieder, T. P. Rivellini, J. T. Schofield, A. Seiff, R. B. Singer, P. H. Smith, L. A. Soderblom, D. A. Spencer, C. R. Stoker, R. Sullivan, N. Thomas, S. W. Thurman, M. G. Tomasko, R. M. Vaughan, H. Wanke, A. W. Ward, and G. R. Wilson (1999), Overview of the Mars Pathfinder Mission: Launch through landing, surface operations, data sets, and science results, *J. Geophys. Res., 104*, 8523-8553.

Gooding, J. L., R. E. Arvidson, and M. Y. Zolotov (1992), Physical and Chemical Weathering, in *Mars*, H. H. Kieffer, B. M. Jakosky, C. W. Snyder, M. S. Matthews (Eds.), pp. 626-651, University of Arizona Press, Tucson.

Grant, J. A., R. E. Arvidson, L. S. Crumpler, M. P. Golombek, B. C. Hahn, A. F. C. Haldemann, R. Li, L. A. Soderblom, S. W. Squyres, S. P. Wright, and W. A. Watters (2006), Crater gradation in Gusev crater and Meridiani Planum, Mars, *J. Geophys. Res., 111*, doi:10.1029/2005JE002465.

Greeley, R., and J. E. Guest (1987), Geologic Map of the Eastern Equatorial Region of Mars, *USGS Atlas of Mars – Geologic Series I-1802B*.

Greeley, R., N. Lancaster, S. Lee, and P. Thomas (1992) Martian Aeolian Processes, Sediments, and Features, in *Mars*, edited by H. H. Kieffer, B. M. Jakosky, C. W. Snyder, M. S. Matthews, pp. 730-766, University of Arizona Press, Tucson.

Grotzinger, J. P., R. E. Arvidson, J. F. Bell, W. Calvin, B. C. Clark, D. A. Fike, M. golombek, R. Greeley, A, Haldemann, K. E. Herkenhoff, B. L. Jolliff, A. H. Knoll, M. Malin, S. M. McLennan, T. Parker, L. Soderblom, J. N. Sohl-Dickstein, S. W. Squyres, N. J. Tosca, and W. A. Watters (2005), Stratigraphy and sedimentology of a dry to wet eolian deposition system, Burns formation, Meridiani Planum, Mars, *Earth Planet. Sci. Lett., 240*, 11-72.

Hahn, B. C., and S. M. McLennan (2008), Martian surface heat production and crustal heat flow from Mars Odyssey Gamma-Ray Spectrometry, *Lunar and Planetary Science Conference XXXIX*, Houston, TX, Abstract #2032.

Hahn, B. C., S. M. McLennan, G. J. Taylor, W. V. Boynton, J. M. Dohm, M. J. Finch, D. K. Hamara, D. M. Janes, S. Karunatillake, J. M. Keller, K. E. Kerry, and R. M. S. Williams (2007) The Odyssey GRS Science Team, Mars Odyssey Gamma-Ray Spectrometer Elemental Abundances and Apparent Relative Surface Age: Implications for Martian Crustal Evolution, *J. Geophys. Res., 112*, doi:10.1029/2006JE002821.

Haining, R. (2003), *Spatial Data Analysis: Theory and Practice*, Cambridge Univ. Press, Cambridge.

Halliday, A. N., H. Wänke, J. L. Birck, and R. N. Clayton (2001), The accretion, composition and early differentiation of Mars, *Space Sci. Rev., 96*, 197-230.

Hamilton, V. E., P. R. Christensen, and J. L. Bandfield (2003), Searching for the source regions of martian meteorites using MGS TES: Integrating martian meteorites into the global distribution of igneous materials on Mars, *Meteor. Planet. Sci., 38*, 871-885.

Hartmann, W. K. (2005), Martian cratering 8: Isochron refinement and the chronology of Mars, *Icarus, 174*, 294-320.

Hartmann, W. K., and G. Neukum (2001), Cratering chronology and the evolution of Mars, *Space Sci. Rev., 96,* 165-194.

Hartmann, W. K., J. Anguita, M. A. de la Casa, D. C. Berman, and E. V. Ryan (2001), Martian cratering 7: The role of impact gardening, *Icarus, 149*, 37-53.

Haskin, L. A., A. Wang, B. L. Joliff, H. Y. McSween, B. C. Clark, D. J. DesMarais, S. M. McLennan, N. J. Tosca, J. A. Hurowitz, J. D. Farmer, A. Yen, S. W. Squyres, R. E. Arvidson, G. Klingelhöfer, C. Schröder, P. A. de Souza, D. W. Ming, R. Gellert, J. Zipfel, J. Brückner, J. F. Bell, K. Herkenhoff, P. R. Christensen, S. Ruff, D. Blaney, S. Gorevan, N. A. Cabrol, L. Crumpler, J. Grant, and L. Soderblom (2005), Water alteration of rocks and soils on Mars at the Spirit rover site in Gusev Crater, *Nature, 436*, 66-69.

Haskin, L. A., J. J. Gillis, R. L. Korotev, and B. L. Jolliff (2000), The materials of the lunar Procellarum KREEP Terrane: A synthesis of data from geomorphological mapping, remote sensing, and sample analyses, *J. Geophys. Res., 105*, 20403-20415.

Head, J. W., R. Greeley, M. P. Golombek, W. K. Hartmann, E. Hauber, R. Jaumann, G. Neukum, L. E. Nyquist, and M. H. Carr (2001), Geologic processes and evolution, *Space Sci. Rev., 96*, 263-292.

Hurowitz J. A., S. M. McLennan, N. J. Tosca, R. E. Arvidson, J. R. Michalski, D. W. Ming, C. Schröder, and S. W. Squyres (2006), In situ and experimental evidence for acidic weathering of rocks and soils on Mars, *J. Geophys. Res., 111*, doi:10.1029/2005JE002515.

Hurowitz, J. A., and S. M. McLennan (2007), A similar to 3.5 Ga record of water-limited, acidic weathering conditions on Mars, Earth Planet. Sci. Lett., 260, 432-443.

Hurowitz, J. A., S. M. McLennan, H. Y. McSween, P. A. DeSouza, and G. Klingelhofer (2006), Mixing relationships and the effects of secondary alteration in the Wishstone and Watchtower classes of Husband Hill, Gusev Crater, Mars, *J. Geophys. Res., 111*, doi:10.1029/2006JE002795.

Hynek, B. M., R. E. Arvidson, and R. J. Phillips (2002), Geologic setting and origin of Terra Meridiani hematite deposit on Mars. *J. Geophys. Res., 107,* doi:10.1029/2002JE001891.

Ivanov, B. A. (2001), Mars/Moon Cratering Rate Ratio Estimates, *Space Sci. Rev.*, *96*, 87-104.

Jagoutz, E. (1991), Chronology of SNC Meteorites, *Space Sci. Rev., 56*, 13-22.

Jaupart, C., and J.-C. Mareschal (2006) Constraints on crustal heat production from heat flow data. In: Rudnick, R. L. (ed.) *Treatise on Geochemistry*, Vol. 3: The Crust, Elsevier, pp. 65-84.

Jerram, D. A., and M. Widdowson (2005), The anatomy of Continental Flood Basalt Provinces: geologic constraints on the processes and products of flood volcanism, *Lithos, 79*, 385-405.

Jolliff, B. L., B. C. Clark, D. W. Mittlefehldt, R. Gellert, and the Athena Science Team (2007), Composition of spherules and rock surface at Meridiani, *Seventh International Conference on Mars*, Abstract #3374.

Kahn, R. A., T. Z. Martin, R. W. Zurek, and S. W. Lee (1992) The Martian Dust Cycle, in *Mars*, edited by H. H. Kieffer, B. M. Jakosky, C. W. Snyder, M. S. Matthews, pp. 1017-1053, University of Arizona Press, Tucson.

Karunatillake, S, J. M. Keller, S. W. Squyres, W. V. Boynton, J. Bruckner, D. M. Janes, O. Gasnault, and H. E. Newsom (2007), Chemical compositions at Mars landing sites subject to Mars Odyssey Gamma Ray Spectrometer constraints, *J. Geophys. Res., 112*, doi:101029/2006JE002859.

Karunatillake, S., S. W. Squyres, G. J. Taylor, J. M. Keller, O. Gasnault, L. G. Evans, R. C. reedy, R. D. Starr, W. V. Boynton, D. M. Janes, K. E. Kerry, J. M. Dohm, A. L. Sprague, B. C. Hahn, and D. K. Hamara (2006) Composition of northern low-albedo regions of Mars: Insights from the Mars Odyssey Gamma Ray Spectrometer, *J. Geophys. Res., 111,* doi:10.1029/2006JE002675.

Karunatillake, S., S. W. Squyres, J .J. Wray, G. J. Taylor, O. Gasnault, S. M. McLennan, W. V. Boynton, M. R. El Maarry, and J. M. Dohm (2009), Chemically striking regions on Mars and Stealth revisited, *J. Geophys. Res.,* doi:10.1029/2008JE003303 (*in press*).

Keller, J. M., W. V. Boynton, S. Karunatillake, V. R. Baker, J. M. Dohm, L. G. Evans, M. J. Finch, B. C. Hahn, D. K. Hamara, D. M. Janes, K. E. Kerry, H. E. Newsom, R. C. Reeder, A. L. Sprague, S. W. Squyres, R. D. Starr, G. J. Taylor and R. M. S. Williams (2006), Equitorial and midlatitude distribution of chlorine measured by Mars Odyssey GRS, *J. Geophys. Res., 111, doi:*10.1029/2006JE002679.

Kieffer, H. H., and A. P. Zent (1992) Quasi-Periodic Climate Change on Mars, in *Mars*, edited by H. H. Kieffer, B. M. Jakosky, C. W. Snyder, M. S. Matthews, pp. 1080-1218, University of Arizona Press, Tucson.

Knoll, A. H., M. Carr, B. C. Clark, D. J. Des Marais, J. D. Farmer, W. W. Fischer, J. P. Grotzinger, S. M. McLennan, M. Malin, C. Schröder, S. W. Squyres, N. J. Tosca, and T. Wdowiak (2005) An astrobiological perspective on Meridiani Planum, *Earth Planet. Sci. Lett., 240*, 179-189.

Korotev, R. L., (1998), Concentrations of radioactive elements in lunar materials, *J. Geophys. Res., 103*, 1691-1701.

Korotev, R. L., B. L. Jolliff, R. A. Zeigler, J. J. Gillis, and L. A. Haskin (2003), Feldspathic lunar meteorites and their implications for compositional remote sensing of the lunar surface and the composition of the lunar crust, *Geochim Cosmochim Acta, 67*, 4895-4923.

Laul, J. C., M. R. Smith, H. Wänke, E. Jagoutz, G. Dreibus, H. Palme, B. Spettel, A. Burghele, M. E. Lipschutz, and R. M. Verkouteren (1986), Chemical systematic of the shergotty meteorite and the composition of its parent body (Mars), *Geochim. Cosmochim. Acta, 50,* 909-926.

Lemoine, F. G., D. E. Smith, D. D. Rowlands, M. T. Zuber, G. A. Neumann, D. S. Chinn, and D. E. Pavlis (2001), An improved solution of the gravity field of Mars (GMM-2B) from Mars Global Surveyor, *J. Geophys. Res., 106,* 23,359-23,376.

Lewis, J. W., O. Aharonson, J. P. Grotzinger, S. W. Squyres, J. F. Bell, L. S. Crumpler, and M. E. Schmidt (2008), Structure and stratigraphy of Home Plate from Spirit Mars Exploration Rover, *J. Geophys. Res., 113*, doi:10.1029/2007JE003025.

Lucey, P., R. L. Korotev, J. J. Gillis, L. A. Taylor, D. Lawrence, B. A. Campbell, R. Elphic, B. Feldman, L .L. Hood, D. Hunten, M. Mendillo, S. Noble, J. J. Papike, R. C. Reedy, S. Lawson, T. Prettyman, O. Gasnault, and S. Maurice (2006), Understanding the Lunar Surface and Space-Moon Interactions, *Space Sci. Rev., 60*, 83-219.

McEwen, A. S., B. S. Preblich, E. P. Turtle, N. A. Artemieva, M. P. Golombek, M. Hurst, R. L. Kirk, D. M. Burr, and P. R. Christensen (2005), The rayed crater Zunil and interpretations of small impact craters on Mars, *Icarus*, *176*, 351-381.

McGovern, P. J., S. C. Solomon, D. E. Smith, M. T. Zuber, M. Simons, M. A. Wieczorek, R. J. Phillips, G. A. Neumann, O. Aharonson, and J. W. Head (2002), Localized gravity/topography admittance and correlation spectra on Mars: Implications for regional and global evolution, *J. Geophys. Res., 107,* doi:10.1029/2002JE001854.

McGovern, P. J., S. C. Solomon, D. E. Smith, M. T. Zuber, M. Simons, M. A. Wieczorek, R. J. Phillips, G. A. Neumann, O. Aharonson, and J.W. Head (2004) Correction to "Localized gravity/topography admittance and correlation spectra on Mars: Implications for regional and global evolution". *J. Geophys. Res., 107,* doi:10.1029/2002JE001854.

McLennan, S. M. (2001), Crustal heat production and the thermal evolution of Mars. *Geophys. Res. Lett., 28*, 4019-4022.

McLennan, S. M. (2001), Relationships between the trace element composition of sedimentary rocks and upper continental crust. *Geochem. Geophys. Geosys., 2*, doi:2000GC000109.

McLennan, S. M. (2003), Large-ion lithophile element fractionation during the early differentiation of Mars and the composition of the martian primitive mantle, *Meteor. Planet. Sci., 38*, 895-904.

McLennan, S. M., and S. R. Taylor (1996), Heat flow and the chemical composition of continental crust, *J. Geo., 104*, 369-377.

McLennan, S. M., J. F. Bell, W. M. Calvin, P. R. Christensen, B. C. Clark, P. A. de Souza, J. Farmer, W. H. Farrand, D. A. Fike, R. Gellert, A. Ghosh, T. D. Glotch, J. P, Grotzinger, B. C. Hahn, K. E. Herkenhoff, J. A. Hurowitz, J. R. Johnson, S. S.Johnson, B. Jolliff, G. Klingelhofer, A. H. Knoll, Z. Learner, M. C. Malin, H. Y. McSween, J. Pocock, S. W. Ruff, L. A. Soderblom, S. W. Squyres, N. J. Tosca, W. A. Watters, M. B. Wyatt, and A. Yen (2005), Provenance and diagenesis of the evaporite-bearing Burns formation, Meridiani Planum, Mars, *Earth Planet. Sci. Lett., 240*, 95-121.

McLennan, S. M., S. R. Taylor, and S. R. Hemming (2006) Composition, differentiation, and evolution of continental crust: Constraints from sedimentary rocks and heat flow, in: Evolution and Differentiation of the Continental Crust, edited by M. Brown, T. Rushmer, *Cambridge Univ. Press*, pp. 92-134.

McNutt, M. K. (1984), Lithospheric flexure and thermal anomalies, *J. Geophys. Res., 89*, 11,180-11,194.

McSween, H. Y. (2002), The rocks of Mars, from far and near, *Meteor. Planet. Sci., 37*, 7-25.

McSween, H. Y., G. J. Taylor, and M. B. Wyatt (2009), Elemental composition of the Martian crust, *Science, 324*, 736-739.

McSween, H. Y., T. L. Grove, and M. B. Wyatt (2003), Constraints on the composition and petrogenesis of the Martian crust, *J. Geophys. Res., 108*, doi:10.1029/2003JE002175.

Meyer, C. (2006), *Mars meteorite compendium*, NASA Lyndon B. Johnson Space Center, Houston, TX.

Mitchell, D. L., R. J. Lillis, R. P. Lin, J. E. P. Connerney, and M. H. Acuna (2007), A global map of Mars' crustal magnetic field based on electron reflectometry, *J. Geophys. Res*., *112*, doi: 10.1029/2005JE002564.

Montési, L. G. J., and M. T. Zuber (2003), Clues to the lithospheric structure of Mars from wrinkle ridge sets and localization instability. *J. Geophys. Res., 108*, doi:10.1029/2002JE001974.

Nekvasil, H., F. M. McCubbin, A. Harrington, S. Elardo, D. H. Lindsley (2009), Linking the Chassigney meteorite and the Martian surface rock Backstay: Insight into igneous crustal differentiation processes on Mars, *Meteor. Planet. Sci., 44*, 853-869.

Neukum, G., B. A. Ivanov, and W. K. Hartmann (2001), Cratering Records in the Inner Solar System in Relation to the Lunar Reference System, *Space Sci. Rev., 96,* 55-86.

Neumann, G. A., M. T. Zuber, M. A. Wieczorek, P. J. McGovern, F. G. Lemoine, and D. E. Smith (2004) Crustal structure of Mars from gravity and topography. *J. Geophys. Res., 109*, doi:10.1029/2004JE002645.

Newsom, H. E., L. S. Crumpler, R. C. Reedy, M. T. Petersen, G. C. Newsom, L. G. Evans, G. J. Taylor, J. M. Keller, D. M. Janes, W. V. Boynton, K. E. Kerry, and S. Karunatillake (2007), Geochemistry of Martian soil and bedrock in mantled and less mantled terrains with gamma ray data from Mars Odyssey, *J. Geophys. Res., 112,* doi:10.1029/2006JE002680.

Nimmo, F., and K. L. Tanaka (2005), Early Crustal Evolution of Mars, *Annu. Rev. Earth Planet. Sci., 33,* 133-161.

Norman, M. D., (1999), The composition and thickness of the crust of Mars estimated from rare earth elements and neodymium-isotopic compositions of Martian meteorites, *Meteor. Planet. Sci., 34*, 439-449.

Norman, M. D., (2002), Thickness and Composition of the Martian Crust Revisited: Implications of an Ultradepleted Mantle with a Nd Isotopic Composition like that of QUE94201, *Lunar and Planetary Science Meeting XXXIII*, Abstract #1175.

Nunes, D. C., and R. J. Phillips (2006), Radar subsurface mapping of the polar layered deposits on Mars, *J. Geophys. Res., 111,* doi:10.1029/2005JE002609.

Nyblade, A. A., and Pollack, H. N. (1993), A Global Analysis of Heat-Flow from Precambrian Terrains – Implications for the Thermal Structure of Archean and Proterozoic Lithosphere, *J. Geophys. Res., 98,* 12,207-12,218.

Nyquist, L. E., D. D. Bogard, C. Y. Shih, A. Greshake, D. Stoffler, and O. Eugster (2001), Ages and geologic histories of Martian meteorites, *Space Sci. Rev., 96*, 105-164.

Phillips, R. J., M. T. Zuber, S. C. Solomon, M. P. Golombek, B. M. Jakosky, W. B. Banerdt, D. E. Smith, R. M. E. Williams, B. M. Hynek, O. Aharonson, and S. A. Hauck (2001), Ancient geodynamics and global-scale hydrology on Mars, *Science, 291,* 2587-2591.

Phillips, R. J., M. T. Zuber, S. E. Smrekar, M. T. Mellon, J. W. Head, K. L. Tanaka, N. E. Putzig, S. M. Milkovich, B. A. Campbell, J. J. Plaut, A. Safaeinili, R. Seu, D. Biccari, L. M. Carter, G. Picardi, R. Orosei, P. S. Mohit, E. Heggy, R. W. Zurek, A. F. Egan, E. Giacomoni, F. Russo, M. Cutigni, E. Pettinelli, J. W. Holt, C. J. Leuschen, and L. Marinangeli (2009), Mars North Polar Deposits: Stratigraphy, Age, and Geodynamical Response, *Science, 320*, 1182-1185.

Plank, T., and C. H. Langmuir (1998), The chemical composition of subducting sediment and its consequences for the crust and mantle, *Chem. Geol., 145*, 325-394.

Prettyman, T. W. C., D. J. Feldman, G. W. Lawrence, A. B. McKinney, R. C. Binder, O. M. Elphic, S. Maurice, and K. R. Moore (2002), Library least squares analysis of Lunar Prospector gamma ray spectra, *Lunar and Planetary Science Conference XXXII*, Houston, TX, Abstract #2012.

Richter, F. M., D. B. Rowley, and D. J. DePaolo (1992), Sr isotope evolution of seawater: the role of tectonics, *Earth Planet. Sci. Lett., 109*, 11-23.

Rieder, R., R. Gellert, R. C. Anderson, J. Brückner, B. C Clark, G. Dreibus, T. Economou, G. Klingelhöfer, G. W. Lugmair, D. W. Ming, S. W. Squyres, C. d'Uston, H. Wänke, A. Yen, and J. Zipfel (2004), Chemistry of Rocks and Soils at Meridiani Planum from the Alpha Particle X-ray Spectrometer*, Science, 306*, 1746-1749.

Ronov, A. B. (1983), The Earth's sedimentary shell: Quantitative patterns of its structure, compositions, and evolution, *Amer. Geol. Inst. Reprint Series V*, pp. 80.

Rudnick, R. L., and S. Gao (2003), Composition of the continental crust, in The Crust, edited by R. L. Rudnick, *Treatise on Geochemistry*, pp. 1-64, Elsevier vol. 3.

Ruiz, J., R. Tejero, and P. J. McGovern (2006), Evidence for a differentiated crust in Solis Planum, Mars, from lithospheric strength and heat flow. *Icarus, 180*, 308-313.

Schröder, C., D. S. Rodionov, T. J. McCoy, B. L. Jolliff, R. Gellert, L. R. Nittler, W. H. Farrand, J. R. Johnson, S. W. Ruff, J. W. Ashley, D. W. Mittlefehldt, K. E. Herkenhoff, I. Fleischer, A. F. C. Haldemann, G. Klingelhöfer, D. W. Ming, R. V. Morris, P. A. de Souze Jr., S. W. Squyres, C. Weitz, A. S. Yen, J. Zipfel, and T. Economou (2008), Meteorites on Mars observed with the Mars Exploration Rovers, *J. Geophys. Res., 113*, doi:10.1029/2007JE002990.

Scott, D. H., and K. L. Tanaka (1986) Geologic Map of the Western Equatorial Region of Mars, *USGS Atlas of Mars – Geologic Series I-1802A*.

Scott, D.H., and M. H. Carr (1978), Geologic map of Mars, *USGS Atlas of Mars – Geologic Series I-1083*.

Searls, M. L., W. B. Banerdt, and R. J. Phillips (2006), Utopia and Hellas basins, Mars: Twins separated at birth, *J. Geophys. Res., 111,* doi:10.1029/2005JE002666.

Soffen, G. A. (1977), The Viking Project, *J. Geophys. Res., 82*, 3959-3970.

Spohn, T., M. H. Acuna, D. Breuer, M. Golombek, R. Greeley, A. N. Halliday, E. Hauber, R. Jaumann, and F. Sohl (2001) Geophysical constraints on the evolution of Mars. *Space Sci. Rev., 96*, 231-262.

Squyres, S. W., R. E. Arvidson, D. Bollen, J. F. Bell, J. Bruckner, N. A. Cabrol, W. Calvin, M. H. Carr, P. R. Christensen, B. C. Clark, L. Crumpler, D. J. Des Marais, C. d'Uston, T. Economou, J. Farmer, W. Farrand, W. Folkner, R. Gellert, T. D. Glotch, M. Golombek, S. Gorevan, J. A. Grant, R. Greeley, J. Grotzinger, K. E. Herkenhoff, S. Hviid, J. Johnson, G. Klingelhofer, A. Knoll, G. Landis, M. Lemmon, R. Li, M. B. Madsen, M. C. Malin, S. M. McLennan, H. Y. McSween, D. W. Ming, J. Moersch, R. V. Morris, T. Parker, J. W. Rice, L. Richter, R. Rieder, C. Schroder, M. Sims, M. Smith, P. Smith, L. A. Soderblom, R. Sullivan, N. J. Tosca, H. Wanke, T. Wdowiak, M. Wolff, and A. Yen (2006), Overview of the Mars Exploration Rover mission to Meridiani Planum: Eagle crater to Purgatory ripple, *J. Geophys. Res., 111,* doi:10.1029/2006JE002771.

Squyres, S. W., R. E. Arvidson, J. F. Bell, J. Bruckner, N. A. Cabrol, W. Calvin, M. H. Carr, P. R. Christensen, B. C. Clark, L. Crumpler, D. J. Des Marais, C. d'Uston, T. Economou, J. Farmer, W. Farrand, W. Folkner, M. Golombek, S. Gorevan, J. A. Grant, R. Greeley, J. Grotzinger, L. Haskin, K. E. Herkenhoff, S. Hviid, J. Johnson, G. Klingelhofer, A. Knoll, G. Landis, M. Lemmon, R. Li, M. B. Madsen, M. C. Malin, S. M. McLennan, H. Y. McSween, D. W. Ming, J. Moersch, R. V. Morris, T. Parker, J. W. Rice, L. Richter, R. Rieder, M. Sims, M. Smith, P. Smith, L. A. Soderblom, R. Sullivan, H. Wanke, T. Wdowiak, M. Wolff, and A. Yen (2004a), The Spirit Rover's Athena Science Investigation at Gusev Crater, Mars, *Science, 305*, 794-799.

Squyres, S. W., R. E. Arvidson, J. F. Bell, J. Bruckner, N. A. Cabrol, W. Calvin, M. H. Carr, P. R. Christensen, B. C. Clark, L. Crumpler, D. J. Des Marais, C. d'Uston, T. Economou, J. Farmer, W. Farrand, W. Folkner, M. Golombek, S. Gorevan, J. A. Grant, R. Greeley, J. Grotzinger, L. Haskin, K. E. Herkenhoff, S. Hviid, J. Johnson, G. Klingelhofer, A. Knoll, G. Landis, M. Lemmon, R. Li, M. B. Madsen, M. C. Malin, S. M. McLennan, H. Y. McSween, D. W. Ming, J. Moersch, R. V. Morris, T. Parker, J. W. Rice, L. Richter, R. Rieder, M. Sims, M. Smith, P. Smith, L. A. Soderblom, R. Sullivan, H. Wanke, T. Wdowiak, M. Wolff, and A. Yen (2004b), The Opportunity Rover's Athena Science Investigation at Meridiani Planum, Mars, *Science, 306*, 1698-1703.

Squyres, S. W., R. E. Arvidson, S. Ruff, R. Gellert, R. V. Morris, D. W. Ming, L. Crumpler, J. Farmer, D. J. Des Marais, A. Yen, S. M. McLennan, W. Calvin, J. F. Bell, B. C. Clark, A. Wang, T. J. McCoy, M. E. Schmidt, and P. A. de Souza (2008) Detection of silica-rich deposits on Mars, *Science, 320*, 1063-1067.

Tanaka, K. L. (1986), The Stratigraphy of Mars, *J. Geophys. Res.*, *91*, 139-158.

Tanaka, K. L., and D. H. Scott (1987) Geologic Map of the Polar Regions of Mars, *USGS Atlas of Mars – Geologic Series I-1802C*.

Tanaka, K. L., D. H. Scott, and R. Greeley (1992), Global Stratigraphy, in *Mars*, edited by H. H. Kieffer, B. M. Jakosky, C. W. Snyder and M. S. Matthews, pp. 345-382, University of Arizona Press, Tucson, AZ.

Tanaka, K. L., J. A. Skinner, T. M. Hare, T. Joyal, and A. Wenker (2003), Resurfacing history of the northern plains of Mars based on geologic mapping of Mars Global Surveyor data, *J. Geophys. Res., 108*, doi:10.1029/2002JE001908.

Tanaka, K. L., Skinner, J. A. Jr., and Barlow, N. G. (2006), How geology affects crater size-frequency distributions and determination of the crater production function for craters >5 km in diameter on Mars, *Workshop on Surface Ages and Histories: Issues in Planetary Chronology, Houston, Lunar and Planetary Institute,* abstract #6014.

Tanaka, K.L., J. A. Skinner, and T. M. Hare (2005), Geologic map of the northern plains of Mars, *USGS Scientific Investigations Map SIM-2888*.

Taylor, G. J., J. Stopar, W. V. Boynton, S. Karunatillake, J. M. Keller, J. Brückner, H. Wänke, G. Dreibus, K. E. Kerry, R. C. Reedy, L. G. Evans, R. D. Starr, L. M. V. Martel, S. W. Squyres, O. Gasnault, S. Maurice, C. d'Uston, P. A. Englert, J. M. Dohm, V. R. Baker, D. K. Hamara, D. M. Janes, A. L. Sprague, K. Kim, D. M. Drake, S. M. McLennan, and B. C. Hahn (2006a), Causes of Variation in K/Th on Mars, *J. Geophys. Res., 111,* doi:10.1029/2006JE002676.

Taylor, G. J., W. V. Boynton, J. Brückner, H. Wänke, G. Dreibus, K. E. Kerry, J. M. Keller, R. C. Reedy, L. G. Evans, R. D. Starr, S. W. Squyres, S. Karunatillake, O. Gasnault, S. Maurice, C. d'Uston, P. A. Englert, J. M. Dohm, V. R. Baker, D. Hamara, D. M. Janes, A. L. Sprague, K. Kim, and D. M. Drake (2006b), Bulk Composition and Early Differentiation of Mars, *J. Geophys. Res., 111,* doi: 10.1029/2005JE002645.

Taylor, S. R. (1982), *Planetary Science: A Lunar Perspective*, Lunar and Planetary Institute, Houston, TX.

Taylor, S. R. (2001), *Solar System Evolution – A New Perspective*, 2nd ed., Cambridge University Press, Cambridge, UK.

Taylor, S. R. and S. M. McLennan (1985), *The Continental Crust: Its Composition and Evolution*, Blackwell Scientific Publications, Oxford, UK.

Taylor, S. R., and S. M. McLennan (1995), The geochemical evolution of the continental crust, *Rev. Geophys., 33*, 241-265.

Taylor, S. R., and S. M. McLennan (2009), *Planetary Crusts: Their Composition, Origin and Evolution*, Cambridge University Press, Cambridge, UK.

Tosca, N. J., S. M. McLennan, B. C. Clark, J. P. Grotzinger, J. A. Hurowitz, A. H. Knoll, C. Schröder, and S. W. Squyres (2005), Geochemical modeling of evaporation processes on Mars: Insight from the sedimentary record at Meridiani Planum, *Earth Planet. Sci. Lett., 240,* 122-148.

Tosca, N. J., S. M. McLennan, D. H.. Lindsley, and M. A. A. Schoonen (2004) Acid-sulfate weathering of synthetic Martian basalt: The acid fog model revisited, *J. Geophys. Res., 109,* doi:10.1029/2003JE002218.

Treiman, A. H., J. D. Gleason, and D. D. Bogard (2000), The SNC meteorites are from Mars, *Planet. Space Sci., 48*, 1213-1230.

Treiman, A. H., M. J. Drake, N.-J. Janssens, R. Wolf, and M. Enihara (1986) Core formation in the Earth and shergottite parent body, *Geochim. Cosmochim. Acta, 50,* 1061-1070.

Turcotte, D. L., and G. Schubert (2001), *Geodynamics* (Cambridge University Press, Cambridge, UK, ed. 2), pp. 136-138.

Veizer, J. (1979), Secular variations in chemical composition of sediments: A Review, *Phys. Chem. Earth, 11*, 269-278.

Veizer, J., and F. T. Mackenzie (2003), Evolution of sedimentary rocks, in: Sediments, Diagenesis, and Sedimentary Rocks, edited by F. T. Mackenzie, Treatise on Geochemistry, *Elsevier, vol. 7*, pp. 369-407.

Veizer, J., and S. L. Jansen (1985), Basement and Sedimentary Recycling 2: Time Dimension to Global Tectonics, *J. of Geo., 93*, 625-643.

Wang, A., J. F. Bell, R. Li, J. R. Johnson, W. H. Farrand, E. A. Cloutis, R. E. Arvidson, L. Crumpler, S. W. Squyres, S. M. McLennan, K. E. Herkenhoff, S. W. Ruff, A. T. Knudson, W. Chen, and R. Greenberger (2008) Light-toned salty soils and soexisting Si-rich species deiscovered by the Mars Exploration Rover Spirit in Columbia Hills, *J. Geophys. Res., 113*, doi:10.1029/2008JE003126.

Wang, A., L. A. Haskin, S. W. Squyres, B. L. Jolliff, L. Crumpler, R. Gellert, C. Schröder, K. Herkenhoff, J. A. Hurowitz, N. J. Tosca, W. H. Farrand, R. Anderson, and A. T. Knudson (2006), Sulfate deposition in subsurface regolith in Gusev Crater, Mars, *J. Geophys. Res.*, *111*, doi:10.1029/2005JE002513.

Wänke, H. (2001), Chemistry, Accretion, and Evolution of Mars, *Space Sci. Rev., 56*, 1-8.

Wänke, H., and G. Dreibus (1988), Chemical composition and accretion history of the terrestrial planets, *Phil. Trans. R. Soc. London, A325*, 545-557.

Wänke, H., and G. Dreibus (1992) Chemistry and accretion history of Mars, *Phil. Trans. R. Soc. London, A349*, 285-293.

Wood, C. A., and L. D. Ashwal (1981), SNC Meteorites: Igneous rocks from Mars?, Procedures from the Lunar and Planetary Science Conference 12, *Geochim. Cosmochim. Acta Supplement, 16*, 1359-1375.

Wyatt, M. B., H. Y. McSween (2002), Spectral evidence for weathered basalt as an alternative to andesite in the northern lowlands of Mars, *Nature, 417*, 263-266.

Yen, A. S., D. W. Mittlefehldt, S. M. McLennan, R. Gellert, J. F. Bell, H. Y. McSween, D. W. Ming, T. J. McCoy, R. V. Morris, M. Golombek, T. Economou, M.B. Madsen, T. Wdowiak, B. C. Clark, B. L. Jolliff, C. Schroder, J. Bruckner, J. Zipfel, and S.W. Squyres (2006), Nickel on Mars: Consstraints on meteoritic material at the surface, J. *Geophys. Res., 111*, doi:10.1029/2006JE002797.

Yen, A. S., R. Gellert, C. Schröder, R. V. Morris, J. F. Bell, A. T. Knudson, B. C. Clark, D. W. Ming, J. A. Crisp, R. E. Arvidson, D. Blaney, J. Brückner, P. R. Christensen, D. J. DesMarais, P. A. de Souza, T. E. Economou, A. Ghosh, B. C. Hahn, K. E. Herkenhoff, L. A. Haskin, J. A. Hurowitz, B. L. Joliff, J. R. Johnson, G. Klingelhöfer, M. B. Madsen, S. M. McLennan, H. Y. McSween, L. Richter, R. Rieder, D. Radionov, L. Soderblom, S. W. Squyres, N. J. Tosca, A. Wang, M. Wyatt, and J. Zipfel (2005), An integrated view of the chemistry and mineralogy of martian soils, *Nature, 436*, 49-54.

Zuber, M. T. (2001) The crust and mantle of Mars. *Nature, 412*, 220-227.

Zuber, M. T., S. C. Solomon, R. J. Phillips, D. E. Smith, G. L. Tyler, O. Aharonson, G. Balmino, W. B. Banerdt, J. W. Head, C. :. Johnson, F. G. Lemoine, P. J. McGovern, G. A. Neumann, D. D. Rowlands, and S. J. Zhong (2000), Internal structure and early thermal evolution of Mars from Mars Global Surveyor topography and gravity, *Science, 287*, 1788-1793.